NOAA Technical Memorandum ERL NHRL-98

U.S. DEPARTMENT OF COMMERCE
NATIONAL OCEANIC AND ATMOSPHERIC ADMINISTRATION
Environmental Research Laboratories

Development of a Seven-Level, Balanced, Diagnostic Model and Its Application to Three Disparate Tropical Disturbances

HARRY F. HAWKINS, JR.

National
Hurricane
Research
Laboratory
CORAL GABLES,
FLORIDA
January 1972

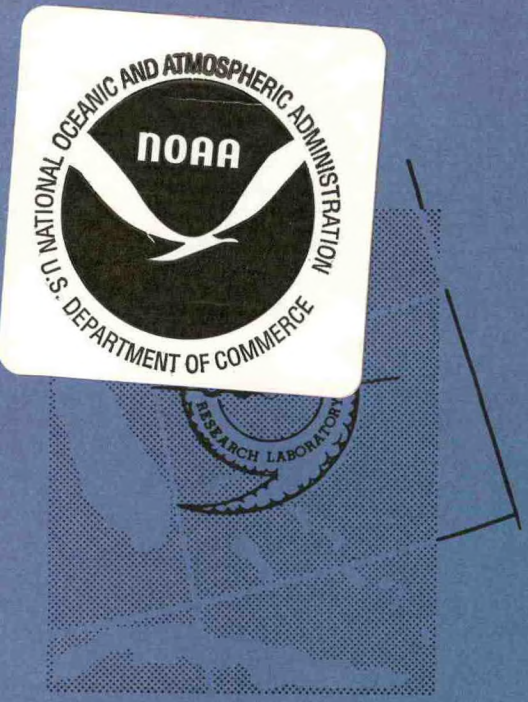

NATIONAL OCEANIC AND ATMOSPHERIC ADMINISTRATION

ENVIRONMENTAL RESEARCH LABORATORIES

NATIONAL HURRICANE RESEARCH LABORATORY TECHNICAL MEMORANDA

Reports by units of the NOAA Environmental Research Laboratories, contractors, and cooperators working on the hurricane problem are preprinted in this series to facilitate immediate distribution of the information among the workers and other interested units. As the limited reproduction and distribution in this form do not constitute formal scientific publication, reference to a paper in the series should identify it as a preprinted report.

Other reports in this series have been prepared by the National Hurricane Research Project of the U.S. Weather Bureau, by the National Hurricane Research Laboratory, as a part of the Weather Bureau Technical Note Series, and as NHRL Technical Memoranda, a subseries of the Institute of Environmental Research Technical Memoranda series.

Beginning with No. 81, they are identified as NHRL Technical Memoranda, a subseries of the ESSA Research Laboratories (ERL). Beginning with No. 90, they are identified as ERL NHRL Technical Memoranda, a subseries of the NOAA Environmental Research Laboratories (ERL).

The reports are available, at a cost of $3.00 per hard copy (microfiche 95 cents), from the National Technical Information Service, Operations Division, Springfield, Virginia 22151.

U.S. DEPARTMENT OF COMMERCE
National Oceanic and Atmospheric Administration
Environmental Research Laboratories

NOAA Technical Memorandum ERL NHRL-98

DEVELOPMENT OF A SEVEN-LEVEL, BALANCED, DIAGNOSTIC MODEL AND ITS APPLICATION TO THREE DISPARATE TROPICAL DISTURBANCES

Harry F. Hawkins, Jr.

National Hurricane Research Laboratory
Coral Gables, Florida
January 1972

TABLE OF CONTENTS

LIST OF SYMBOLS

a	radius of earth
C_d	drag coefficient
C_P	specific heat capacity at constant pressure
C_v	specific heat capacity at constant volume
D	divergence, $D \equiv \nabla \cdot \vec{V}$
F_H	horizontal frictional force per unit mass
f	coriolis parameter
g	acceleration due to gravity
$\hat{i}$	unit vector in the x - direction
$\hat{j}$	unit vector in the y - direction
J	Jacobian, $J(\psi_x, \psi_y) = \psi_{xx}\,\psi_{yy} - (\psi_{xy}^2)$
$\hat{k}$	unit vector in the vertical (up) direction
L	latent heat of evaporation
n	distance in a right hand normal direction
P	pressure
Q	heat energy
q	specific humidity
R	specific gas constant
s	distance along a streamline or counterclockwise along a boundary
T	Kelvin temperature
t	time
u	component of velocity in x - direction
v	component of velocity in y - direction
V	magnitude of velocity, $V \equiv \lvert\vec{V}\rvert$
$\vec{V}$	total horizontal velocity vector

x	eastward coordinate
y	northward coordinate
Z	abbreviation for Greenwich Meridian Time (GMT)
α	specific volume, relaxation coefficient
β	rate of change of coriolis parameter with distance northward
δ	a small increment
ζ	relative vorticity about the vertical, $\hat{k}\cdot\nabla x\vec{V}$
η	absolute vorticity about the vertical, $\eta = \zeta + f$
θ	potential temperature
κ	$R/C_p = 0.286$
σ	static stability
ϕ	latitude
Φ	geopotential height ($\Phi \equiv gZ$)
χ	velocity potential
ψ	stream function
ω	vertical velocity in the x, y, p, t system of coordinates
∇	isobaric gradient operator $(\frac{\partial}{\partial x}\hat{i} + \frac{\partial}{\partial y}\hat{j})_p$

Used as subscripts

b	satisfies the balance equation
g	geostrophic
H	horizontal, at top of the boundary layer
n	partial differentiation with respect to the outward directed normal
p	partial differentiation with respect to the P coordinate
s	in saturated cloud environment, partial differentiation with respect to distance along a streamline

t	partial differentiation with respect to time
x	partial differentiation with respect to the x coordinate
y	partial differentiation with respect to the y coordinate
χ	irrotational component of the wind ($\vec{V}_\chi$)
ψ	non-divergent component of the wind ($\vec{V}_\psi$)

ABSTRACT

Large scale vertical motions are computed using a 7-level diagnostic model in which the streamfunction and contours are related through the balance equation. The model with grid-point spacing of about 205 km is designed primarily for synoptic-scale studies over the subtropical ocean and island areas where moisture is relatively abundant. Consequently, an idealized moisture supply, driven by surface frictional convergence, releases latent heat which is partitioned in the vertical in a modified Kuo fashion. This model has been applied to a late season, strong, cold low; an easterly wave deepening into a closed system, and, to a weakening easterly low.

If one considers the simplest form of the model, i.e., without surface frictional effects and without latent heating, introduction of frictional effects increases central updraft velocities up to 50% in strong circulations. Further, the introduction of the release of latent heat increases the central updrafts by an additional factor of 2 to 5. With both of these effects included, grid scale vertical motions of the strongest circulations considered reached values of 10^{-4} cb/sec (about one cm/sec) and a tenth of this value in the weakest system. The vertical motions and fields of divergence associated with them relate to the observed weather in satisfactory fashion although they correlate very poorly with the kinematic divergences.

Test runs were made in which the weightings of stream function (derived from the wind field analysis) and analyzed heights were varied. Diagnostic results were relatively stable and suggested that wind analyses alone are adequate for most purposes.

The effects of latent heating are greatest at higher levels (250 and 400 mbs) with maximum heating equivalent to 4 or 5° C/12 hrs noted. Vertical motion accompanying the heat release is just about enough to counteract the heating through "adiabatic" expansion. The net heating or cooling is a very small residual.

Vorticity budgets revealed that in the weaker disturbances where divergence is small almost all of the vorticity change can be attributed to advection. In stronger systems with stronger vertical velocities the divergence term may equal or even dominate the advective term at those levels where divergence is most marked. The vertical advection and twisting terms seldom become very large, but on occasion when the advective and divergence terms are weak they may contribute significantly to the vorticity change at that particular level. Correlations show that the calculated vorticity tendency relates to the observed tendency best in the more quiescent situations. In the strongly disturbed state we find evidence that up through the 550 mb level the cumulus scale activity seems to be effecting vorticity changes which are proportional to the vertical gradient of vorticity between 1000 mb and the level under consideration. The inference to be drawn is that in intensely active, convective situations the vertical transport of vorticity by synoptic scale vertical velocity is too small and that the transport must occur at something more nearly approaching cumulus scale velocities.

DEVELOPMENT OF A SEVEN-LEVEL, BALANCED, DIAGNOSTIC MODEL AND ITS APPLICATION TO THREE DISPARATE TROPICAL DISTURBANCES

Harry F. Hawkins, Jr.

1. INTRODUCTION

A. Statement of the Problem

The application of numerical weather prediction (NWP) and analysis techniques to the realm of tropical meteorology is currently demanding much effort and attention. If we are to minimize the pragmatic approach which characterized much of the development of NWP methods at middle latitudes, we would be well advised to concentrate much of our early effort on diagnostic studies of tropical weather systems. Through such a procedure we would aim to establish those salient features and processes which must be retained in the numerical prediction models if they are to produce meaningful and useful forecasts for the tropics. In addition to satisfying this utilitarian role,we can also contribute to the knowledge and understanding of these tropical weather systems, per se.

In pursuit of these objectives the present paper describes the development of a seven-level, balanced, diagnostic model which includes frictional convergence of moisture in low levels and parameterized release of latent heat in the vertical. Vertical velocities, computed in two different ways, are compared to each other and to the attendant weather. The more sophisticated of these velocities is used in an evaluation of the various terms of the vorticity equation in order to determine which terms are usually dominant and which acquire importance in particular situations.

The conduct of this kind of research cannot be divorced from the inadequacies and inaccuracies of tropical data and data networks. The

network has been augmented on occasion, by choosing situations in which the usual coverage is sometime supplemented by research flight data. Special attention has been paid to the question of the well known inadequacies in the height data by merging the wind and height data with various weightings. Examples are presented in which the height data are derived solely from the windfield analysis with little or no perceptible loss of useful information.

B. Previous Studies

It has been recognized for quite some time that the horizontal velocity vector is usually measured with sufficient accuracy to satisfactorily define the major features of the horizontal flow field. This is in contrast to the vertical component of motion which is never measured directly without special instrumentation. Instead, it must be derived by indirect methods. Even these must be chosen with care because restrictive assumptions or blind application of academically logical techniques may lead to serious error. Because this most significant component of motion in producing hydrometeors is almost impossible to observe instrumentally on a synoptic scale, numerous methods have been devised which yield quantitative estimates of the vertical velocity. These include the kinematic, adiabatic, vorticity and NWP methods.

The simplest and most direct of techniques and the one involving (seemingly) the least assumptions is the kinematic. It uses the observed or analyzed wind field to define the divergence at pre-selected levels of the atmosphere. One then integrates the continuity equation, $\omega_p = -(u_x+v_y)$, from the ground to successively higher levels, assuming omega, dp/dt, is zero at the ground or is determined by the surface wind and the ground

terrain. By this means discrete values of the vertical velocity are obtained. The basic assumption implied in this approach is that the raw or manipulated winds are accurate enough for this purpose and that they are representative on the desired scale. For instance, Palmén (1958) has successfully treated the conversion of hurricane Hazel into an extratropical wave via the basic kinematic method using analyzed u and v wind fields from which were estimated the mean winds around the sides of areas 5° of latitude by 5° of longitude. In this particular example and for the scale considered, his treatment produced acceptable results. For many research projects the winds are specially prepared, e.g. minor inconsistencies in the wind field are frequently removed by smoothing horizontally (Shuman, 1957) or vertically or both.

Lateef (1967) has treated the vertical velocities in an easterly wave by modifying the kinematic divergences in a manner suggested by B. I. Miller (unpublished). This method involves differentiating the divergences in the vertical and integrating $\omega_{pp} = -\frac{\partial Div}{\partial p} = -(u_{xp} + v_{yp})$ with suitable boundary values. In a limited test this technique appeared to work reasonably well; O'Brien (1970) has shown analytically how this arbitrary approach might be objectively improved. Pfeffer (1962) used the basic kinematic approach but averaged the divergences in the vertical and set the mean equal to zero. The divergence at any level was taken to be $\overline{D}_{adj} = D - \overline{D}$ which has much in common with Lateef's approach.

In more relevant tropical applications we may cite first the study of Rex (1958) who treated a low latitude disturbance in the Pacific. Despite better than average data available from the bomb test network, he found vertical velocities increasing with elevation although they appeared otherwise reasonable. Yanai (1961) utilized data from the same

site and network in a now classical study of the formation of a typhoon. He, too, employed the kinematic approach to evaluate the divergence and vertical motion fields. However, in order to check the accuracy of his analyses and computations, Yanai computed the local vorticity tendency from successive 6-hourly maps and correlated these values with those computed from the vorticity equation using his calculated values of divergence and vertical velocity. The correlations below 500 mb were fairly good (.46 to .81) but were poorer at the higher elevations (.75 to -.45). His vertical velocities also tended to be strongest at higher elevations, i.e. at 300 mb and above. In their use of the kinematic approach both of these investigators avoided any specifications of the pressure-wind relation. Yanai also included the effects of diabatic and latent heating by considering the individual change in potential temperature and water vapor, but these effects were not incorporated in the vertical velocity determinations.

Despite encouraging results obtained by a select number of investigators who used special techniques in applying the kinematic method, the technique itself has been accepted with some hesitation. This is because of numerous instances where direct application of the method to raw data produced unrealistic vertical velocities. Appreciation of the extreme sensitivity of the technique to relatively minor fluctuations in the wind occurred fairly early and was, perhaps, inescapable after the graphical-slide-rule aids developed by Bellamy (1949) and Graham (1953). Thus, despite the simplicity of the kinematic method, many researchers turned to more laborious approaches due to a lack of confidence in the results that could be obtained kinematically.

The adiabatic method suffers from a number of handicaps: (1) It assumes that no heat is added to or lost by the system, (2) the temperature tendency must be observed (restricting its use to historical research), and (3) the vertical velocities are extremely sensitive to the lapse rate when instability is approached. In essence the method requires the conservation of potential temperature, and one way of expressing this fact is $\omega = -\frac{(\theta_t + V\theta_s)}{\theta_p}$. The local rate of change of θ on an isobaric surface, θ_t, is usually evaluated from successive synoptic charts, θ_p, from the sounding or a vertical cross section and the advection, $V\theta_s$, from the analysis. This latter may be difficult to estimate due to the tendency of the isotherms to parallel the streamlines or contours. If the situation does not concern significant release of latent heat and is not critically involved with the lower atmospheric levels where diabatic effects are largest, the adiabatic assumption is not overly restrictive (when periods of 24 to 36 hours are considered). Up until the acceptance of Numerical Weather Prediction (NWP) a few years ago, it was the most commonly used technique in spite of its inherent unsuitability for synoptic use. Panofsky (1946) presented one of the earliest formal discussions of the kinematic and adiabatic methods and also discussed variations in their application. Epstein (1959) and Craig, Lateef, and Mitchem (1961) employed a computer-adapted form of the adiabatic method. In a more recent tropical application Lateef (1968) used the technique to determine vertical motions at 100 mbs, a level where the stability presents no problem and the necessary assumptions are quite well satisfied.

The vorticity method is a rather laborious approach which shares some of the time dependency disadvantages of the adiabatic method. Nevertheless, Petterssen (1956) deemed it: ". . .perhaps, the one that is most

suitable for general use. . . ." The first post World War II use of this approach, by Sawyer (1949), utilized a simplified form of the vorticity equation, $\nabla\cdot\vec{V} = -\frac{d}{dt}(\ell n \eta)$, and graphical manipulation of successive synoptic maps which differed in time by 6 hrs. Eliassen and Hubert (1953) similarly ignored both the twisting term and frictional effects to arrive at the equivalent expression $\left.\frac{\omega}{\eta}\right|_{p_1} = \left.\frac{\omega}{\eta}\right|_{p_0} - \int_{P_1}^{P_0} \frac{(\zeta_t + \vec{V}\cdot\nabla\eta)}{\eta^2}\, dP$. The integral was evaluated by trapezoidal integration from one level to the next; ζ_t was computed from synoptic charts 12 hours apart and the simultaneous advection was calculated from mean maps formed by averaging the two synoptic charts together. The results from these early experiments were definitely encouraging but not uniformly satisfactory.

Recently Yanai and Nitta (1967) have employed this basic approach in a somewhat more sophisticated form in a tropical application: the study of vertical motions in an easterly wave. Winds were objectively analyzed by a scheme programmed for the computer by Yanai (1964). The derived grid point winds were used to define the vorticity from which the stream-function and the rotational part of the wind fields were obtained. The vorticity tendency was computed from successive maps and the complete vorticity equation together with the continuity equation and Helmholtz theorem were combined in an iterative procedure which yielded successively more accurate estimates of ω as long as the absolute vorticity was not too small. The method avoids specification of the wind pressure relationship and does not explicitly include any heating effects or friction. The vertical motions appeared reasonably well oriented relative to the axis of the easterly wave, cloudiness, and active precipitation but they had a tendency to increase with height, a weakness also commonly associated with the kinematic method. Aside from this

possible deficiency, the principal drawbacks are related to its time dependency and to the operationally observed fact that point by point evaluations of the vorticity tendency from analyses based on observed winds seem to fluctuate somewhat erratically, presumably due to noise in the observed wind data.

Inherent in every baroclinic Numerical Weather Prediction model is a set of instantaneous, simultaneous vertical motions. In the early days of NWP these "diagnostic" vertical velocities were regarded rather lightly, i.e., as a by-product of the numerical technique. The main attention was focused on the forecast of trough-ridge positions and their intensities. In time the value of these "diagnostics" became apparent and they now receive considerable attention in their own right because of the insight they provide into synoptic events. In the 1950's work began to be published which paid significant heed to "diagnostic" or NWP vertical velocities which differed from the older adiabatic and kinematic approaches because the wind-pressure relationship and thermodynamics are specified.

Bushby (1952) first studied the omega equation using Sumner's (1950) modification of the Sutcliffe (1947) development theory. He determined the field of mean vertical velocity in the 1000-500 mb layer using a static stability that was not permitted to vary in the horizontal or the vertical.

In 1955, Gates, Pocinki and Jenkins presented sets of vertical velocities for January 1953. These were derived from a thermotropic forecast model and the major aim of the paper was to compare the forecasts produced by this model with those by a barotropic model. Nevertheless, Miller and

Panofsky (1957) studied these vertical motions and found them to be usefully correlated to the observed weather.

Aubert (1957) developed one of the early sophisticated, multi-level models. In investigating the importance of the release of latent heat in large scale atmospheric motions he examined the differences in the vertical velocities produced with and without latent heat. Aubert forecast at six levels but interpolated the results to seven standard levels for verification. One of his conclusions was that the inclusion of the latent heating significantly influenced the vertical motions compared to those obtained without this effect.

As other multi-layer models were developed and tested it became clear that increasing the number of levels, i.e., the vertical resolution, increased not only the details in the flow field but also resulted in increasing the magnitude of the centers of rising and sinking motion. Knighting (1960) used a 9-level quasi-geostrophic model with constant static stability. He found that the larger vertical motions occur at mid-tropospheric levels, have predominantly parabolic shaped profiles and may change character completely over small horizontal distances. Sanders, Wagner, and Carlson (1960) compared vertical motions computed from a 10-level model with those from a 2-level model. The vertical velocity fields were in broad agreement but the more sophisticated model gave increased maxima in the centers of rise and fall. Despite the increased vertical resolution, vertical motions from the 10-level model were no better related to the observed cloudiness and precipitation than were those from the 2-level model. Stuart (1964) used the geostrophic omega equation with 8 levels of input data to determine vertical velocities which were then employed to investigate the baroclinic terms in the vorticity

equation. Among other points, his results indicated that at higher levels, particularly near the jet stream (in the development case considered), the relative importance of the twisting and divergence terms in producing vorticity changes on a parcel was far from negligible.

Many of the studies cited to this point have considered middle latitude events almost exclusively. Not a few of them employed the geostrophic relation and many of them ignored the effects of latent heat.

A contemporary development to this one, a relatively complete diagnostic formulation, is that of Krishnamurti (1968). The balance equation is used to specify the pressure-wind relation and, in a tropical application of this model (Baumhefner, 1968), the balance equation was used to derive the stream function, given the geopotential. The fact that a solution is not always mathematically possible was avoided by using the observed, i.e., analyzed, velocity components in place of ψ_x and ψ_y in the Jacobian term. Full cognizance of the wind field and its analysis was taken by making the geopotential analysis fit the calculated geostrophic gradients. Also included in the model are: the effects of surface friction, latent heating and, for the version used at higher latitudes (Krishnamurti, 1968) terrain effects and sensible heat transfer over water surfaces.

A unique feature of Krishnamurti's model is the explicit formulation of the "balanced omega equation" and an iterative approach which allows the contribution (to the vertical velocity) of each of the 12 terms in the forcing function to be evaluated separately. Using essentially this same model with 5 levels (1000, 800, 600, 400, 200 mb) of input data from the geopotential, humidity and wind analysis, Baumhefner studied the various terms contributing to the vertical motion in an easterly wave.

The vertical motions seemed reasonably oriented relative to the wave axis with synoptic scale magnitudes of about 1 cm/sec in large weather disturbances. Five of his forcing functions made negligible contributions to the final velocity. Those functions proving to be of major importance included: differential vorticity advection, Laplacion of the thermal advection, differential time dependent deformation of the stream function, differential divergence vorticity effect, frictional effect and the diabatic heating. All in all the attack by Krishnamurti and Baumhefner represents the most comprehensive approach yet addressed to the vertical motion problem.

C. Outline of the Current Study

The current study deals with three synoptic sequences in the lower latitudes: 1) a vigorous October cyclonic vortex which maintains its identity throughout the troposphere, 2) an easterly wave which deepens into a closed low as the sequence progresses and, 3) an easterly wave which weakens with time. These sequences are studied with the aid of a 7-level balanced diagnostic model which contains an idealized latent heat release partitioned after the manner of Kuo (1965). In the course of these studies the following items are among those treated:

1. Vertical velocities derived "geostrophically" are compared with those obtained from the more sophisticated balanced model. The vertical motions are also related to the reported clouds and weather.

2. The information contributions of analyzed height fields over and above the information content of the streamline-isotach field are considered.

3. Heating in the upper troposphere with the Kuo partitioning is touched upon.

4. Various terms in the vorticity equation are evaluated for the three sequences and comparisons are offered.

5. The computed vorticity tendency is compared to the "observed" and differences are examined in the light of what cumulus-scale activity may have achieved in the way of vertical transport of vorticity.

II. THE DIAGNOSTIC EQUATIONS AND MODEL

A. The Diagnostic Equations

The complete set of hydrodynamical equations are a mathematical expression of the known physical laws governing fluid motion. Although the major effects have been recognized and explicitly formulated for many years, there are still many facets that need explanation and definition, i.e., the details of radiative exchange in the atmosphere, the values for the exchange coefficients for momentum, heat and moisture, the synoptic-scale effects of cumulus-scale activity in the release of latent heat, redistribution of vorticity, etc., etc. Consequently, despite the fact that the hydrodynamical equations can be expressed as a closed set, the forecasts which can be obtained from them and the diagnostic values of divergence and vertical velocity which can be derived with their aid, depend on the validity with which the equations define the actual processes which are operative as well as on the faithfulness with which the finite difference expressions and computer manipulations approximate the differential equations.

1. The Vorticity Equation

If one takes the vertical component of the curl of the horizontal equation of motion, i.e. $\hat{k}\cdot\nabla\times$, the result is the well-known vorticity equation.

$$\hat{k}\cdot\nabla\times\vec{V}_t = -\hat{k}\cdot\nabla\times[\vec{V}\cdot\nabla\vec{V} + \omega\vec{V}_p + \nabla\phi + f\hat{k}\times\vec{V} - \alpha\vec{F}_H], \text{ or}$$

$$\zeta_t = -\vec{V}\cdot\nabla(\zeta+f) - (\zeta+f)\,\nabla\cdot\vec{V} - \omega\zeta_p - \hat{k}\cdot\nabla\omega\times\vec{V}_p + \hat{k}\cdot\nabla\times(\alpha\vec{F}_H) \qquad (1)$$

where the symbols are conventionally defined in the x, y, p, t coordinate

system, but may be found listed on page xiv preceding this text if clarification is needed. In this study the vorticity equation was not taken to include the frictional torque term throughout, although at the lowest level (1000 mb) the surface stresses are allowed to define a vertical velocity, ω_H, at the top of the friction layer in a manner suggested by Cressman (1960).

2. The Balance Equation

According to the Helmholtz Theorem a three-dimensional vector can be written as the three-dimensional gradient of a scalar and the three-dimensional curl of a vector. In turn, it can be shown that the horizontal or two-dimensional "total" wind, $\vec{V}$, can be expressed as the sum of two parts: a nondivergent part, $\vec{V}_\psi$, and an irrotational part, $\vec{V}_\chi$, where ψ is the stream function and χ is the velocity potential. Thus $\vec{V} = \vec{V}_\psi + \vec{V}_\chi = -\psi_y \hat{i} + \psi_x \hat{j} + \chi_x \hat{i} + \chi_y \hat{j}$ and we define $\nabla^2\chi = -\omega_p$ = Divergence. We seek an expression which will relate the stream function and the geopotential, preferably a reasonably sophisticated expression. We have chosen to use the Balance Equation to define this relationship.

If we take $\nabla\cdot$ the horizontal equation of motion and use $D = \nabla\cdot\vec{V}$, we obtain from $\vec{V}_t + \vec{V}\cdot\nabla\vec{V} + \omega\vec{V}_p + f\hat{k}\times\vec{V} + \nabla\phi = 0$, omitting friction and using

$$\vec{V}\cdot\nabla\vec{V} = \zeta\hat{k}\times\vec{V} + \nabla\left(\frac{\vec{V}\cdot\vec{V}}{2}\right)$$

$$D_t + \nabla\cdot(\eta\hat{k}\times\vec{V}) + \nabla\omega\cdot\vec{V}_p + \omega D_p + \nabla^2\Phi + \nabla^2\left(\frac{\vec{V}\cdot\vec{V}}{2}\right) = 0$$

$$D_t + \vec{V}\cdot\nabla D + \omega D_p + \nabla\omega\cdot\vec{V}_p - f\zeta + \nabla^2\Phi + \vec{V}\cdot(\nabla\times f\hat{k}) + D^2 + 2J(v,u)$$

$$- \frac{\vec{V}\cdot\vec{V}}{a^2} - \frac{\mathrm{Tan}\phi}{a}\frac{\delta(2\vec{V}\cdot\vec{V})}{\delta y} = 0$$

Scale analysis for subtropical synoptic systems (see Appendix A) suggests that if only terms $10^{-10}\,\mathrm{sec}^{-2}$ or larger are retained, then this expression

reduces to the familiar Balance Equation:

$$L(\psi) \equiv f\nabla^2\psi + \psi_y f_y + 2[\psi_{xx}\psi_{yy} - \psi_{xy}^2] = \nabla^2\Phi \qquad (2)$$

This defines the pressure-wind relation since it specifies the stream function given the geopotential or vice versa. The Jacobian term takes cognizance of the curvature of the streamlines.

3. The Thermodynamic Equation

In view of the importance generally conceded the release of the latent heat of condensation in tropical systems, we deemed it highly desirable to include this heating effect. For this purpose the following form of the thermodynamic equation was used:

$$\frac{dQ}{dt} = C_P \frac{dT}{dt} - \alpha\frac{dp}{dt} = C_P\frac{T}{\theta}\frac{d\theta}{dt}$$

On a constant pressure surface $\frac{1}{\theta}\frac{d\theta}{dt}\Big|_p = \frac{1}{T}\frac{dT}{dt}\Big|_p = \frac{1}{\alpha}\frac{d\alpha}{dt}\Big|_p$. If we use the hydrostatic relation, $\alpha = -gZ_p = -\Phi_p$, one can show

$$\Phi_{tp} = -\vec{V}\cdot\nabla\Phi_p - \omega\sigma - \frac{R}{C_P P}\frac{dQ}{dt} \qquad (3)$$

where $\sigma \equiv -\frac{\alpha}{\theta}\theta_p$ is the static stability. Equations 1, 2 and 3 can be shown to be energetically consistent (Appendix B). Such consistency is often mandatory for successful runs of iterative models and is highly desirable in diagnostic models.

Since independent temperature analyses were not available for all of these sequences, the above expression for sigma was deemed inconvenient to use. It was formulated in handier terms by using the Poisson Equation, $\frac{1}{\theta}\theta_p = \frac{1}{T}T_p - \frac{R}{C_P P}$, and the equation of state, $\frac{1}{p} + \frac{1}{\alpha}\alpha_p = \frac{1}{T}T_p$, to show that $\sigma = \phi_{pp} + \frac{C_V}{C_P P}\phi_p$.

4. The "Geostrophic" Omega Equation

The basic equations for the complete model are (1), (2), and (3). Actual application of the model showed that convergence (in a manner to

be defined shortly) did not always occur readily. In an effort to supply a reasonably intelligent first guess of the vertical velocity fields, we found that the "geostrophic" omegas served this purpose quite admirably. If one uses a simplified but still energetically consistent form of the vorticity, balance and thermodynamic equations (See Appendix B), the following equalities are realized:

Vort. Eqn. $\nabla^2\psi_t = -\vec{V}\cdot\nabla\eta + f_o\omega_p$

Where f_o is the mean coriolis parameter over the domain of interest.

Bal. Eqn. $\nabla^2\psi = \frac{1}{f_o}\nabla^2\Phi$

Thermo. Eqn. $\Phi_{tp} = -\vec{V}\cdot\nabla\Phi_p - \sigma\omega - \frac{R}{C_pP}\frac{dQ}{dt}$

If we take $\partial/\partial p$ of the first equation and the Laplacian of the third and make use of the geostrophic relationship defined in the second, we find

$$\frac{1}{f_o^2}\nabla^2(\sigma\omega) + \omega_{pp} = \frac{1}{f_o}\frac{\partial}{\partial p}[\vec{V}\cdot\nabla\eta] - \frac{1}{f_o^2}\nabla^2[\vec{V}\cdot\nabla\Phi_p] - \frac{1}{f_o^2}\nabla^2\left[\frac{R}{C_pP}\frac{dQ}{dt}\right]$$

which provides the fourth basic working relationship. We define the omegas so determined to be the "geostrophic" vertical velocities.

5. Parameterization of the Release of Latent Heat

The primary use for which the diagnostic model is intended is in the study of tropical weather systems. Charney (1963) has pointed out that the synoptic-scale systems in the tropics require diabatic and viscous affects for the occurrence of significant vertical motions. Most of the systems studied will be located over tropical maritime areas. Consequently, no cognizance has been taken of terrain effects. Furthermore, not all of the synoptic sequences on which it was immediately planned to use the model had separate analyses of the moisture parameter. Nevertheless, it was felt that the moisture could be satisfactorily

represented by using the appropriate normal distributions for the location and season. The normals used were Jordan's (1958) mean monthly values for the West Indies area. This rationale is substantiated in part, at least, by studies (unpublished) made at the National Hurricane Research Laboratory. These studies consisted of series of charts showing the vertical distribution of moisture and the total precipitable water content analyzed over the Gulf of Mexico, Caribbean Sea and southwestern North Atlantic for several summer seasons. Inspection of these charts led to the conviction that where water vapor was readily available, moisture values rose suddenly and with little warning from continuity whenever the synoptic situation turned favorable for upward motion. Our conviction from this series was that over such regions there was little prognostic (although certain diagnostic) information to be gleaned from charts of water content and that there was always more than adequate moisture available which could be "pumped up" under a favorable synoptic development. For these reasons it is felt that little harm has been done through neglect of the moisture analysis.

Another possibly mitigating factor in this seemingly cavalier treatment is the unsolved problem of cumulus heat release and transport. There is little question that significant atmospheric warming occurs through cumulus activity, particularly over the tropics. It is extremely difficult, however, to know how to partition the heat release. A number of able investigators have treated this subject (Kuo, 1965; Ooyama, 1967; Charney and Eliassen, 1964; and Ogura, 1964). The method of parameterization employed in this model is most similar to that of Kuo although, as will be noted, modifications have been made to his philosophy. Kuo calculates the mass of vapor (in tons/m^2) which must be

condensed to bring the environmental air at temperature T to the cloud temperature, T_S, as: $\frac{1}{g} \int_{P_T}^{P_B} \frac{C_P}{L} (T_S - T)\, dP$

where P_B and P_T refer to the pressures at the bottom and top of the column considered. He also computes the mass of vapor (in tons) required to saturate the environment as: $\frac{1}{g} \int_{P_T}^{P_B} (q_S - q)\, dP$. If ω_H is taken as the frictional vertical velocity at the top of the friction layer and q_H is a reasonable value for q at that level, then I is defined as $I \equiv \frac{\omega_H q_H}{g}$ tons of water vapor/m^2 sec i.e., the amount of water vapor made available per square meter per second. The heating rate at a particular point is then defined as

$$\frac{dQ}{dt} = -C_P (T_S - T) \frac{I}{N} \text{ where } N = \frac{1}{g} \int_{P_T}^{P_B} \frac{C_P}{L} (T_S - T)\, dP + \frac{1}{g} \int_{P_T}^{P_B} (q_S - q)\, dP$$

There are obvious weaknesses in the above formulation which should be pointed out. The frictional vertical velocities used to drive the latent heating will be grid-scale (200 km) values, i.e., much smaller than the local velocities experienced under cumulus cells, cloud lines and the like where the physical processes actually take place. Where cumulus activity is occurring the activity itself results in raising T toward T_S and q toward q_S so that the climatological values of T and q will be generally smaller than those found in disturbed situations. In strongly disturbed areas T and q become nearly equal T_S and q_S, respectively, so that nearly all of the moisture entering at cloud base condenses and falls as rain while releasing its latent heat. In the present formulation this can never occur since we are using a constant, climatological N. Consequently, we know a priori, due to both scale and practical considerations that the mean climatological expression will lead to underestimates of the latent heat release.

It should be emphasized that this underestimate is not due to the use of climatology alone. It is partly a result of the differences between the grid-scale and the scale of the phenomenon. Rosenthal (1970) has arrived at a similar expression for the partitioning of latent heat using a different rationale. However, much of his work is on a 10-km grid which compares well with the scale of the phenomenon. Thus, he is able to use the expression without any arbitrary adjustment. On this smaller scale, and with an explicit water vapor cycle, his model seems to reproduce the intensification of a tropical cyclone quite realistically.

If we consider the total "potentially available latent heat" is $\frac{\omega_H q_H L}{g}$, we might consider partitioning it vertically according to the expression

$$\frac{C_p\ (T_S - T)}{C_p \int (T_S - T) \frac{dP}{g}}$$

which is similar to the distribution used by Rosenthal (1969), but now superseded. This would ensure that all of the "available latent heat" was used in warming the atmosphere, a bit of an overestimate. Later discussion will reveal what modification was made to Kuo's original formulation for the present sequences.

The frictional vertical velocity, ω_H, at the top of the friction layer is essentially that of Cressman (1960) with a minor modification, i.e.

$$\omega_H = \frac{\rho g C_d}{f} \left[\frac{\partial}{\partial y} \left(u\sqrt{u^2 + v^2}\right) - \frac{\partial}{\partial x} \left(v\sqrt{u^2 + v^2}\right)\right]$$

where C_d is a linear function of velocity as expressed by Miller (1966)

$$C_d = (1.00 + 0.07\ \sqrt{u^2 + v^2}) \times 10^{-3}$$

In both of these equations u and v are defined by the streamfunction at the 1000-mb level.

In summary then the humidity parameter was not analyzed. The appropriate normal values of humidity and temperature are used in conjunction with the vertical velocity due to low level frictional convergence. Where there is upward motion at low levels, heat is released (above the lifting condensation level) in proportion to the difference between the ambient (normal) air temperature and the saturation adiabat through the lifting condensation level. Heat is released from the LCL to that level where the sounding indicates no positive (parcel) buoyancy remains.

B. The Seven-Level Diagnostic Model

1. The Physical Dimensions

A model with 7 levels was selected for a variety of reasons. In order to simplify the programming, it was desirable to maintain a uniform separation between information levels. In addition to this characteristic, we wanted to have at least one level in the stratosphere and as many as could be readily carried in the troposphere. Since the map analysis is not an inconsiderable part of the whole task, one cannot afford too many levels. The compromise here was to separate the levels by 150-mb intervals. Consequently, the levels were at: 1000, 850, 700, 550, 400, 250 and 100 mb. These are conventional meteorological levels except for that at 550 mb.

The mesh size chosen was 2° of longitude at 22.5° N latitude which gives a grid size of about 206 km on a side. This can be altered by a control card. Analyses were to be made on a Mercator projection true at 22.5° N latitude and the distance between grid points varied from 217 km at 13° N to 183 km at 35° N. Because of computer limitations, the grid was restricted to a relatively small number of points (10 x 13 = 130) but

the coding was designed so that the grid was movable to any area of interest and was keyed by giving the latitude of the southernmost grid row. We intended to resolve systems with wavelengths generally of the order of 1000 km, and this design allowed for some 4 to 5 data points in a typical wavelength.

2. Merging Wind and Height Data

The analysis projected called for analysis of the streamlines, isotachs and contours at each of the 7 levels. Since the streamfunction was to be determined from the wind field and the streamfunction is also related to the geopotential heights through the balance equation, the situation is overspecified if the geopotential is also given. (This is not altogether true since the geopotentials are needed in order to determine σ, the static stability.) The data presented an opportunity for investigation of how the geopotential heights should be merged with the wind data to achieve a "best" estimate of both the wind and height fields.

This problem has been treated by Charney (1962) in working with higher latitude systems. He suggested that where one has wind and heights available the balanced values be determined by: 1) at a given level calculate ζ from the actual wind field, 2) determine the stream function, ψ, from $\nabla^2\psi_1 = \zeta_1$, 3) use ψ_1 in the balance equation to obtain Φ_1, 4) a corrected $\zeta = \zeta_2$ is determined from $f(\zeta_2-\zeta_1) = \nabla^2(\Phi_1-\Phi_0)$ where Φ_0 is the original analyzed geopotential, and 5) steps (2), (3) and (4) are repeated twice to yield ψ_2, Φ_2 and ψ_3, Φ_3. The latter ones were to be accepted as the balanced fields of ψ and Φ. The approximation in step (4) is based on the fact that the actual vorticities are approximated

by the geostrophic vorticities, $\frac{1}{f}\nabla^2\Phi$. In the research reported on here, Charney's suggested method failed to converge in early runs (perhaps due to the low latitudes involved) and was abandoned in favor of the following scheme. If (see equation 2) $\nabla^2({}_b\Phi) \equiv A\nabla^2{}_a\Phi + (1-A)L({}_a\psi) \equiv L({}_b\psi)$, where subscripts a and b refer to "analyzed" and "balanced" respectively, then we can vary A from 0 to 1 and allow the weighting of the respective contributions of height and wind fields to vary from 0 percent to 100 percent.

While this may appear at first glance to be a rigorous and fair test of the value of each of these parameters, in actual execution this is far from the case. Geopotential height values are notoriously poor in latitudes where relatively weak gradients coincide with significant wind speeds. Experience has shown that one cannot draw to the reported height values alone and produce a meteorologically meaningful map. Consequently, the analyst usually draws mainly for the winds but includes as much geopotential height information as he deems consistent with the analysis demanded by the wind field. This is not entirely different from the approach at middle latitudes, but the opportunities to satisfy both the reported height and wind fields are much more infrequent, and the differences between analyzed and reported heights, particularly at higher levels, are most conspicuous in these latitudes where gradients are weak. In consequence, the height analyses are not independent inputs; they are closely related to the wind field analysis. With the current standards of rawinsonde accuracy, no meaningful evaluation of the independent contribution of the height field is possible. Nevertheless, within these limitations we can still see whether the contour fields add significantly to the results when the diagnostic model is applied. It

will also be interesting to see if comparable results can be obtained without the height field analyses (cf. Bedient and Vederman, 1964).

3. The Proposed Cycle and Boundary Conditions

From the analyses at each level, we propose to read the meteorological wind direction and speed, DDDVV, and the heights, HHHHH, at the grid intersections. The major steps in the cycle are shown schematically in flow chart form, figure 1; a detailed expansion proceeds as follows:

a. Control of Operational Modes and Input Constants

One of the input parameters punched into the cards preceding each data set was the latitude of the southernmost grid row. From this datum the following parameters are calculated: the latitude of each grid row, the coriolis parameter for each row, the value of β for each row and the map factor and grid distance in meters for each row.

These leading data cards also contained other parameters of use in the model, such as, the year, month, day and hour of the synoptic map time, the normal heights of the 7 levels, the value of the relaxation coefficient, α, various tolerances for relaxations and various switches, i.e., for conversion of units from knots and geopotential feet to the meter - ton - second system which is used throughout this paper, etc.

b. Wind Smoothing

The winds are broken down into u and v components and smoothed with the Shuman (1957) nine-point smoothing routine. On the outer boundaries the smoothing does not involve 9 points but retains the same relative weighting of the possible adjacent points to obtain a smoothed value. This technique suppresses much of the "noise" in the original individual reports and also suppresses the extremely short wavelengths of two grid lengths or less.

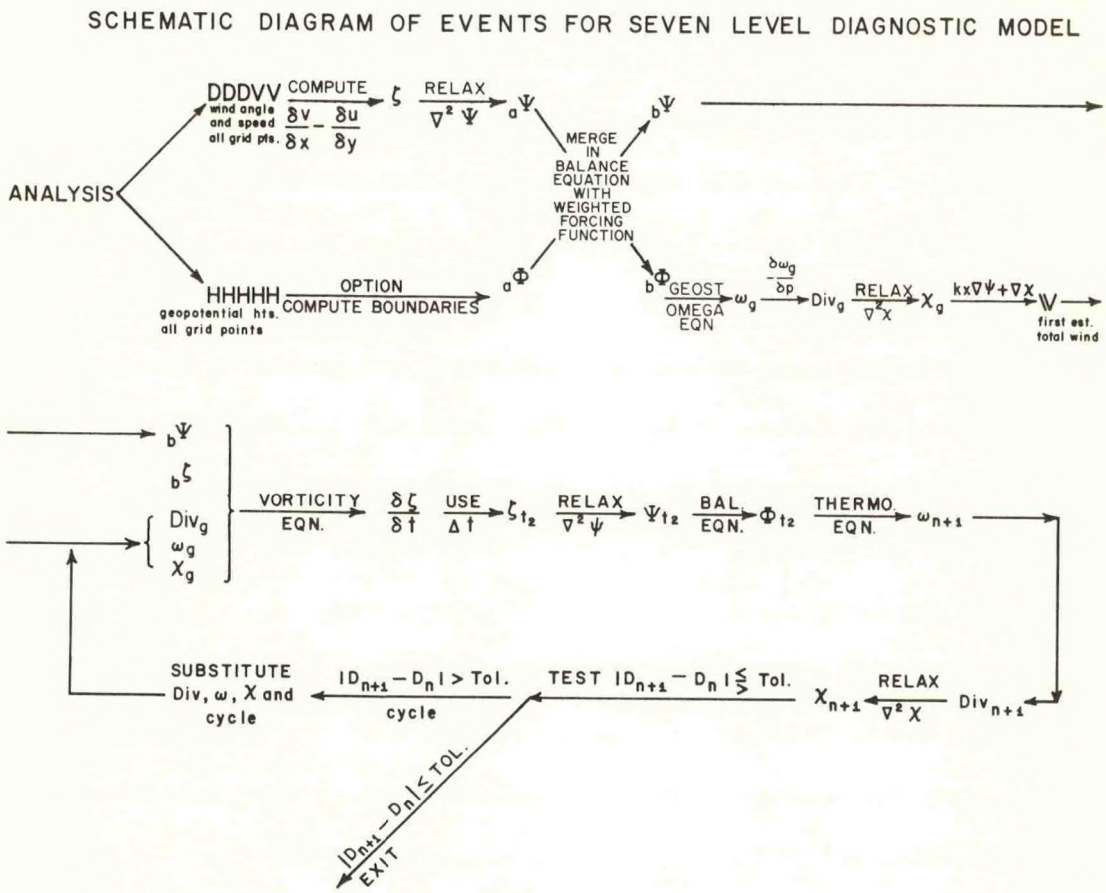

Figure 1. A schematic flow diagram of the diagnostic model outlining the ordered sequence of steps which are followed in obtaining refined vertical velocities. Subscripts a and b refer to analyzed and balanced, respectively; subscript g refers to geostrophic and t_2 to the value of the parameter at time t_2 which is Δt later than the initial time.

c. Deriving the Vorticity

The relative vorticity of the wind field is computed from the equation $\zeta = v_x - u_y$, using the usual centered finite difference approximations for the differentials. Only interior values can be determined this way, so a simple method of extrapolating values out to the border was employed as a subroutine. In essence it used the Shuman smoothing weightings omitting the central value (and any other missing values) and correcting the weighting for this omission. For instance, a mid-point on the western boundary would be determined by taking twice the value of the grid point due east of it, adding the values of the points north and south of this latter point and dividing by 4.

d. Computing the Stream Function

The stream function is derived next from the relationship $\nabla^2\psi = \zeta$ using a boundary routine derived by Hawkins and Rosenthal (1965). If we consider the regular 10 x 13 grid to be bounded by boundary A and an interior grid one row and/or one column in as bounded by B, we use the following equations as indicated:

(a). $\nabla^2\psi = \zeta$

(b). $\nabla^2\chi = u_x + v_y$

(c). $\psi_n = V_S - \chi_s$

(d). $\psi_s = -V_N + \chi_n$

where n is the outward directed normal and

s is distance measured (counter-clockwise, positive) along the boundary.

(1). Solve b for boundary B, using $\chi = 0$ on A.

(2). Evaluate χ_n on B using centered differences.

(3). Integrate (d) trapezoidally along inner boundary, B.

(4). Solve (a) over interior of B using ψ values from (3) as boundary values on B.

(5). Integrate (c) trapezoidally from B to A with χ_s evaluated by centered differences thus obtaining ψ on boundary A.

(6). Using ψ on boundary A solve (a) over the interior. This field is denoted ${}_a\psi$ or the analyzed stream function after the corner values are extrapolated by the amended 9-point formula and the field is altered so that the lower left-hand corner value is zero. The use of $\chi = 0$ on the boundary of A has the result of maximizing the portion of the kinetic energy carried by the ψ field and minimizing the portion carried by the χ field as shown by Sangster (1960).

e. Merging the Stream Function and Contour Heights

The analyzed geopotential heights are smoothed with the Shuman 9-point smoothing routine and converted to meters to comprise ${}_a\Phi$. The two parameters, ψ and Φ are now weighted (through the arbitrary argument A) to compute the forcing function: $FF \equiv A\nabla^2{}_a\Phi + (1-A)L({}_a\psi)$. Then $\nabla^2({}_b\Phi) \equiv FF \equiv L({}_b\psi)$ is solved for both ${}_b\Phi$ and ${}_b\psi$, the balanced values. In relaxing for ${}_b\Phi$ the boundary values of Φ are constrained to be "pseudo-geostrophic". On the northern and southern boundaries ${}_b\Phi = f{}_a\psi$ or $\delta_b\Phi = f\delta_a\psi$. This procedure is begun at the lower left-hand corner and procedes counter-clockwise to the upper right-hand corner. We momentarily ignore the small term involving beta on the eastern and western boundaries. The same procedure is then used in a clockwise sense to the upper right-hand corner, thus establishing a second value for Φ at that point. These two values are averaged and the final value for that grid corner is taken as the mean of the two. The top row phi's are now computed geostrophically going counter-clockwise to the upper

left-hand corner. We now have values for both top and bottom rows. If we differentiate twice, we obtain ${}_b\Phi_{yy} = 2f_y\, {}_a\psi_y + f\, {}_a\psi_{yy} + {}_a\psi\, f_{yy}$ where the third term on the right may be neglected. This equation is then used for a one-dimensional relaxation on the eastern and (separately) on the western boundaries using the relevant corner values as bounds. The values are obviously keyed to the lower left-hand corner value; however, they can, by simple addition or subtraction, be keyed to any grid point value which the analyst selects. If no ${}_a\Phi$ values are available, or if one wishes to disregard the field of ${}_a\Phi$ completely, the program is so designed that the average values of ${}_b\Phi$ over the boundary can be set equal to the normal value of phi for that level. This would be even more appropriate if the grid were somewhat larger. In any event the interior values of ${}_b\Phi$ are obtained by relaxation of the Laplacian using the 'weighted' forcing function and the boundary values just described.

Manipulating the balance equation in order to evaluate the stream function is a more time-consuming proposition. Relaxation methods are usually employed and convergence is not always achieved because the radical term may become imaginary at times. Following Shuman (1957) we set

$$f\nabla^2\psi + \nabla f \cdot \nabla\psi + 2(\psi_{xx}\psi_{yy} - \psi_{xy}^2) - FF = 0$$

If we add and subtract $\frac{\psi_{xx}^2}{2}$, $\frac{\psi_{yy}^2}{2}$ and $f^2/2$ we obtain

$$\tfrac{1}{2}(\psi_{xx} + \psi_{yy} + f)^2 - \tfrac{1}{2}(\psi_{xx} - \psi_{yy})^2 - 2\psi_{xy}^2 + \beta\psi_y - \frac{f^2}{2} - FF = 0$$

or

$$\eta = \sqrt{(\psi_{xx} - \psi_{yy})^2 + 4\psi_{xy}^2 + 2FF + f^2 - 2\beta\psi_y}$$

This expression has the desired form with the central point implicit only in the first term on the left when ordinary centered differences are used. Although the first two terms under the radical are positive

definite, the expression may become imaginary if $(2FF + f^2 - 2\beta\psi_y) < 0$. In order to circumvent this possibility, we make the field $(2FF + Bf^2) \geq 0$. This is done by scanning the field for negative values of this quantity and when one is encountered reducing the value at the surrounding four points by $\left|\left(\frac{2FF + Bf^2}{4}\right)\right|$ and setting the value at the point equal to zero. B is an arbitrary constant, $0 \leq B \leq 1$, which allows us to use a portion of the quantity f^2 to meet the test. According to Shuman, this procedure does not alter the mean value of the field nor (in practice) the major features of the field. The value of the radical is next computed (including the unused portion of f^2, i.e., $((1-B)\ f^2)$. This expression is tested to see if it is less than zero. On the rare occasions when it is, it is set equal to zero after testing to see if its absolute magnitude exceeds $.2\ f^2$; if it does, such points are tabulated (and found to be quite rare). The relaxation for ${}_b\psi$ can now proceed maintaining previous boundary values for the stream function. From the new field of ${}_b\psi$, the 'balanced' vorticity field is derived using ${}_b\zeta = {}_b\psi_{xx} + {}_b\psi_{yy}$. Values are extrapolated to the boundaries and smoothed to insure a minimum of discontinuity with the interior field.

The balanced values of geopotential are next derived using:

$$\nabla^2 {}_b\Phi = f\nabla^2({}_b\psi) + \nabla f \cdot \nabla({}_b\psi) + 2({}_b\psi_{xx}\ {}_b\psi_{yy} - {}_b\psi_{xy}^2)$$

maintaining the previous border values as bounds for the relaxation.

f. Calculating the Static Stability

The static stability is computed using the balanced contour heights in the expression $\sigma = {}_b\Phi pp + \frac{C_v}{C_p P}({}_b\Phi p)$. Sigma appears in the denominator of the expression for omega and, as it approaches zero, the value becomes indeterminate. On a synoptic scale such a physical state of affairs is highly unlikely and negative values are completely unrealistic. The

possibility of negative values and unrealistic small values is avoided by: 1) testing sigma at each point in the field to see if it is less than one tenth of the normal sigma for that level. If it is, then it is replaced with one tenth of the normal value of sigma for the level. The field is then smoothed with the 9-point smoothing routine to eliminate any possible discontinuities. Thus the sense of pattern of the sigmas is maintained but extreme values tend to be minimized. In general, negative values were almost never found in the interior of the field of sigma. Because of the way in which the boundaries of the balanced phi field were determined, occasional boundary values of sigma were slightly negative. This occurred only at the lower levels where the values of sigma are small. Average values of sigma at each level are maintained for use in determining the geostrophic vertical motions since energetic consistency with a geostrophic approximation (see Appendix B) requires sigma be a function of pressure only.

g. Computation of Frictional Vertical Velocities

The frictionally-induced vertical velocity is calculated from the equation

$$\omega_H = \frac{\rho g C_d}{f}\left[\frac{\partial}{\partial y}\left(u\sqrt{u^2+v^2}\right) - \frac{\partial}{\partial x}\left(v\sqrt{u^2+v^2}\right)\right]$$

where $C_d = (1.00 + 0.07\sqrt{u^2+v^2}) \times 10^{-3}$ is a function of the wind speed. The values of u and v are computed from the balanced stream function using centered differences and are extrapolated to the boundary so the differentials could be calculated for the interior grid. A mean value, $\rho = 1.15 \times 10^{-3}$ tons/m^3 and $g = 9.8$ m/sec^2, is used for this equation.

h. Computation of the Heating Function

We have specified the heating function:

$$\frac{dQ}{dt} = -C_P(T_S - T)\frac{I}{N}$$

where $I = \frac{\omega_H q_H}{g}$ and

$$N = \frac{1}{g} \{ \int_{P_T}^{P_B} \frac{C_P}{L} (T_S - T)\, dP + \int_{P_T}^{P_B} (q_S - q)\, dP \}$$

We take C_P = 1004 kj/ton °C

$L = 2.5 \times 10^6$ kj/ton

$g = 9.8$ m/sec^2

The quantity N is computed from a tephigram plot (see Appendix C) of the appropriate monthly mean sounding for the West Indies (Jordan, 1958). Surface air is lifted dry adiabatically to the lifting condensation level and moist adiabatically thereafter. The cloud top is assumed to coincide with that level at which no free parcel buoyancy remains. From the two soundings, i.e., the monthly normal and the "cloud sounding," we compute the mean values of T_S, T, q_S and q from the cloud base to 850 mb, then upward by 150-mb layers, and, finally, to the cloud top. The value of q_H, the specific humidity at the top of the friction layer, is taken at cloud base or the LCL. Since the heating is partitioned according to $(T_S - T)$, the heating should be greatest in the region of 300 to 400 mb where the temperature differences are most marked.

i. The "Geostrophic" Vertical Velocities, Divergence and Velocity Potentials

We compute the geostrophic vorticities from the fields of balanced geopotentials, ${}_b\Phi$. Then from equation,

$$\frac{1}{f_o^2}\nabla^2(\sigma\omega) + \omega_{pp} = \frac{1}{f_o}\frac{\partial}{\partial p}(\vec{V}_g \cdot \nabla\eta_g) - \frac{1}{f_o^2}\nabla^2(\vec{V}_g \cdot \nabla\Phi_p) - \frac{1}{f_o^2}\nabla^2\left(\frac{R}{C_P P}\frac{dQ}{dt}\right)$$

we note that centered difference approximations for both of the terms on the left contain the central point value for ω, and an expression for the residual in an Extrapolated Liebmann relaxation is readily obtained. Sigma may be taken outside of the Laplacian since it is here a function

of pressure only and the average for the level is used. The relaxation is three-dimensional with limits as follows: Omega at 100 mb is taken as zero, since this level is in the stably stratified stratosphere and vertical motions should be small (Lateef, 1968). The lower boundary values at the 1000 mb level are taken as the frictional omegas, ω_H, and the effects of surface friction are thus incorporated in the model without having the expression for it appear explicitly in the "geostrophic" omega equation. The lateral boundaries for the interior levels are also taken to be zero for the relaxation iteration but are extrapolated out to the boundaries after the iteration.

The "geostrophic" divergence is computed from the expression: $Div_g = - \frac{\partial \omega_g}{\partial P}$. The values of the frictional vertical velocity are not used in these finite difference expressions for divergence since we are essentially interested in the synoptic scale divergence. Consequently, one-sided difference expressions are used for the 1000-mb and 100-mb levels which involve only the 850-mb and 250-mb geostrophic omegas respectively.

The "geostrophic" velocity potentials, χ_g, are computed from the equation $\nabla^2 \chi_g = Div_g = - \frac{\partial \omega_g}{\partial P}$. This relaxation is carried out on at expanded grid two rows and two columns larger than the 10 x 13 working grid. The iteration takes place on one level after another with lateral boundaries taken as zero. We have now gone through the upper line of schematic events shown in figure 1.

j. The "Balanced" Omega

At this juncture we must consider the problem of obtaining more accurate vertical velocities employing equations (1), (2) and (3). In a subsequent development (to this one), Krishnamurti (1968) combined the

equations by expressing (1) in terms of $\frac{\partial}{\partial t}\nabla^2\psi = \ldots$ (2) in terms of $\nabla^2\psi = \ldots$, and taking $\partial/\partial t$ of (2). One solves the combination of (1) and (2) for $\frac{\partial}{\partial t}\nabla^2\Phi = \ldots$ and uses (3), $\frac{\partial}{\partial t}\frac{\partial\Phi}{\partial p} = \ldots$. If he differentiates $\frac{\partial}{\partial p}$ (2) $= \ldots$ and takes the Laplacian of (3), ∇^2 (3) $= \ldots$, he then can combine (1), (2) and (3) into a "balanced omega" equation.

We did not attempt this elegant approach in part because of the mathematical obstacles which arise when one considers the solution of the combined equations. Instead, it was felt that a simpler alternate was available which had some advantages of its own. In essence, the original geopotential heights and stream functions are balanced (as described). Then the vorticity equation (1) is used to "forecast" ζ at <u>one</u> later time, t_2. From the "later" vorticity new values of ψ are derived and then new Φ's are determined from the balance equation. We can then approach equation (3) in finite difference form with a known thickness tendency obtained using the values of Φ for the two times and dividing through by the Δt used to evaluate ζ at time t_2 and solve for ω. This procedure allows easy manipulation of the weightings used in merging the original Φ and ψ fields. It also permits the surface frictional convergence to be dropped or altered readily and the latent heating can be experimented with. Nevertheless, it is equivalent to the explicit formulation obtained by Krishnamurti. The details of this approach employ the following cycles:

(1). The vorticity equation is employed to evaluate the vorticity at time t_2. We compute $\zeta_t = -\vec{V}\cdot\nabla\eta - \eta\nabla\cdot\vec{V} - \omega\zeta_p - \hat{k}\cdot\nabla\omega\times(\partial\vec{V}_\psi/\partial p)$ and set $_{t_2}\zeta = {}_{t_1}\zeta + \Delta t\zeta_t$. This is done for computational ease, not because the value of ζ at the two times is of interest. For a first approximation we use the vertical velocities, divergences, and velocity potentials

which we obtained from the "geostrophic" omega computations. The customary centered finite difference approximations are employed.

(2). We make use of the relationship $\nabla^2_{t_2}\psi = {}_{t_2}\zeta$ and by relaxation find ${}_{t_2}\psi$ using (of necessity) the old boundaries.

(3). The border is next adjusted to the changes in the interior field by adding the changes (weighted as in the modified smoothing routine) to the old border values.

(4). We next employ the balance equation to solve for ${}_{t_2}\Phi$ at the interior levels.

(5). Make a border adjustment for the changes in the interior field.

(6). The advection of thickness by the total wind, i.e., $-\vec{V}\cdot\nabla\Phi_p$ is next computed for all points of the grid at all levels using one-sided differences where necessary and multiplied by the time interval Δt. The border values are then smoothed using the modified smoother weighting.

(7). For the 1000 and 100-mb levels, the vorticity equation cannot be used in the centered difference form used for the interior levels. Additionally, at 1000 mb the frictional term becomes increasingly important. For these reasons an alternate method for evaluating Φ at $(t + \Delta t)$ was selected which alleviated some of these drawbacks. At 1000 mb and at 100 mb, ω is essentially taken to be zero (other than the frictional omega at the top of the friction layer to drive the latent heating) and the heating at these levels is essentially nil. Therefore we use $\Phi_{tp} \doteq -\vec{V}\cdot\nabla\Phi_p$. We have ${}_{t_2}\Phi$ at the interior levels and now obtain ${}_{t_2}\Phi$ at 1000 and 100 mb by trapezoidal integration over time Δt.

(8). We now get our first estimate of the refined omegas at all the interior levels by solving the thermodynamic equation $\Phi_{tp} = -\vec{V}\cdot\nabla\Phi_p - \omega\sigma - \frac{R}{C_p P}\frac{dQ}{dt}$ for ω. Note we now have ${}_{t_1}\Phi$ and ${}_{t_2}\Phi$ for all

levels and the time interval, Δt, now is divided into $({}_{t_2}\Phi - {}_{t_1}\Phi)$ rendering the vertical velocities "instantaneous". Since relaxation is not involved, values can be computed even at the lateral boundaries. However, in view of all the manipulation involved in trying to maintain the integrity of the lateral boundaries, little or no weight can be attached to these external points.

k. Computing the Refined Divergence and Velocity Potential

The refined omegas are used to compute the refined divergence (the frictional omegas are ignored for this purpose). Next the velocity potentials are computed (as previously described) using the "geostrophic" estimates as a first guess.

l. Cycling for Convergence

At this point the question is raised as to how much change has been introduced by the last series of steps, i.e., items j and k. A test has been devised keyed to the value of the divergence, namely: Is the most recent value of the divergence significantly different from the next to last obtained value of the divergence? Therefore, at each point on the grid the most recent value of the divergence is compared to the next most recent. If the difference exceeds a certain tolerance, then the latest values are used for a new evaluation of the vorticity equation as described in (1) above and the sequence is repeated using the latest values of ω, divergence and χ. On every third cycle, if three or more are necessary, the most recent and the next most recent values of omega are averaged together and the cycle continued. (The reason for this procedure will become apparent later.) This continues until the value of the change in divergence at each point remains less than or equal to a pre-assigned tolerance. Convergence of the technique is thus defined

and when the criterion is met, values are recorded and cycling is terminated.

4. Products of the Diagnostic Model

In addition to those quantities already mentioned such as, the "geostrophic" ω's, divergence and χ and the refined values of these parameters, the model is also programmed to output other items of interest.

If we express thickness changes in terms of the equivalent mean virtual temperature change through the relevant layer, for a given time interval, Δt, we find $\Delta\overline{T}_* = -\frac{g}{R\ell_n(P_2/P_1)}\Delta[z_2 - z_1] = \frac{\Delta P \Delta t}{R\ell_n(P_2/P_1)}(\vec{V}\cdot\nabla\Phi_p + \omega\sigma + \frac{R}{C_p P}\frac{dQ}{dt})$ where each of the quantities in the parenthesis is available in the core of the computer having been saved from its computation earlier. The following items are prepared using the above expression to compute the mean virtual temperature change per 300-mb layer due to:

a. Thickness advection by the total horizontal wind, i.e.,

$$\Delta\overline{T}_* = \frac{\Delta P \Delta t}{R\ell_n(P_2/P_1)}(V\cdot\nabla\Phi_p)$$

b. advection by vertical motion, i.e.,

$$\Delta\overline{T}_* = \frac{\Delta P \Delta t}{R\ell_n(P_2/P_1)}(\omega\sigma)$$

c. the release of latent heat, i.e.,

$$\Delta\overline{T}_* = \frac{\Delta P \Delta t}{R\ell_n(P_2/P_1)}(\frac{R}{C_p P}\frac{dQ}{dt})$$

d. the sum of quantities a. through c. or the "forecast temperature change" over time Δt.

Other items of interest included the vorticity change which might be expected in time Δt if that part of the local tendency persisted which was due to:

e. the horizontal advection of vorticity by the total wind, i.e.,

$$-\Delta t(\vec{V}\cdot\nabla\eta)$$

f. the divergence term,

$$-\Delta t\ \eta(\nabla\cdot\vec{V})$$

g. the vertical advection of vorticity

$$-\Delta t\ \omega\zeta_p$$

h. the twisting term

$$-\Delta t\hat{\mathbf{k}}\cdot\nabla\omega\times\partial\vec{V}_\psi/\partial p$$

i. the sum of terms e. through h.

The general magnitude, order, interrelationship and significance of these terms will be discussed in appropriate later sections of this report.

5. Programming

The main diagnostic program was originally prepared in Fortran II language for a GE-225 16k machine by chaining program sequences and by frequent tape writing and reading. The program was not in final running shape when our machine activities were transferred to an IBM 7040 with a 32K core. The chains were eliminated and eventually the entire program was made to fit in the 7040 which it filled to capacity.

III. THREE SYNOPTIC SEQUENCES AND THEIR PREPARATION FOR DIAGNOSTIC RUNS

A. General Comments

Analyses for three different synoptic sequences became available for use in the diagnostic model.

1. Sequence #1, October 13-15, 1956: Vigorous Disturbance

The first situation is a late season cold low with fairly vigorous cyclonic circulation which began to turn into a warm core low at upper levels as the series ends. This situation was specifically analyzed by the writer for use in the diagnostic model. It was chosen for the intrinsic merit of the situation and for the added data coverage afforded by; (1) the Atlantic missile range which was then at peak strength, and (2) some aircraft reconnaissance data from the fledgling National Hurricane Research Project (now Laboratory). The latter provided data on the 15th near the 1000, 850 and 555-mb levels. Soundings from Cuba were also available at that time and, on the average, coverage was better then than in more recent years. Of course, not all soundings were present at all synoptic times nor did they all reach our top level of interest, 100 mb. The elements analyzed were heights, streamlines and isotachs at the seven diagnostic levels.

2. Sequence #2, August 25-27, 1962: A Moderately Disturbed Situation

This sequence traces the deepening of a fairly well marked easterly wave in the Caribbean into a closed low. The low eventually (after our period of study) becomes Hurricane Alma. Mr. Clark Smith analyzed this

series for contour heights, streamline, isotachs, temperatures and humidities (Lateef and Smith, 1967) at the desired levels.

3. Sequence #3, August 3-5, 1963: A Slightly Disturbed State

A weak easterly Caribbean wave moves slowly westward weakening further towards the close of the period. Dr. M. A. Lateef analyzed this sequence as a complement to the preceding case in which the easterly wave deepened. (Lateef and Smith, 1967 and Lateef, 1968). Analyses were made at the desired seven levels for streamlines, isotachs, temperature and humidity.

B. Data Preparation

For each case the soundings were processed with the National Hurricane Research Laboratory ADP program developed by J. W. Trout and W. J. Koss. The program interpolates for values at 50-mb intervals from 1000 mb up to 100 mb. These values are then used to make gross consistency checks of the wind shears, static stability and hydrostatic consistency.

Since the research was concerned with synoptic-scale phenomena, it was decided (for the first two sequences only) to reduce the usual noise that accompanies the wind reports at a level and to make them more representative of the layer in which they were embedded. The interior levels were smoothed in the vertical by averaging the u and v components separately in accordance with the following weighting

$$u_{700} = (u_{650} + 2u_{700} + u_{750})/4$$

In this manner winds weighted over a 100-mb interval were derived for each of the interior levels. At the 100-mb level we took $u_{100} = (u_{150} + 2u_{100})/3$ and at the 1000-mb level we used an analogous method which weighted the available winds between the 1000-mb and 950-mb levels.

For all sequences the meteorological data for all 7 levels were plotted on Mercator projection maps true at 22.5° N. The 1000-mb reports were augmented by surface and ship reports and, where possible, by off-hour 1000-mb reports. Although it is recognized that variations in wind from the ship anemometer level to the 1000-mb level are quite common, it was not possible to arrive at a characteristic correction which would materially improve the majority of the situations. This may be due in part to the varying anemometer levels on the different ships but one is inclined, in general, to attribute it to the rather low quality of surface ship reports and to the effects of varying static stability. Even under more stringent conditions, systematic corrections are not too uniform in application and are frequently quite small (Charnock, Francis and Sheppard, 1956).

The third sequence used wind values taken directly from the data. The reason for the differences in approach was that analysis of the three sequences was undertaken independently by the three investigators.

C. Analysis

Analyses were carried out from 5°N to 40 or 45°N and from 50°W to 100°W. Figure 2 shows the data network over the prime area of interest with the grid superimposed.

The following principles were used by the author in his analysis and were used, possibly a bit less rigorously, by the other two analysts. Analysis of the streamlines was begun at the 1000-mb level and proceeded upward using any auxiliary material such as time and space cross-sections which were available from the operational and laboratory historical files. The streamlines were drawn with the following guidelines:

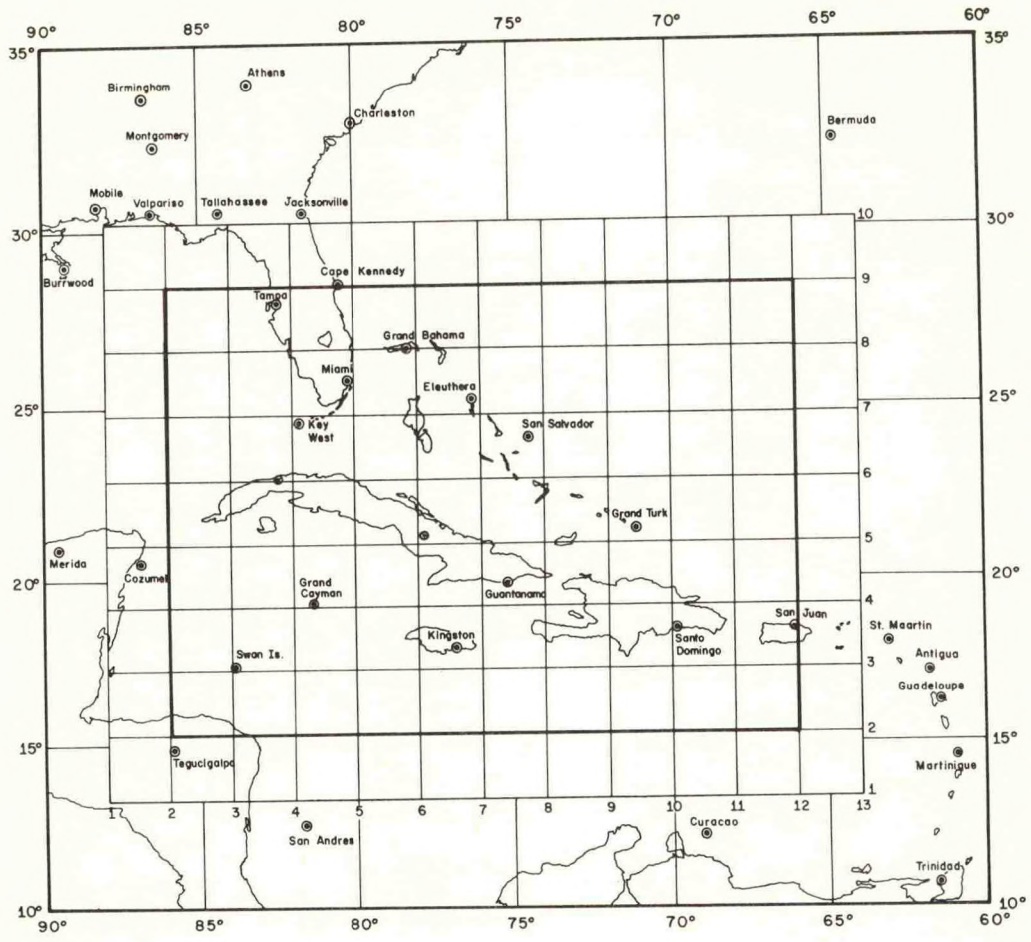

Figure 2. Map of the area of major interest for most of the analysis. Regular upper air reporting stations are indicated by station circles with names. The two unnamed circles are Havana and Camaguay, Cuba, which reported for the October, 1956, weather sequence but not for the other two sequences. The movable 10 x 13 grid is shown in the orientation used for the August, 1963, sequence with the heavier lines outlining the area of more reliable results. Analyses were carried out over a larger area which extended some 5 to 15° further in each direction than the area shown here.

1) Draw as closely to the wind directions as is compatible with experience and reason, 2) favor the higher wind speed where a choice is necessary and all other factors are even, 3) introduce confluence and diffluence only where justification exists or necessity demands, 4) systems are displaced in the vertical as indicated by the data or, if centrally located data are lacking, in accordance with experience as long as peripheral data permit.

The isotachs were drawn to conform with reported wind speeds wherever this was possible and/or reasonable. A most common problem with the speed field is the lack of data encountered in the relatively loose tropical reporting network. The philosophy used in approaching this analysis was to try, while drawing for the data, to minimize the divergence. So, where the data permit, one perpetuates wind speed along a streamline, increases wind speeds in confluent situations, etc. Finally, one guards against inadvertent introduction of divergence.

The analysis of the height fields (undertaken in the first two sequences only) presents even more acute problems, particularly at the higher altitudes. Geopotential heights in the tropics have been notoriously unreliable. Whether they are of poorer quality than higher latitude reports may be a moot point. In some installations both the hot, humid climate and the local employment policies seem to work against the training and maintenance of skilled raob teams. In any event, whether or not errors are larger and more frequent, they are more conspicuous in the tropics since only weak gradients are usually encountered. One cannot draw sensibly to the height values alone. Consequently, the analyst must fall back on what corroborative material is available, i.e.,the wind field, continuity in space and time, etc. Since the motion, even

at latitudes as low as 15°, is essentially quasi-geostrophic (Charney, 1963 and Charney and Eliassen, 1964) there must be quite a close relationship between the streamline-isotach analysis and the contour field. The field of heights, therefore, was analyzed so as to be roughly in geostrophic balance with the winds where this seemed appropriate. Unfortunately, this in effect renders the contour field dependent on the wind field so that it cannot be treated as an independent parameter when it is considered in the light of what new information it brings to the problem.

Analysis of the October case was done in the meter-ton-second system. Contours were analyzed at intervals of 10 geopotential meters and isotachs were drawn every 2 m/sec. The August maps were drawn in the British system with heights in geopotential feet and wind speed in knots, but temperatures were in degrees Celsius. In all three cases the area analyzed was much larger (5 to 10 times as large) than the area covered by the movable grid.

D. Data Tabulation

A transparent overlay bearing the grid network outline was superimposed on the maps, and values at the grid points were read, tabulated and punched. Contour analysis values were interpolated to the nearest meter or nearest foot. Wind directions were read from the streamline analysis to the nearest degree using a specially constructed transparent protractor. Original values read by the analysts were checked against values read by an assistant. For direction, agreement to within 2° was usually obtained without difficulty although when the curvature

was sharp great care was demanded. Even so, extreme disagreements of 5° or more were quite rare. The wind speeds were read off to the nearest meter per second or to the nearest knot as the analysis demanded.

E. Discussion of the Synoptic Sequence

1. Sequence #1

The sequence October 13-15, 1956, was preceded by the intrusion of a cold Canadian high which had penetrated the Central Plains by October 8. The center was located over Lake Michigan on the 10th with cool air reaching the northern Gulf states. Although the cold front had reached the Florida Straits by the 12th, the high center remained well north in Maine. Thus, the air had a long northeasterly fetch over the water. This condition was little changed by the 13th when our series begins (figures 3, 4, 5, 6, a and b). The high center is near Nova Scotia but our map shows only the easterly to northeasterly flow in the latitudes of Florida.

At our first synoptic time, October 13, 15Z a sharp shear zone indicates the remains of the old frontal trough at 1000 mb (figure 3 a and b). The low center is poorly defined at this level and vorticity (figure 3b) is mainly attributable to the cyclonic shear in the strong easterlies to the north of Cuba. In the lower levels (up through 550 mb) the core of the cyclone is somewhat cooler than the environment and intensifies as it tilts northward and slightly eastward. Above 550 mb, the structure is complicated by an abrupt change in the tilt to the west and actually to the south a bit (at 400 mb).

Such irregularities of structure in genetic systems are not too unusual in lower latitudes where vertical coupling of the atmosphere is much weaker than at higher latitudes. It has been frequently pointed out (Riehl, 1954 and Charney, 1963) that the lower level perturbations of the easterlies below mid-tropospheric levels frequently move in ways seemingly unrelated to synoptic events in the upper troposphere and strange superpositions result. In this case a pre-existing trough at 500 mb apparently helped along the cyclo-genesis somewhat in advance of the upper level trough. This apparent discontinuity disappears as the sequence progresses.

The sea-level low has a central pressure of about 1008 mb when the series begins and deepens slowly but steadily at a rate of about 2 mb per day. Analogous deepening is noted at the 850, 700, 550-mb levels and at 400 mb through October 14,15Z (on the final map the center is weaker at the 400 mb level). At the 250-mb level the deepening ceases 12 hours earlier, i.e., on October 14 at 03Z, and the center at that level fills thereafter. These latter effects can be attributed to warming at the upper levels which is apparent in the temperatures (not shown). The total upper-tropospheric warming at the center of the cyclone was not very great, amounting to some 3° to 4°C. Figures 3a through 6a present the fields of geopotential height together with other parameters and bear out these observations. The supplementary fields of stream function, vorticity and total wind are presented in figures 3b through 6b.

It may be noted that the interior winds parallel the stream function with fair fidelity since the divergent part of the wind is quite small and the stream function portion has been constrained to carry the bulk of the kinetic energy. On the boundaries this is not necessarily the case due

Figure 3a. October 13, 1956, 15Z. Weather, vertical motion, contour and divergence fields. The bottom slab depicts the cloud cover and hydrometeors from an independent analysis of the data. Above are slabs from 1000 to 250 mb that show: diagnostic vertical motion (length, (in perspective) of arrow is proportional to speed indicated by tick marks equal to 50 x (10^{-6}) cbs/sec); height contours are solid lines (in tens of geopotential meters, labelled at the east and west limits of the grid only); diagnostic divergences (dashed) with zero line heavier and centers labelled in units of 10^{-6} sec^{-1}. A scale for converting cbs/sec to cm/sec is presented to the right of each slab. North-south direction varies across the grid; its orientation (on extreme right of the grid) is shown on the 250-mb slab.

The overcast squally weather lies mainly in the low-level easterly and northeasterly flow where low-level vertical velocities are upward and the 850-mb convergence is fairly strong. Downdrafts at 850 and 700 mb seem to characterize the better weather to the east and west.

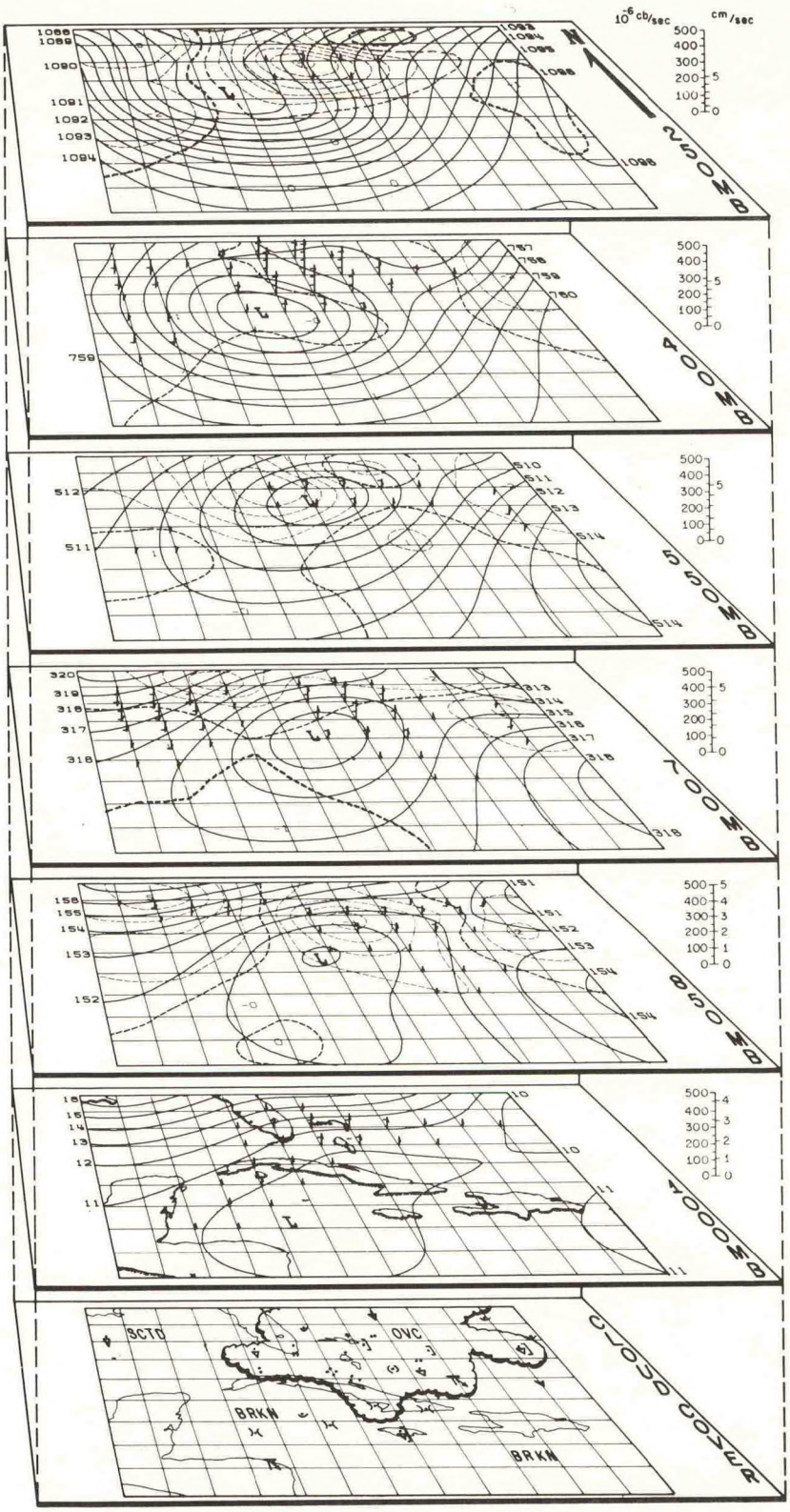
10^{-6} cb/sec
cm/sec
250 MB
400 MB
500 MB
700 MB
850 MB
1000 MB
CLOUD COVER
SCTD
OVC
BRKN
BRKN

Figure 3b. October 13, 1956, 15Z. Streamfunction, vorticity and total wind fields. Perspective drawing for levels from 1000 to 100 mb presenting: the streamfunction (solid lines) which have been zeroed in the lower left corner of the grid and labelled in units of m^2/sec (scaled by 5×10^{-6}); the relative vorticity (dashed lines) with the zero line heavier and centers labelled in units of 10^{-6} sec^{-1}; the total wind speed (in knots) and direction shown in conventional meteorological notation; wind speeds have been converted to knots in order to make evident the smaller variations in speed.

The center of low-level vorticity lies near but slightly north of Cuba just south of the center of active weather. This center is reflected at successively higher levels in a customary fashion until the 400-mb level which suggests that the upper troposphere is not yet completely "in phase" with the lower. This is a commonly noted characteristic of the lower latitude uncoupled troposphere but it appears to diminish as the sequence progresses.

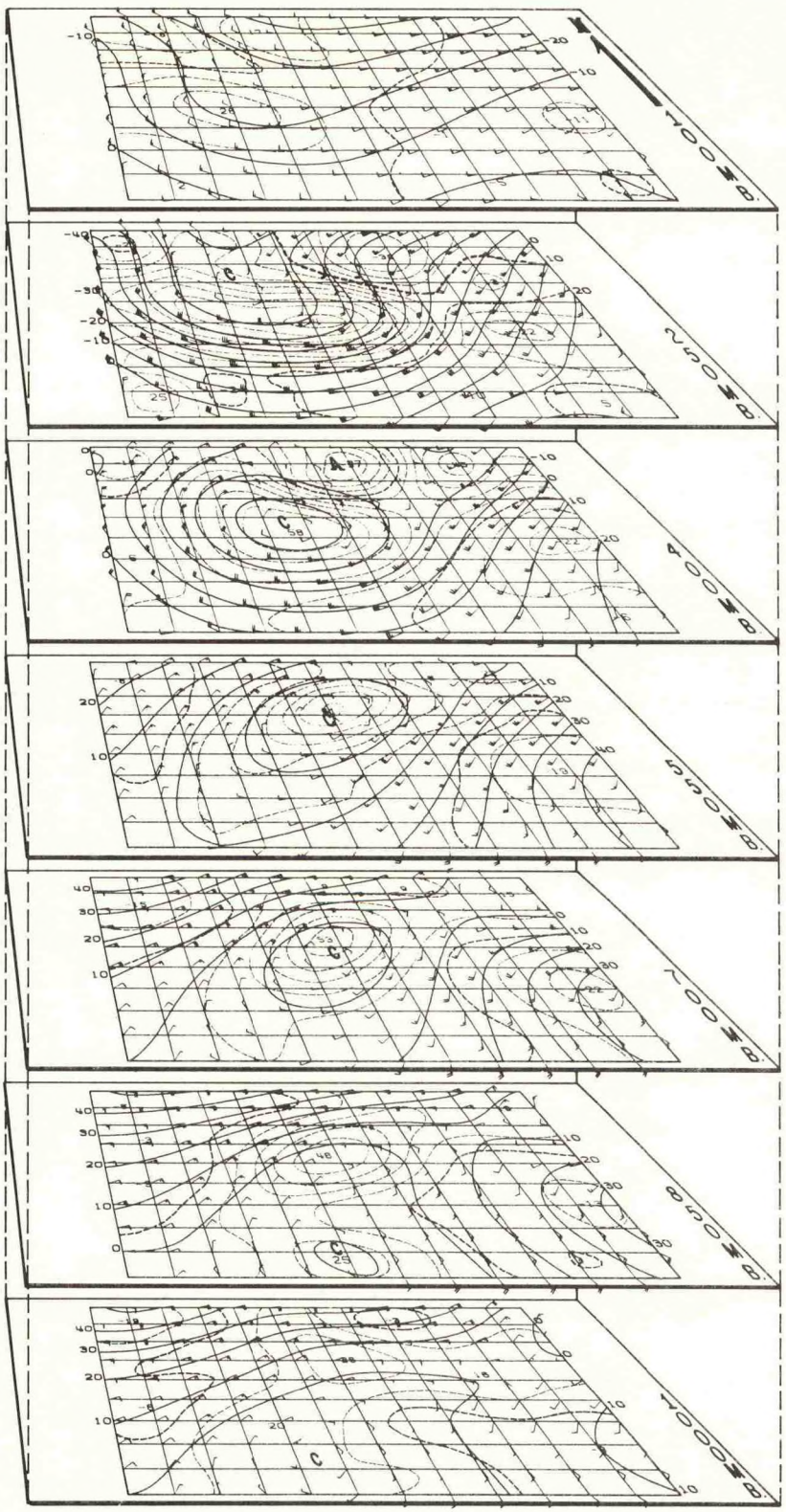
700 MB
500 MB
400 MB
300 MB
250 MB
200 MB
100 MB

Figure 4a. October 14, 1956, 03Z. Weather, vertical motion, contour and divergence fields (see legend figure 3a). Upward vertical velocities of the order of cm/sec (in lower levels) characterize most of the extensive area of bad weather. The western sector characterized by scattered to broken cloudiness shows descent at 850 and 700 mb. The coupling of lower and upper troposphere appears better than in figure 3a with little or no discontinuity apparent between the 550 and 400-mb levels.

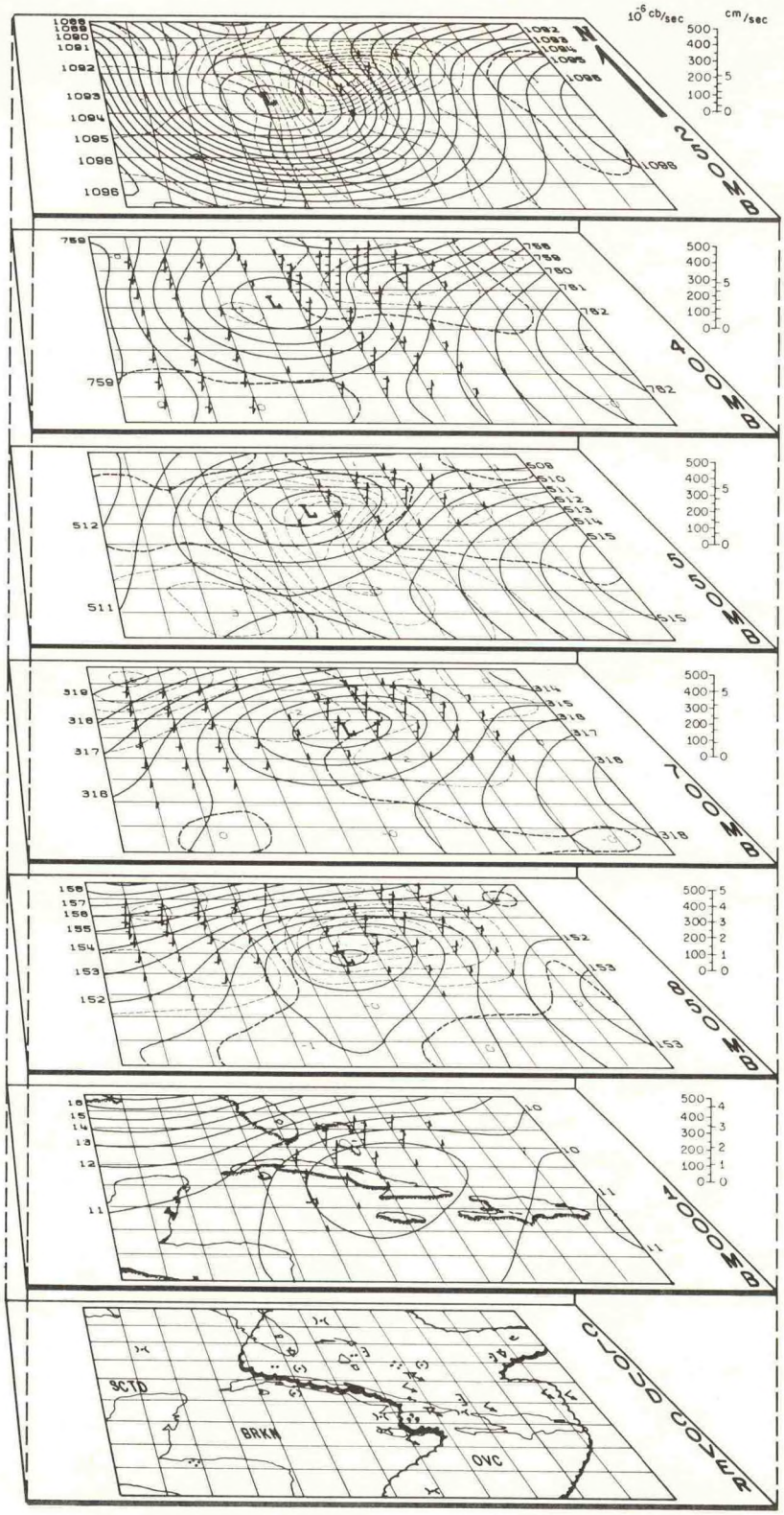
10^6 cb/sec
cm/sec
N
250 MB
400 MB
500 MB
700 MB
850 MB
4000 FT
SURFACE
SCTD
BRKN
OVC

Figure 4b. October 14, 1956, 03Z. Streamfunction, vorticity, and total wind fields (see legend figure 3b). Cyclonic vorticity has increased slightly at the three lowest levels and also at 250 mb where coupling between upper and lower troposphere appears more complete than in figure 4b.

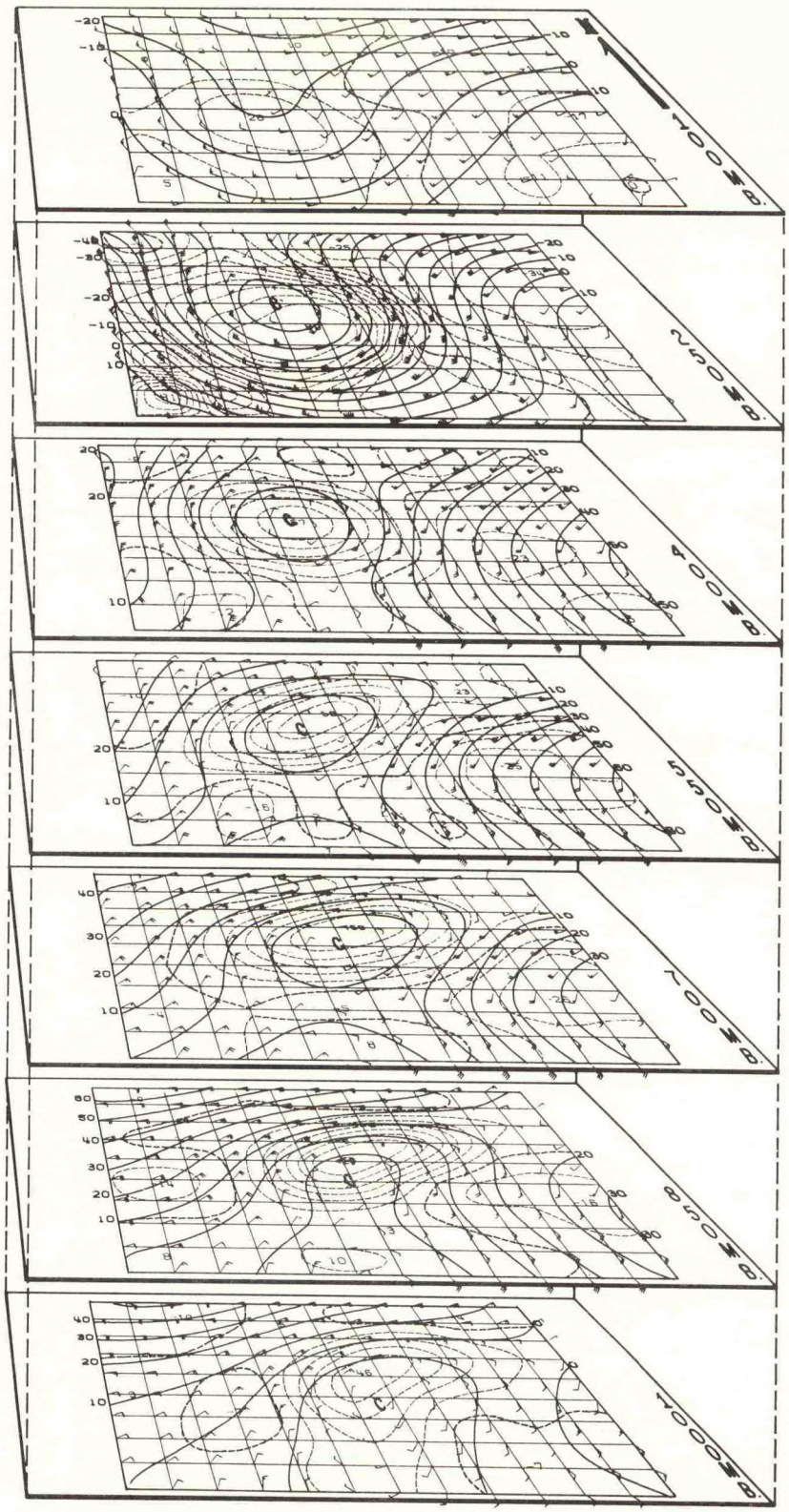

Figure 5a. October 14, 1956, 15Z. Weather, vertical motion, contour and divergence fields (see legend figure 3a). The grid was moved one degree of latitude further north in order to keep the center of cyclonic vorticity (at lower levels) near the center of the grid. Aside from the slight northward shift changes from the preceding 12 hours have been small. There has been some improvement in weather on the northern central Cuban coast and to the east as the vorticity center leaves the immediate coast.

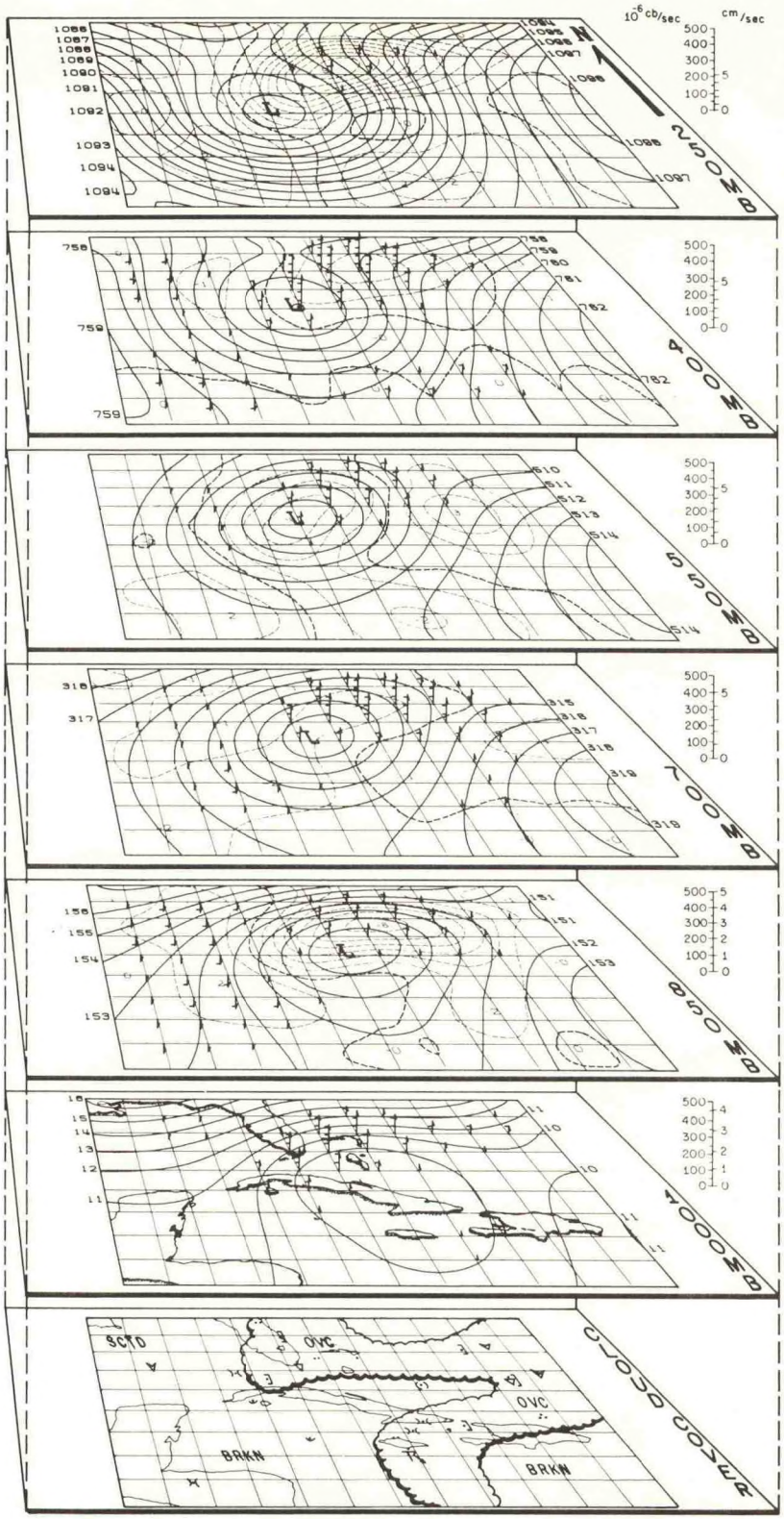
10^{-6} cb/sec
cm/sec
250 MB
400 MB
550 MB
700 MB
850 MB
1000 MB
CLOUD COVER
SCTD
OVC
BRKN

Figure 5b. October 14, 1956, 15Z. Streamfunction, vorticity and total wind fields (see legend figure 3b). Changes in the structure of the low have been relatively small over the 12 hours since figure 4b. The vortex center is now almost vertical throughout the troposphere.

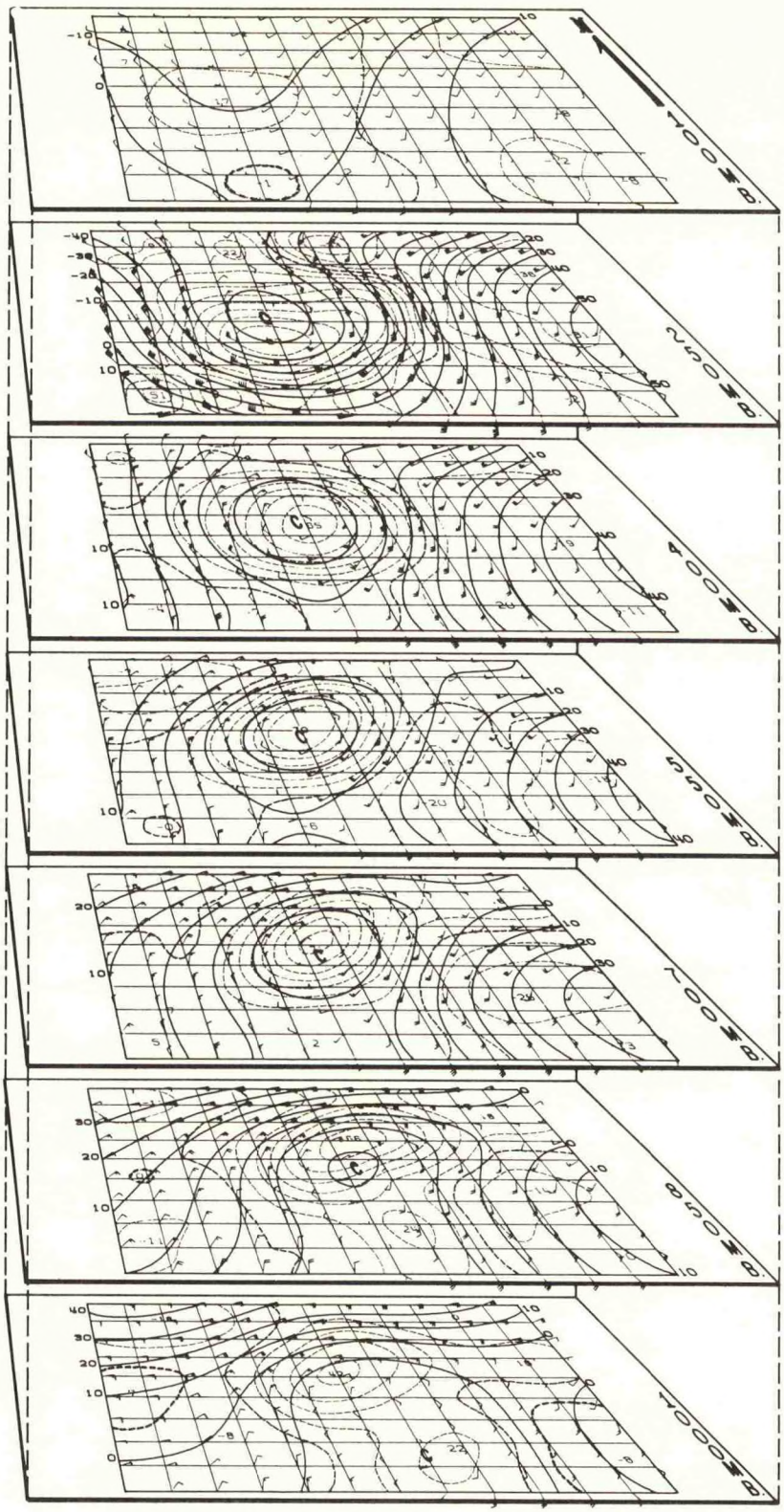

Figure 6a. October 15, 1956, 03Z. Weather, vertical motion, contour and divergence fields (see legend figure 3a). At this map time the upward vertical currents (mostly northeast of the low center) are strongest and most extensive in area, also, they penetrate in strength up through the 400-mb level. Similarly, low level convergence (at 850 mb) reaches a maximum of 10^{-5} sec^{-1} over most of the same area. A widespread area of bad weather covers most of this region.

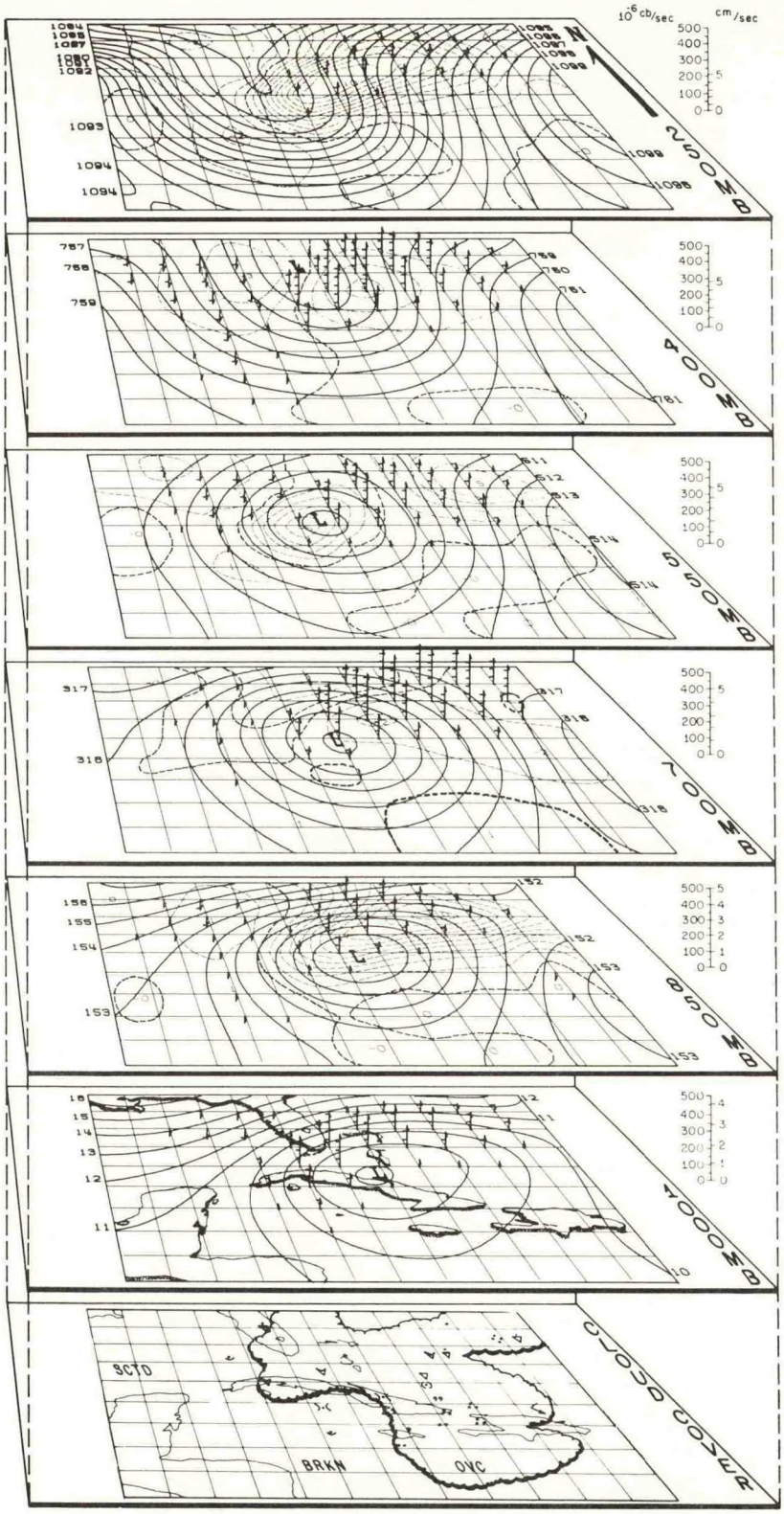
10^6 cb/sec
cm/sec
250 MB
400 MB
500 MB
700 MB
850 MB
40000 MB
CLOUD COVER
SCTD
BRKN
OVC

Figure 6b. October 15, 1956, 03Z. Streamfunction, vorticity and total wind fields (see legend figure 3b). The last maps in this sequence show slight intensification of the low (vorticity increasing) at lower levels and slight decreases at the 400 and 250 mb levels. These signs are interpreted as indicative of the beginning of the establishment of the warm core structure which attends hurricane genesis.

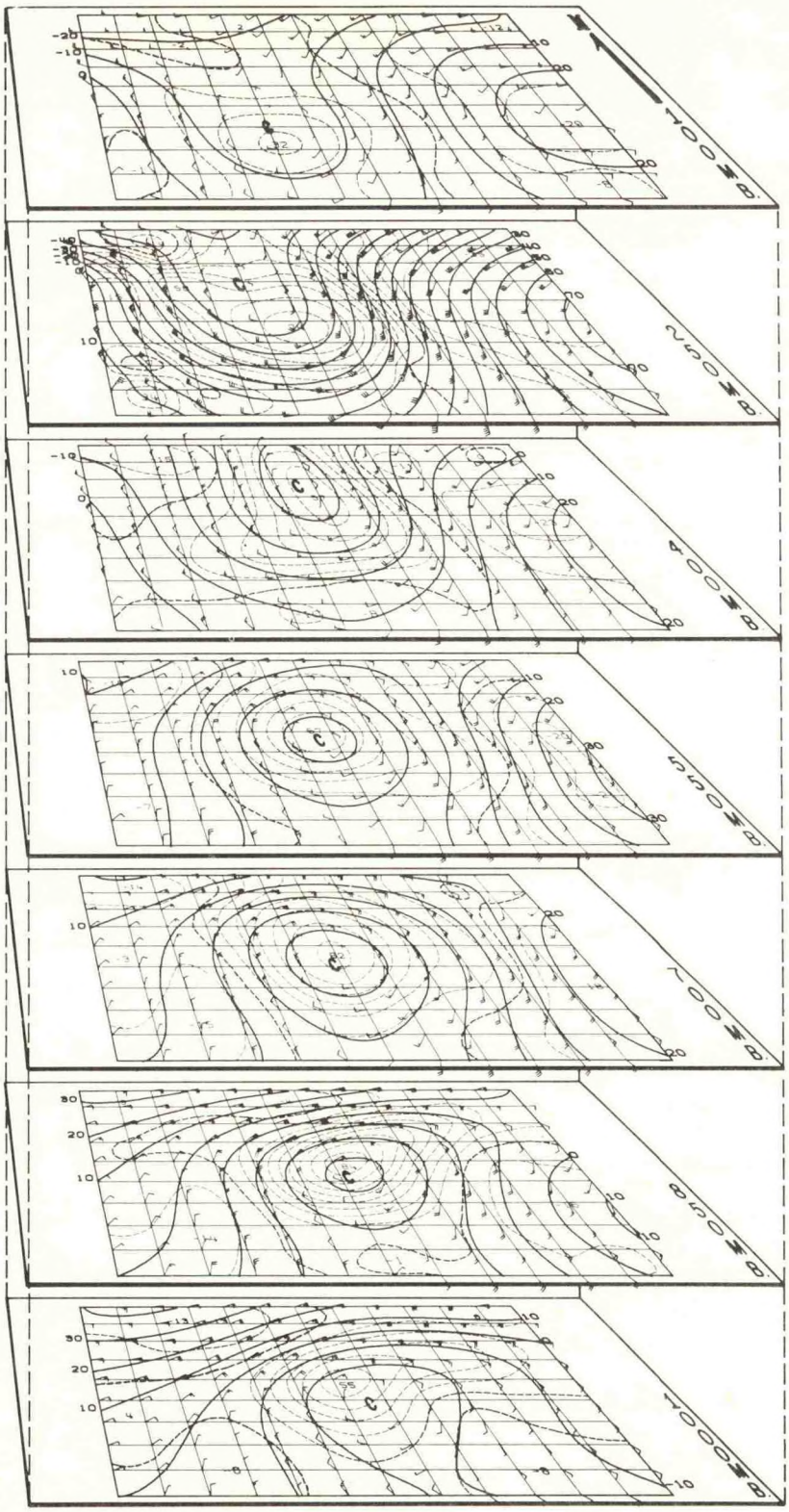

to the fact that here the stream-function component of the wind is calculated by a centered difference and a one-sided difference which leads on occasion to non-representative winds. This effect was even more marked at the corners where only one-sided differences could be used. Grid corner winds have been omitted for this reason.

2. Sequence #2

Sequence #2 presents the deepening easterly wave which preceded Hurricane Alma. The series begins on 00Z of August 25, 1962, and continues through 12Z August 27, 1962. For 00Z and 12Z on the 26th there are two presentations: the original grid orientation and a second in which the grid is shifted 2 grid rows to the north. These have been treated as independent samples because of the scarcity of cases and are presented also to show the very small effects due to varying boundaries.

The sequence begins with a large well-defined easterly wave (which has an almost closed cyclonic center) at 1000 mb (figure 7a and 7b) which tilts eastward and maintains its identity up to the 400-mb level. Above 400 mb the circulation does not appear to be intimately related to conditions below. At 250 mb the flow is dominated by two anticyclones, one over the Gulf of Mexico and the other centered over the eastern Caribbean. The col between these highs is almost centered over the grid.

Aside from some motion to the west, there appears to be little significant change over the next 12 hours. Heights are a little higher in the disturbance at 1000 mb (figure 8a). The cyclonic vorticity center is in evidence up through the 400-mb level, as was the case 12 hours earlier (figure 8b). Circulation on either side of the 250-mb col

appears to have weakened and there is a suggestion of cyclonic circulation becoming weakly evident both here and in the easterlies at 100 mb.

By 00Z of the 26th a closed cyclonic circulation is apparent at 1000 mb over north-central Cuba (even on this space-smoothed pattern) (figure 9a). The vorticity center maintains its identity up through the 250-mb level but shows little effect if any, on the 100-mb pattern. The penetration upwards of the cyclonic system is not necessarily the type of transformation one expects of a perturbation which is to become a hurricane within 60 hours.

The next maps, figure 10a and b,[1] show the low-level center located over the southern Florida peninsula at 12Z, August 26. Oddly enough, the cyclonic circulation has weakened slightly at just about all levels except the surface. This is apparent not only in the closed isopleths but also in the values of the vorticity shown in figure 10b. The weakening aloft, i.e., at 250 and, perhaps, 400 mb is in conformance with our idea that warming aloft will accompany the release of latent heat and will weaken the cyclonic circulation with height. Certainly, at 250 mb the pattern is weak with two new small highs appearing. The very weak circulation at these upper levels does conform to a hypothesis by Gray (1967) which maintains that small shears and weak winds aloft are essential for the significant warming of the upper atmosphere by the release of latent heat and are thus predisposed to favor hurricane genesis.

[1]Tabulations and runs were prepared for August 26, 00 and 12Z using two different lower latitudes for the grid: 15°N and 18.9°N (two grid rows difference). New boundary conditions as well as new data are involved in this change and for certain purposes the duplicate data are considered independent. In the interests of brevity only the 15°N base 00Z analyses and the 18.9°N base 12Z analyses are presented for August 26, 1962.

Figure 7a. August 25, 1962, 00Z. Weather, vertical motion, contour and divergence fields. The bottom slab depicts the cloud cover and hydrometeors from an independent analysis of all available synoptic data. Above are slabs from 1000 to 250 mb that show: the diagnostic vertical motion arrows where the length (in prespective) of the arrow is proportional to the speed indicated by tick marks where each tick now equals 10 ($x10^{-6}$) cbs/sec; the height contours, solid lines, are labelled in tens of geopotential meters (at the east and west limits of the grid only); diagnostic divergences are dashed with the zero line heavier and the centers labelled in units of 2×10^{-7} sec^{-1}. A scale for converting cbs/sec to cm/sec is presented to the right of each slab - it might be noted that 100 of the units used in this study (10^{-6} cbs/sec) are approximately equal to 1 cm/sec.

An easterly wave is located over eastern Cuba with bad weather east of the wave axis over Hispaniola. Vertical motions are generally upward in lower levels where this weather is occurring. Another area of poor weather over the Gulf of Mexico is associated with very weak upward velocities.

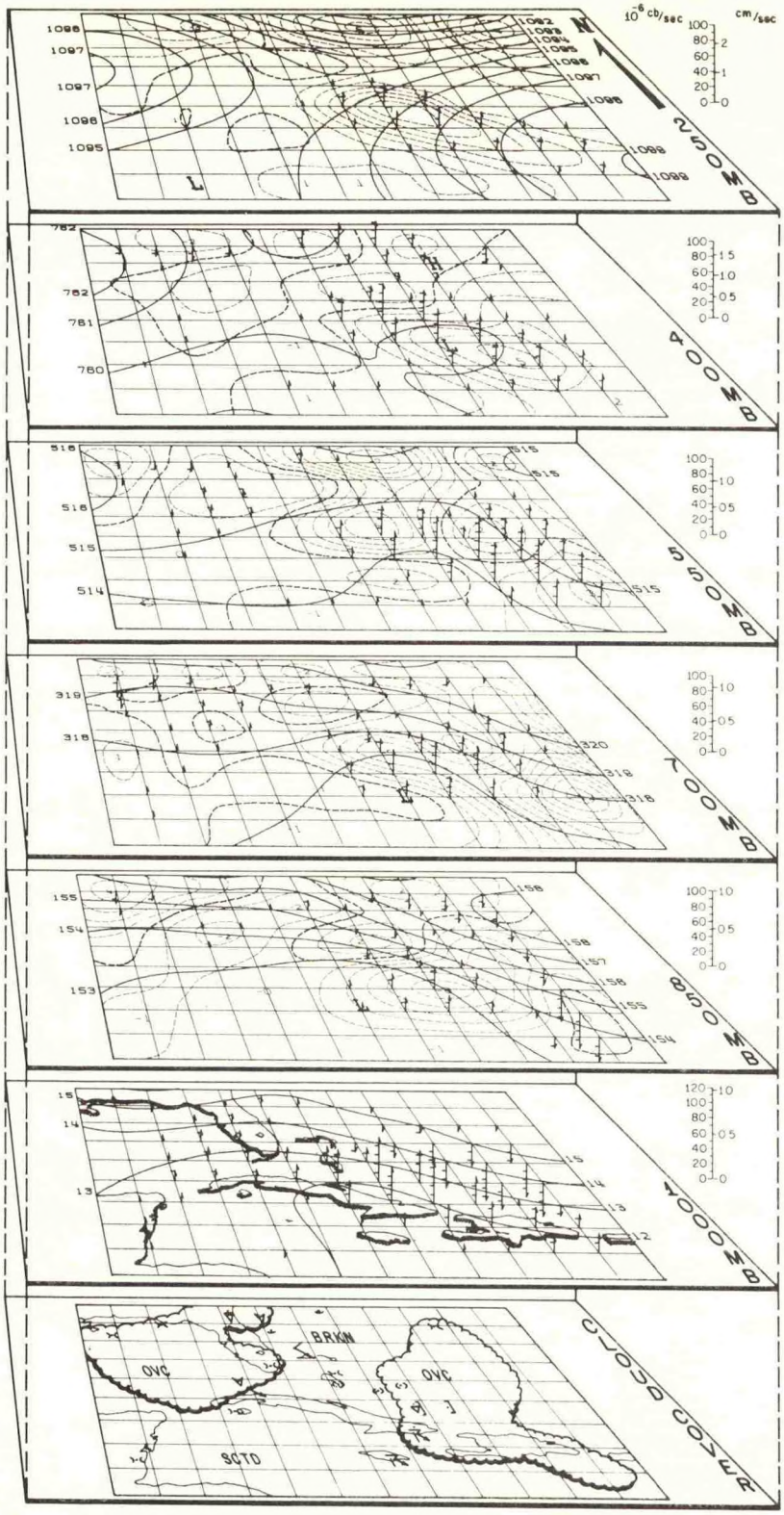
10^{-6} cb/sec
cm/sec
250 MB
400 MB
550 MB
700 MB
850 MB
1000 MB
CLOUD COVER
BRKN
OVC
SCTD

Figure 7b. August 25, 1962, 00Z. Streamfunction, vorticity and total wind fields. Perspective drawing for levels from 1000 to 100 mb presenting: the streamfunction (solid lines) which have been zeroed in the lower left corner of the grid and labelled in units of m^2/sec (scaled by 5×10^{-6}); the relative vorticity (dashed lines) with the zero line heavier and centers labelled in units of 10^{-6} sec^{-1}; the total wind speed (in knots) and direction shown in conventional meteorological notation, wind speeds have been converted to knots in order to make evident the smaller variations in speed.

The wave over eastern Cuba is slightly stronger at 850 mb (note vorticity values) than at 700 or 1000 mb, but the lower levels are of comparable strength all the way up through 400 mb where a very weak closed low is present. In this case coupling up through the 550-mb level seems quite good with the 400-mb level becoming one of transition.

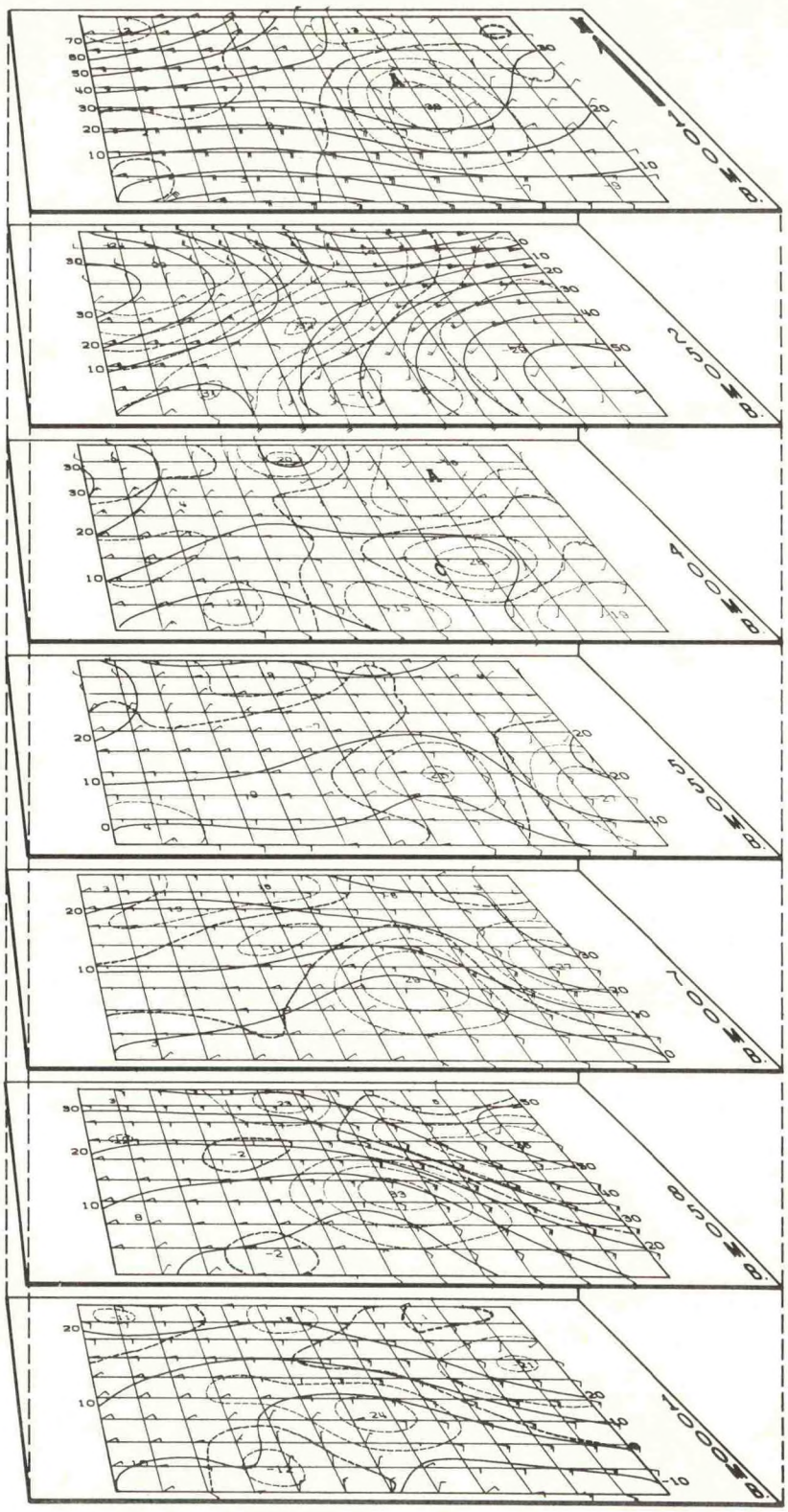

Figure 8a. August 25, 1962, 12Z. Weather, vertical motion, contour and divergence fields (see legend figure 7a). The axis of the wave has moved slightly to the west and the centers of cyclonic vorticity at low levels have shifted a bit west with the axis. The center of rising air at 850 and 700 mbs has not shifted westward and the axis of bad weather has not moved westward.

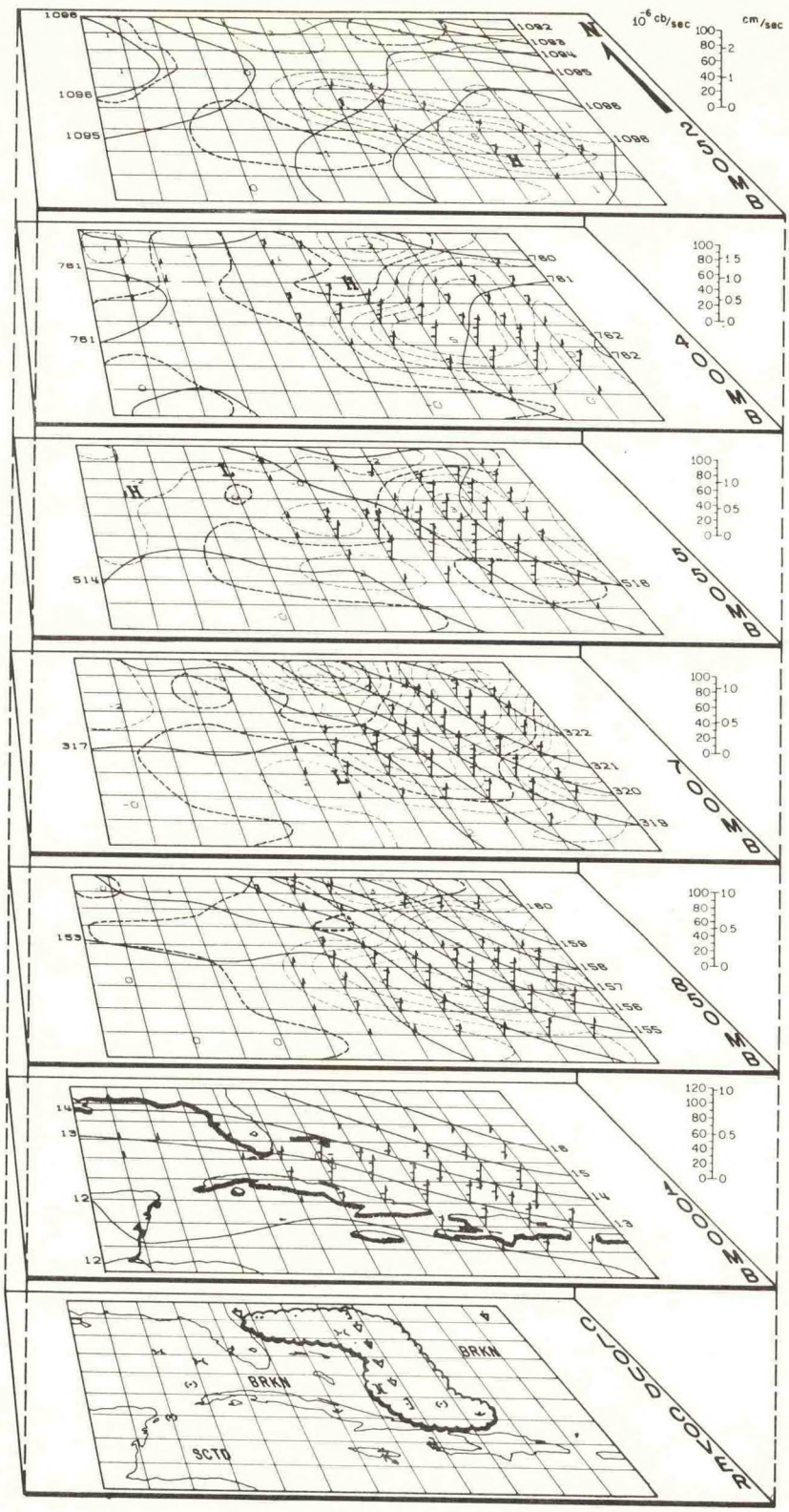
10^{-6} cb/sec
cm/sec
250 MB
400 MB
550 MB
700 MB
850 MB
1000 MB
CLOUD COVER
BRKN
BRKN
SCTD

Figure 8b. August 25, 1962, 12Z. Streamfunction, vorticity and total wind fields (see legend figure 7b). The cyclonic vorticity centers at the 1000 and 400-mb levels have weakened slightly but the intermediate levels have changed very little.

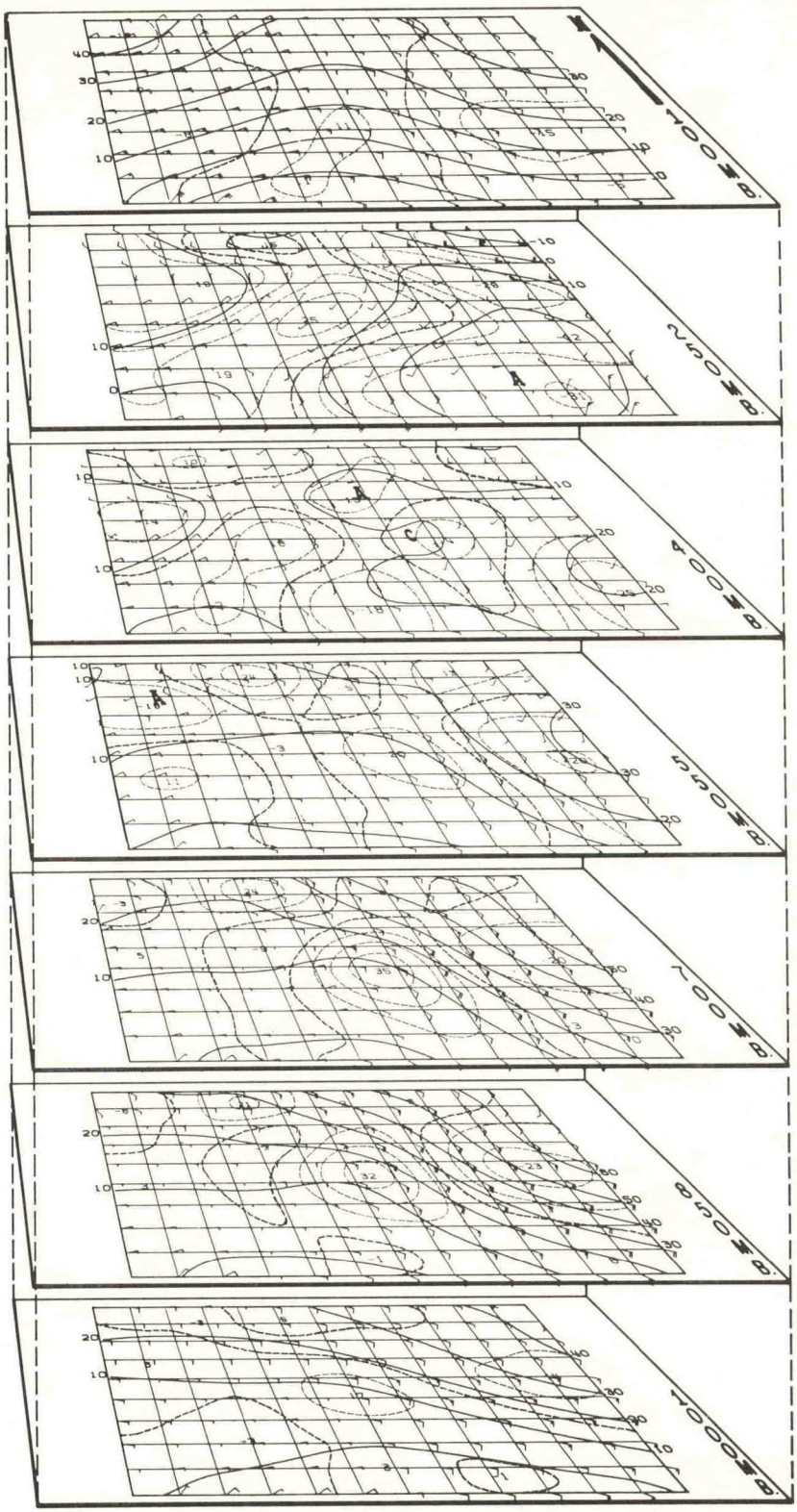

Figure 9a. August 26, 1962, 00Z. Weather, vertical motion, contour and divergence fields (see legend figure 7a). The intensity of the low-level updraft increases as a closed low develops over north central Cuba. This low can now be weakly identified up to the 250-mb level. Almost all of the significant vertical velocities at the lower levels are updrafts associated with the strong field of convergence at 850 mb.

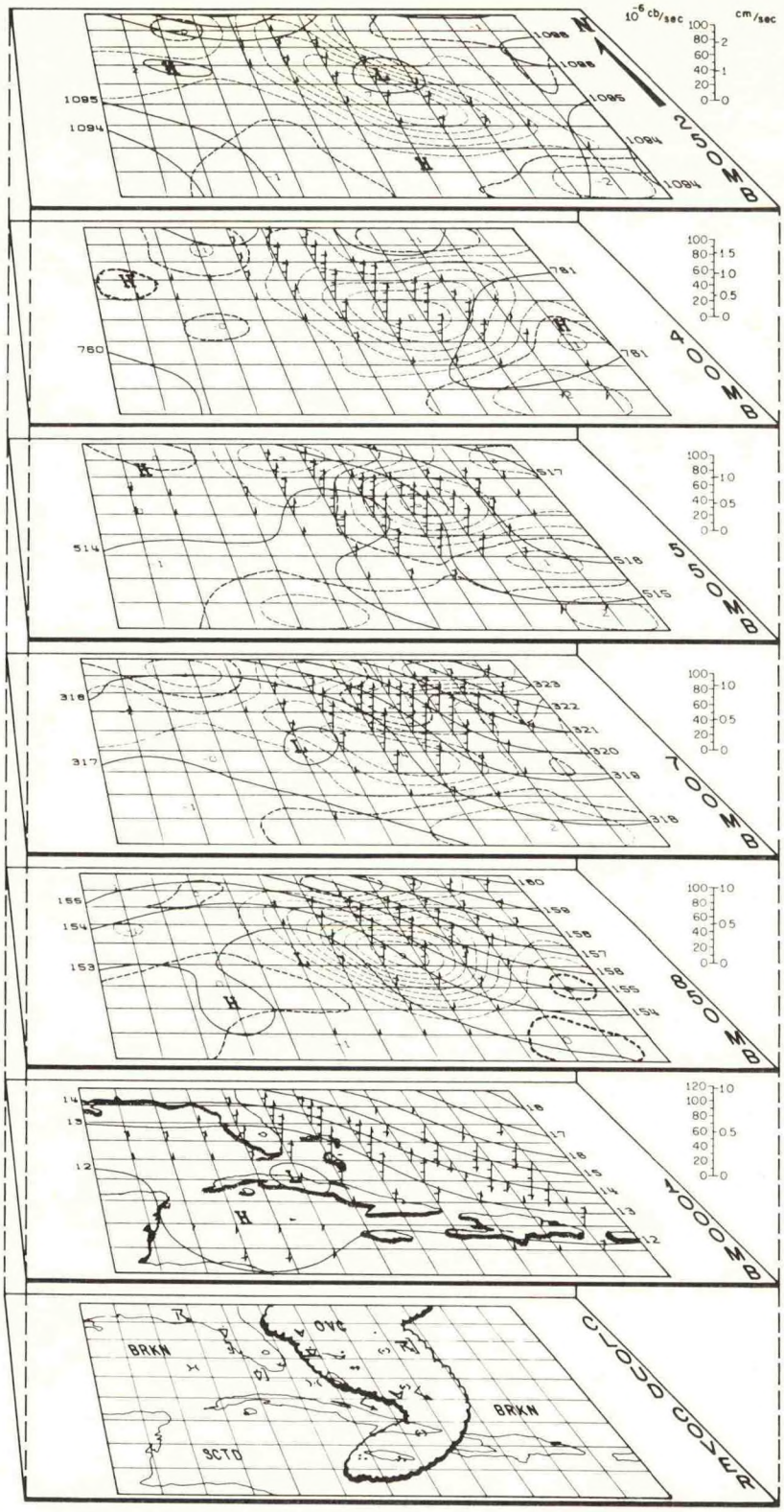
10^{-6} cb/sec
cm/sec
250 MB
400 MB
500 MB
700 MB
850 MB
1000 MB
CLOUD COVER
BRKN
SCTD
BRKN

Figure 9b. August 26, 1962, 00Z. Streamfunction, vorticity and total wind fields (see legend figure 7b). The vertical alignment of the cyclonic vorticity fields from 1000 through 250 mb is now complete. The lower level increase of cyclonic vorticity appears to date from about this time.

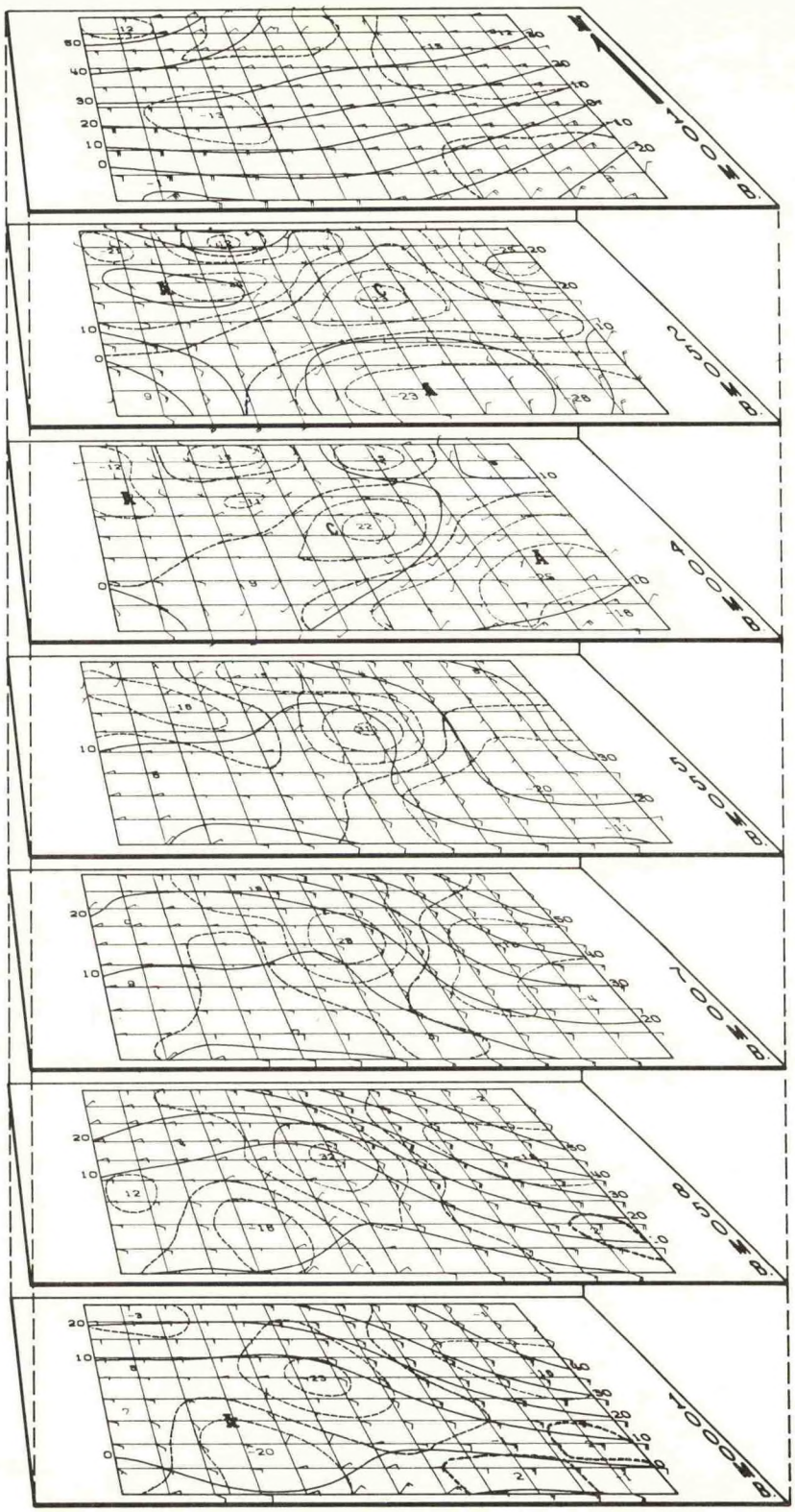

Figure 10a. August 26, 1962, 12Z. Weather, vertical motion, contour and divergence fields (see legend figure 7a). At 1000 mb the vortex intensifies and in association with the strong convergence field at the 850-mb level produces an extensive area of overcast, squally weather. The strong fields of upper level divergence (see figure 9a) are continued as cyclonic circulations at these levels give way to those of increasingly anticyclonic character.

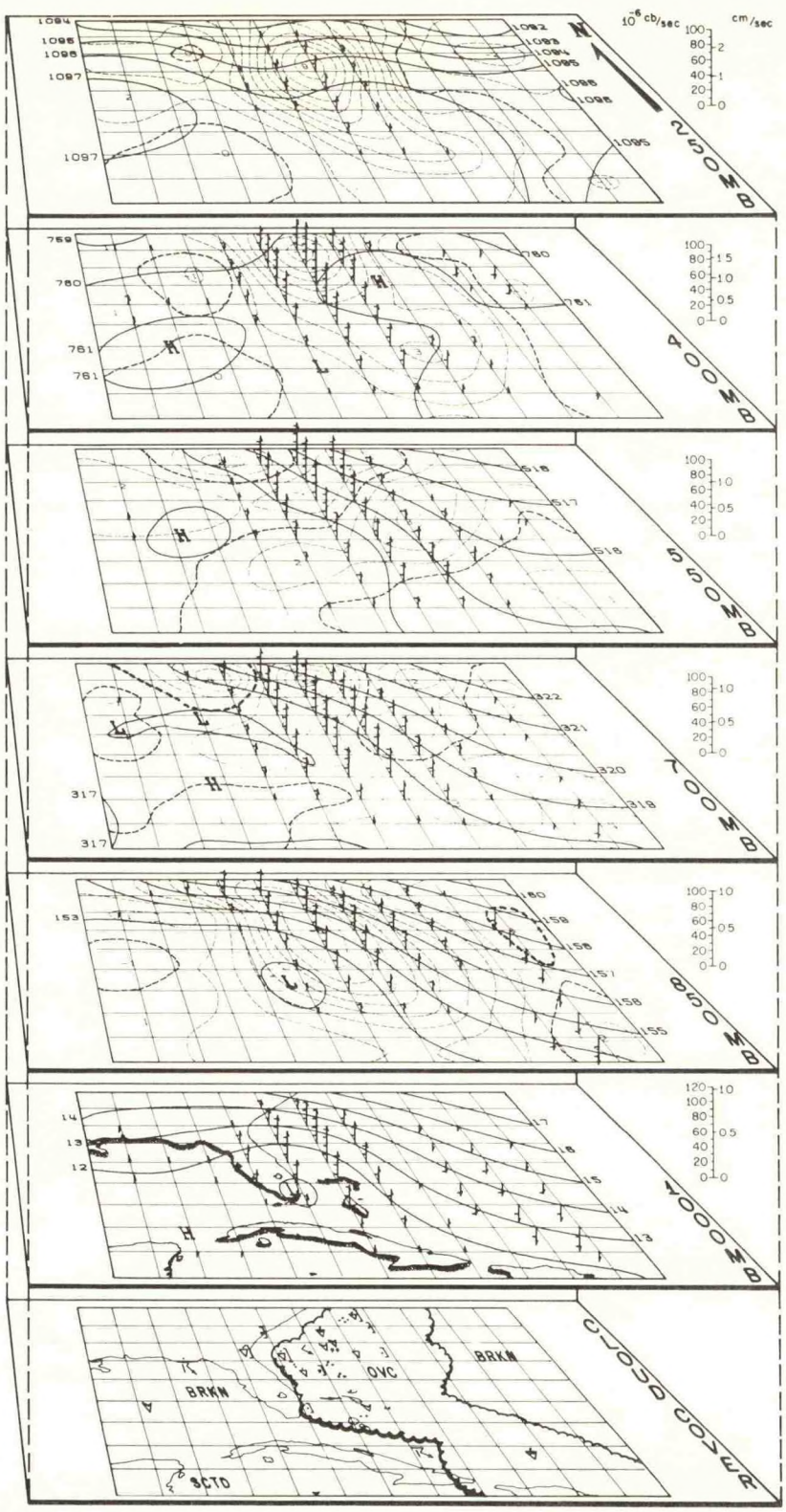
10^{6} cb/sec
cm/sec
N
2000 MB
4000 MB
5500 MB
7000 MB
8500 MB
10000 MB
CLOUD COVER
BRKN
OVC
BRKN
SCTD

Figure 10b. August 26, 1962, 12Z. Streamfunction, vorticity and total wind fields (see legend figure 7b). Upper level divergence has helped in the generation of anticyclonic circulations (at 250 and 400 mb), northeast of the low level cyclonic centers. The low level vorticity is now stronger than at any time heretofore.

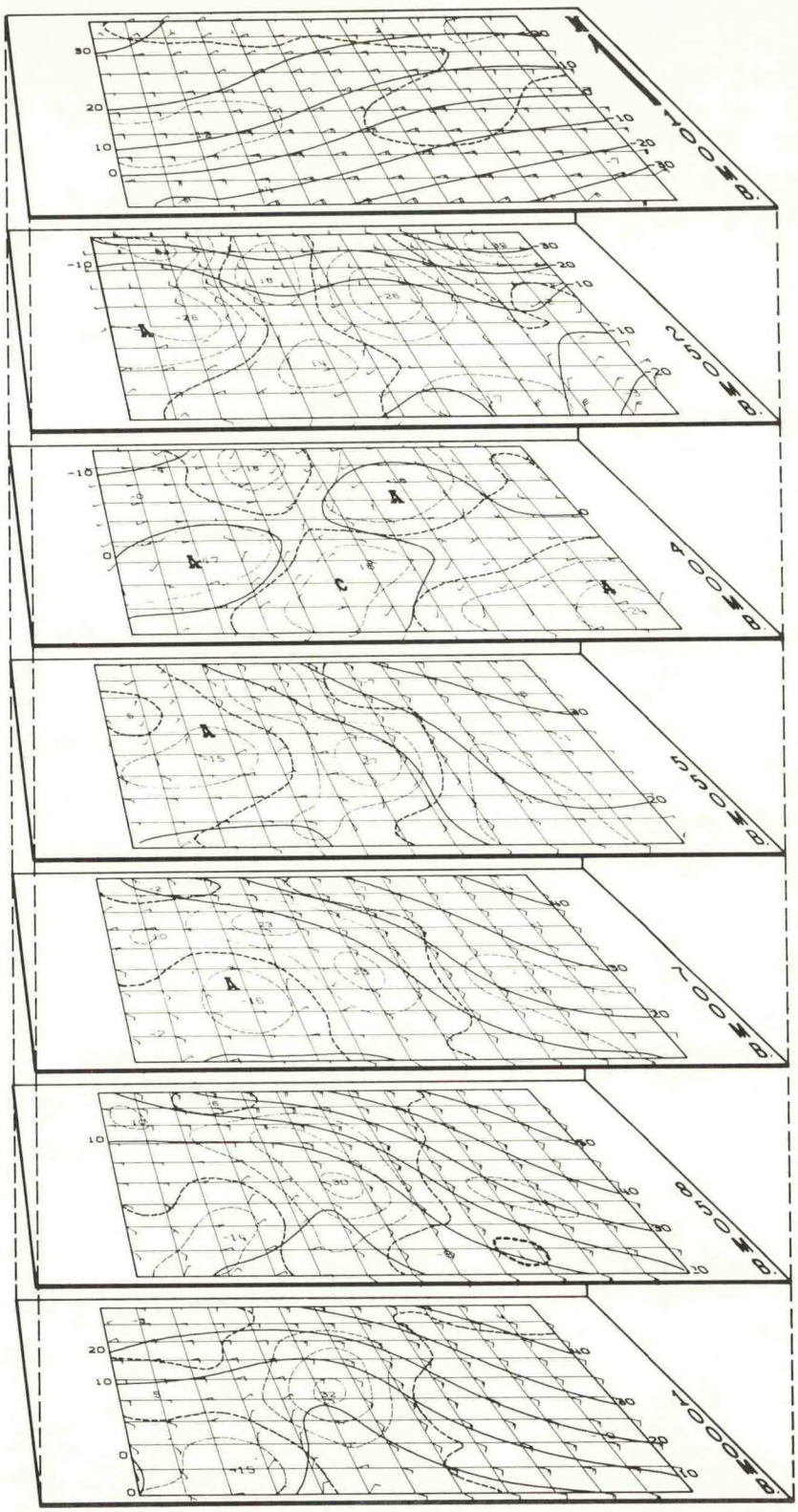

Figure 11a. August 27, 1962, 00Z. Weather, vertical motion, contour and divergence fields (see legend figure 7a). Low level cyclonic vorticity increases as vertical updrafts increase and convergence (850 mb) reaches 10^{-5} sec^{-1}. Upper level divergence more nearly overlies the main center of lower level convergence.

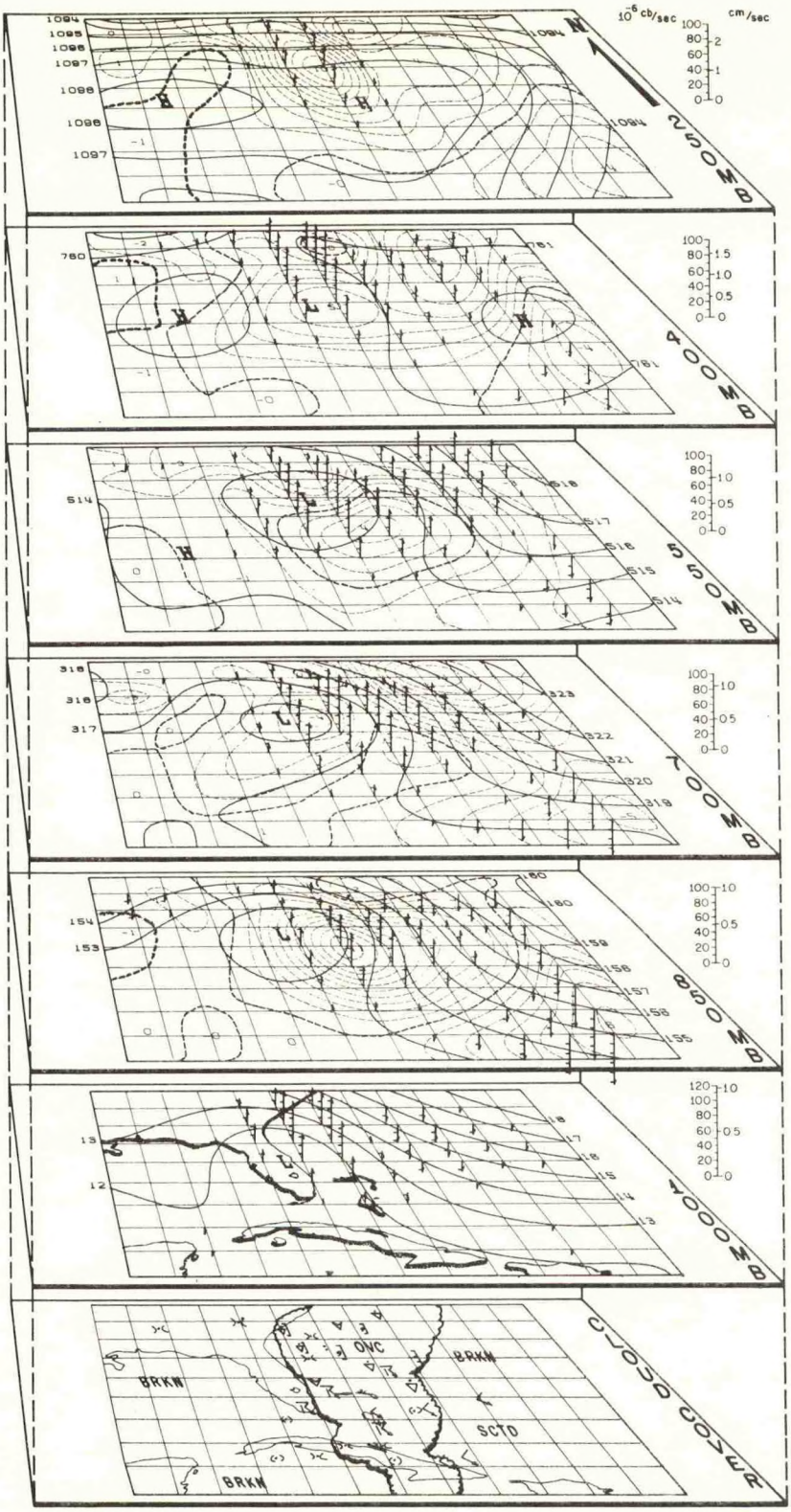
10^{-6} cb/sec
cm/sec
250 MB
400 MB
500 MB
700 MB
850 MB
1000 MB
CLOUD COVER
ONC
BRKN
BRKN
SCTD

Figure 11b. August 27, 1962, 00Z. Streamfunction, vorticity and total wind fields (see legend figure 7b). At lower levels the vortex increases with strength and, for the moment at least, the vortex reappears at the 400-mb level. At 250 mb the anticyclone continues to develop despite the vortex below and to the west.

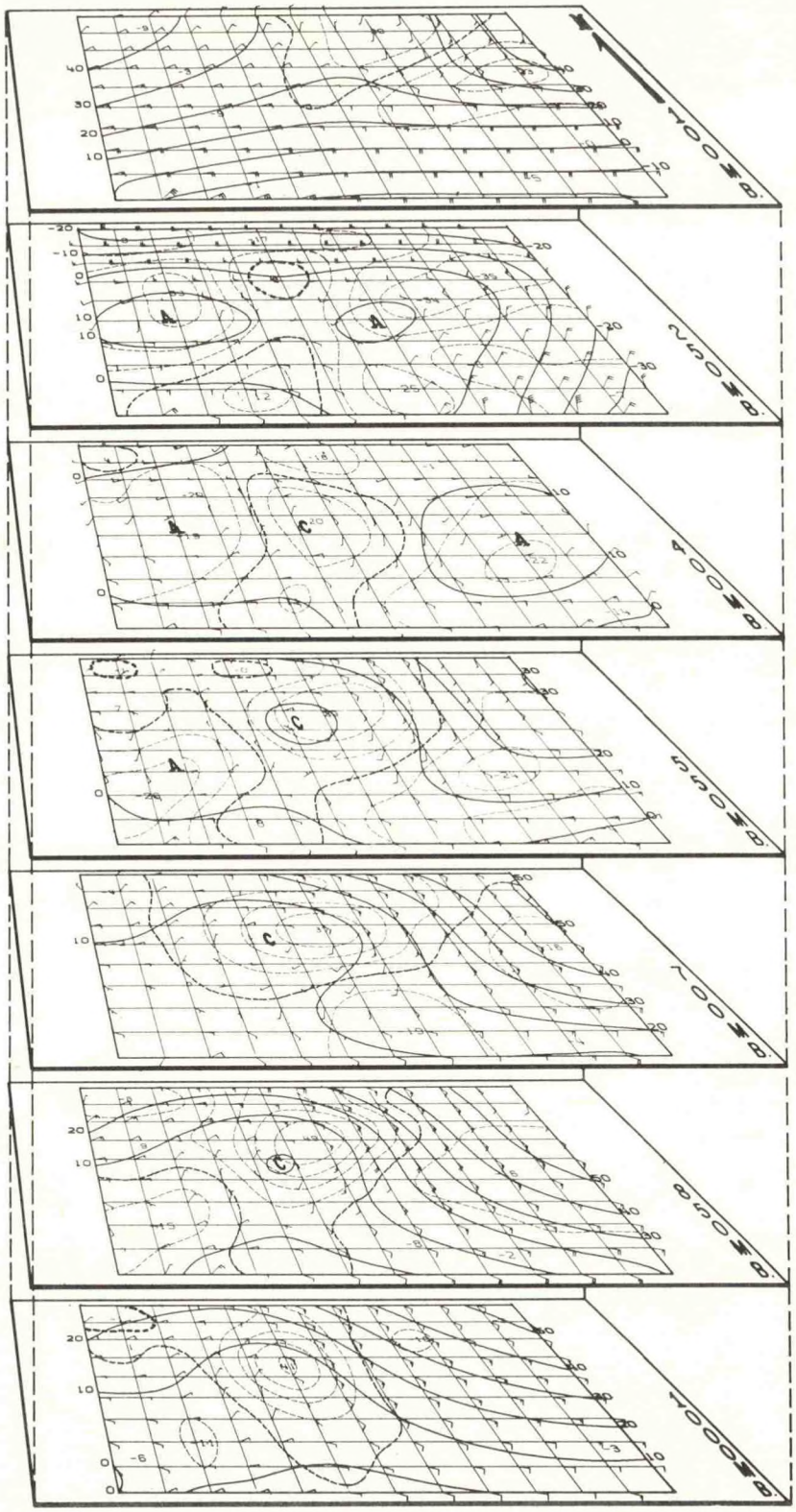

Figure 12a. August 27, 1962, 12Z. Weather, vertical motion, contour and divergence fields (see legend figure 7a). The intense low-level cyclone is now situated off Jacksonville attended by a strong field of convergence and upper-level divergence. Upward vertical velocities are stronger than ever and approach the cm/sec class. Widespread overcast skies, showers and squalls accompany the low.

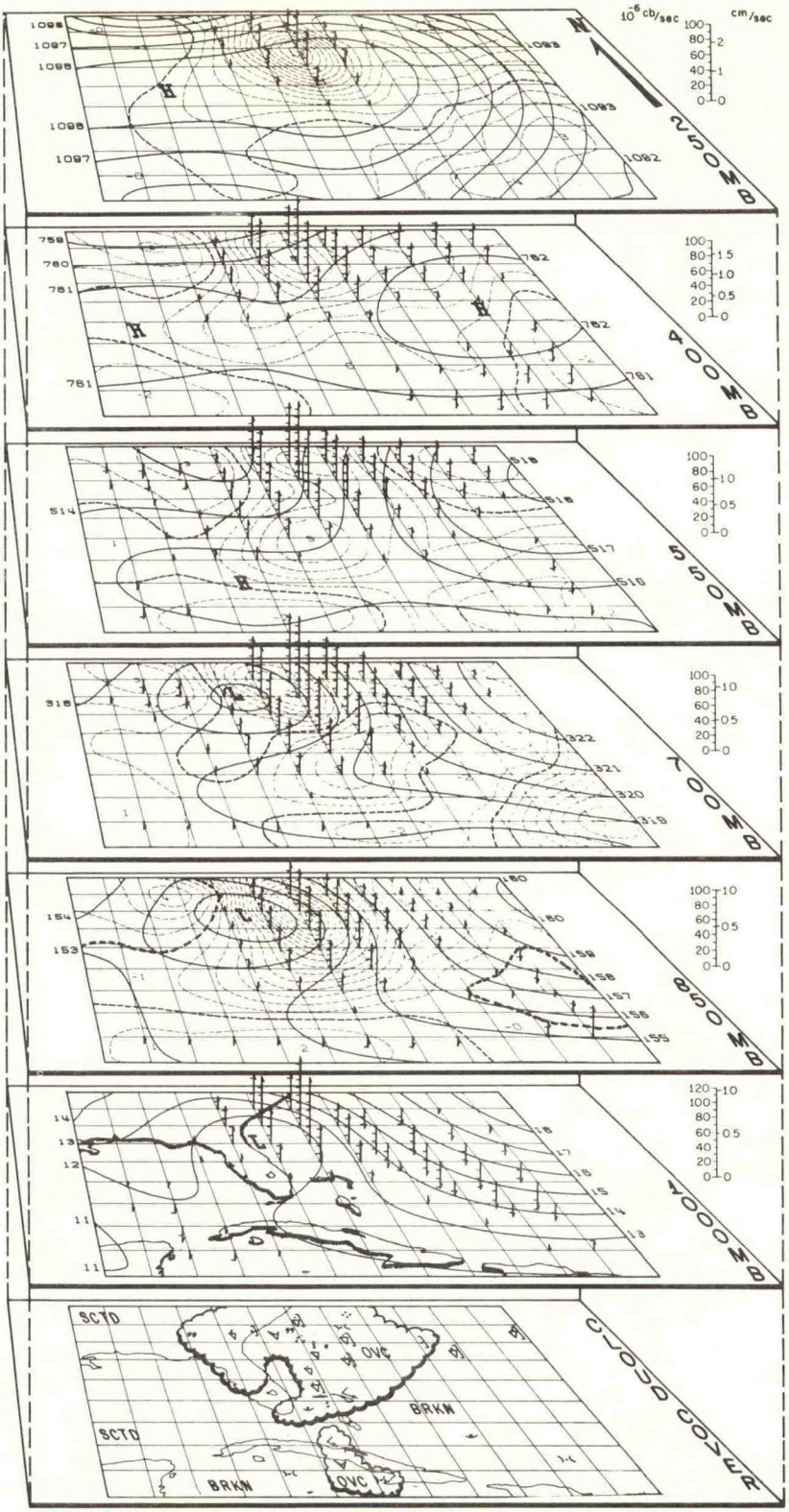
10^{-6} cb/sec
cm/sec
250 MB
400 MB
550 MB
700 MB
850 MB
1000 MB
CLOUD COVER
SCTD
OVC
BRKN
SCTD
BRKN
OVC

Figure 12b. August 27, 1962, 12Z. Streamfunction, vorticity and total wind fields (see legend figure 7b). Cyclonic vorticity continues to increase at the three lowest levels. At the 550 and 400-mb levels it has decreased slightly and the cyclonic circulation center has either disappeared or been displaced off of the northwestern grid area. At the 250-mb level a ridge overlies the surface low.

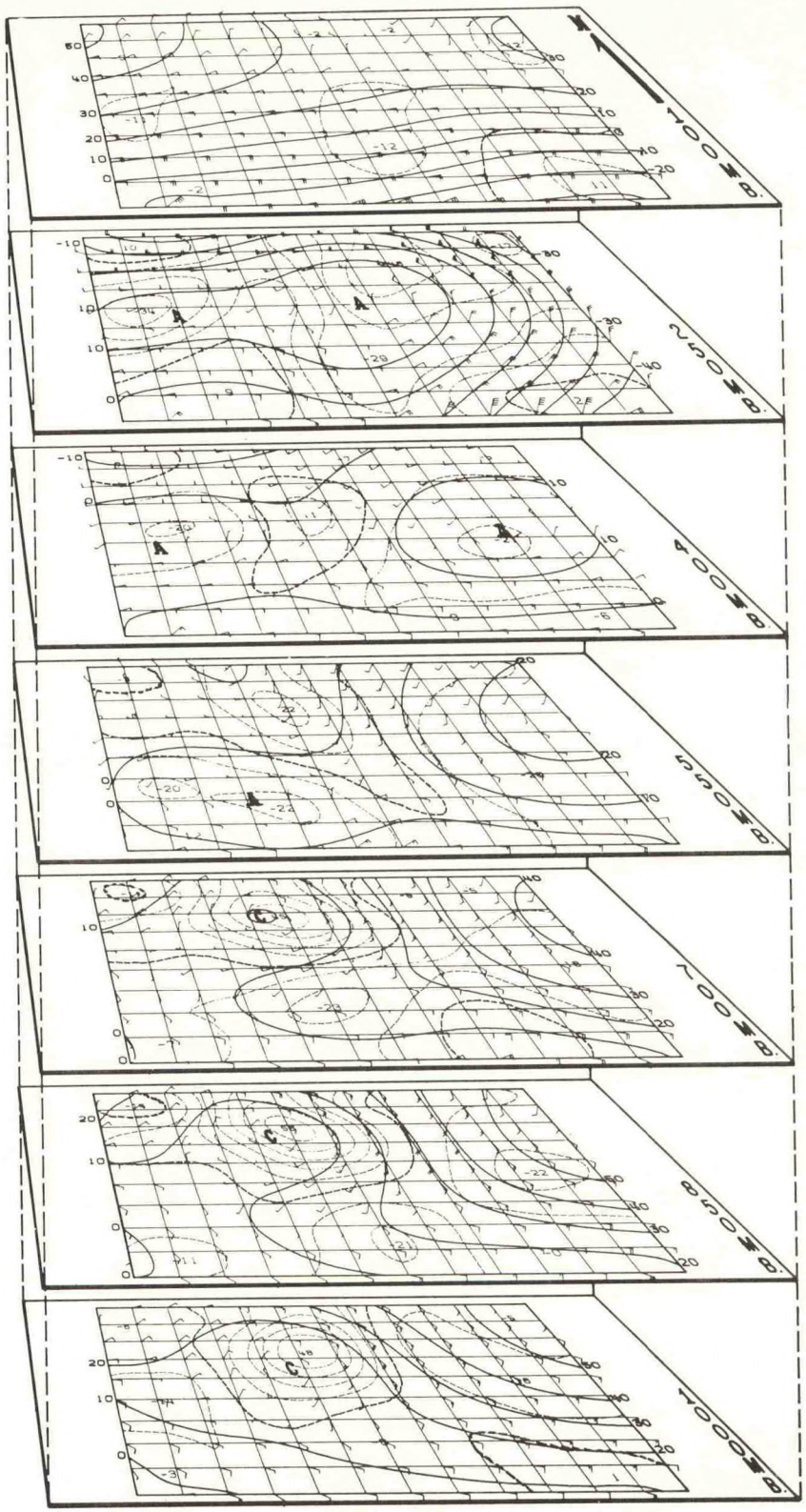

On the 27th (figures 11, 12, a and b) we see that the cyclonic circulation is increasing both in area and intensity in the lower levels (particularly at 850 and 700 mb) as warm anticyclonic conditions dominate the upper troposphere near 250 mb. Tropical storm intensity was attained at 12Z, August 27.

In all, this is a very interesting series with some significant changes occurring during the chosen period.

3. Sequence #3

The third sequence, August 3-5, 1963, shares certain similarities with the second sequence but the wave fails to deepen significantly. At 00Z, August 3, the space smoothing has left a very poorly defined structure at 1000 mb (figure 13a). However, it appears quite well-defined at 850 mb and tilts eastward up through the 550-mb level above which only a trace remains. The upper troposphere is dominated by a large low center located in the area west of Jamaica.

At 12Z of the 3rd, the low-level perturbation appears better marked (figure 14a and b) and the wave can be traced vertically to at least 400 mb. The vorticity field immediately associated with the wave is very similar to that which characterized the predecessor to Alma at the 1000 and 850-mb levels. In the upper troposphere, the low west of Jamaica has moved west-northwestward and a fairly strong field of divergence (at 250 mb) overlays the frictionally driven low-level field of vertical motion.

On 00Z of the 4th (figure 15a and b) the low-level structure again appears quite adequately defined and again the vorticity fields compare

in magnitude with the preceding sequence. The low-level cyclonic vorticity field does not stretch well upstream from the wave axis as had the previous case,and this may have tended to minimize cumulus penetration since the air would not have been greatly moistened by abortive, upstream cumulus towers. The upper-troposphere low has continued to move slowly westward and a well-defined high center dominates the eastern portion of the grid at 250 mb. This in turn means that the perturbation is situated under the southwestern section of an upper-level high - a location which Colon and Nightingale (1963) found favorable for further developments. Despite this "favorable" location, the upper-level divergence was quite restricted in area and small in magnitude and from this time on the disturbance seems to grow slowly weaker.

By 12Z on August 4, low-level frictional velocities are weakly upward over only a limited area. The wave itself is less intense at the 850-mb level and the upper troposphere is dominated by the 250-mb high (figure 16a and b). Upper-level divergence is quite small and it is apparent that the low-level disturbance is not growing vertically in the fashion noted in sequence #2.

Figures 17, 18, a and b (August 5) show the completion of this series. The low-level wave is gradually weakening. Low-level upward velocities grow smaller. Aloft the strong high continues to retrograde and dominates both the 250 and 400-mb levels. The high-level divergence patterns accompanying the anticyclone remain fairly weak and restricted in area (compared to those of figures 11a and 12a),while the effects of the anticyclonic circulation seem to penetrate to lower and lower levels.

Figure 13a. August 3, 1963, 00Z. Weather, vertical motion, contour and divergence fields (see legend figure 7a). The easterly wave appears best-marked at the 700-mb level, weakening at higher levels. It has almost disappeared at 400 mb where the appearance of a vigorous cyclone over the southwestern grid area introduces the main upper-troposphere system. Vertical velocities are very weak although consistent with the weather east of the wave axis.

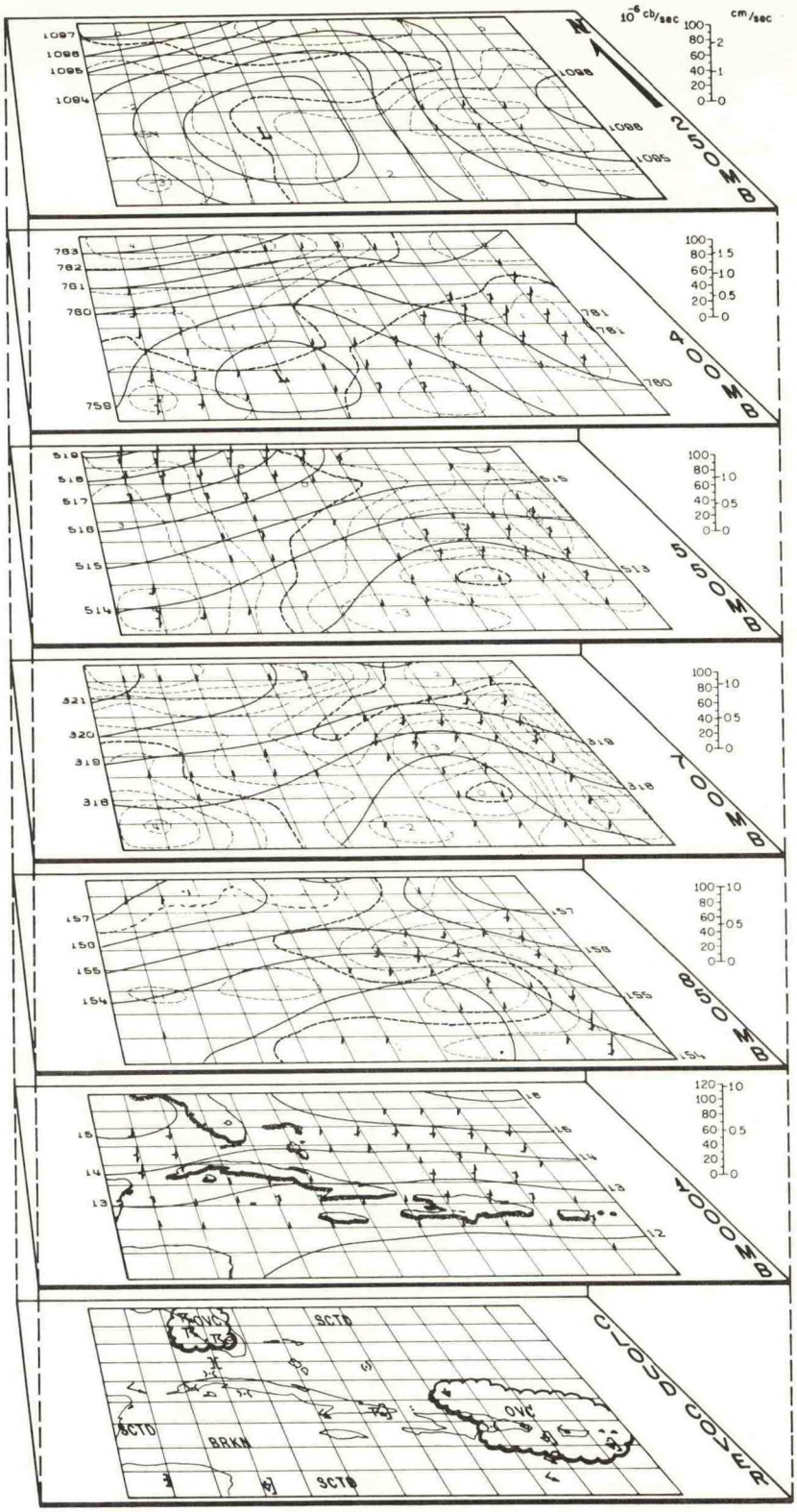
10^{-6} cb/sec
cm/sec
N
250 MB
400 MB
500 MB
700 MB
850 MB
1000 MB
CLOUD COVER
SCTD
OVC
BRKN

Figure 13b. August 3, 1963, 00Z. Streamfunction, vorticity and total wind fields (see legend figure 7b). Cyclonic vorticities at 850 and 700 mb are comparable to those in the August,1962, sequence (see figure 7b) and there is weak divergence indicated aloft over the wave.

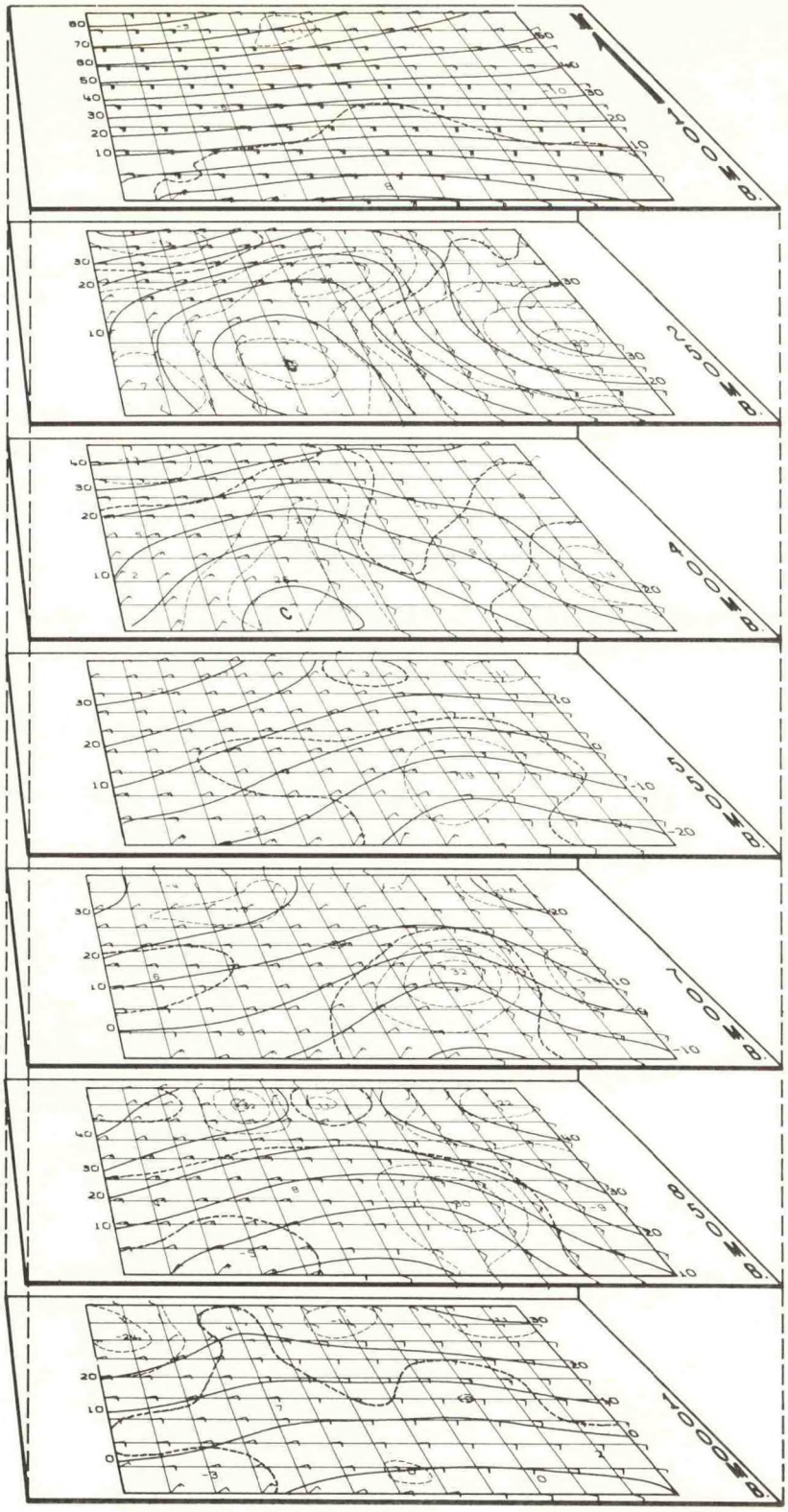

Figure 14a. August 3, 1963, 12Z. Weather, vertical motion, contour and divergence fields (see legend figure 7a). The wave progresses to the west; low-level updrafts increase as does the area of attendant bad weather. The upper level divergence field still appears favorably situated to aid in development.

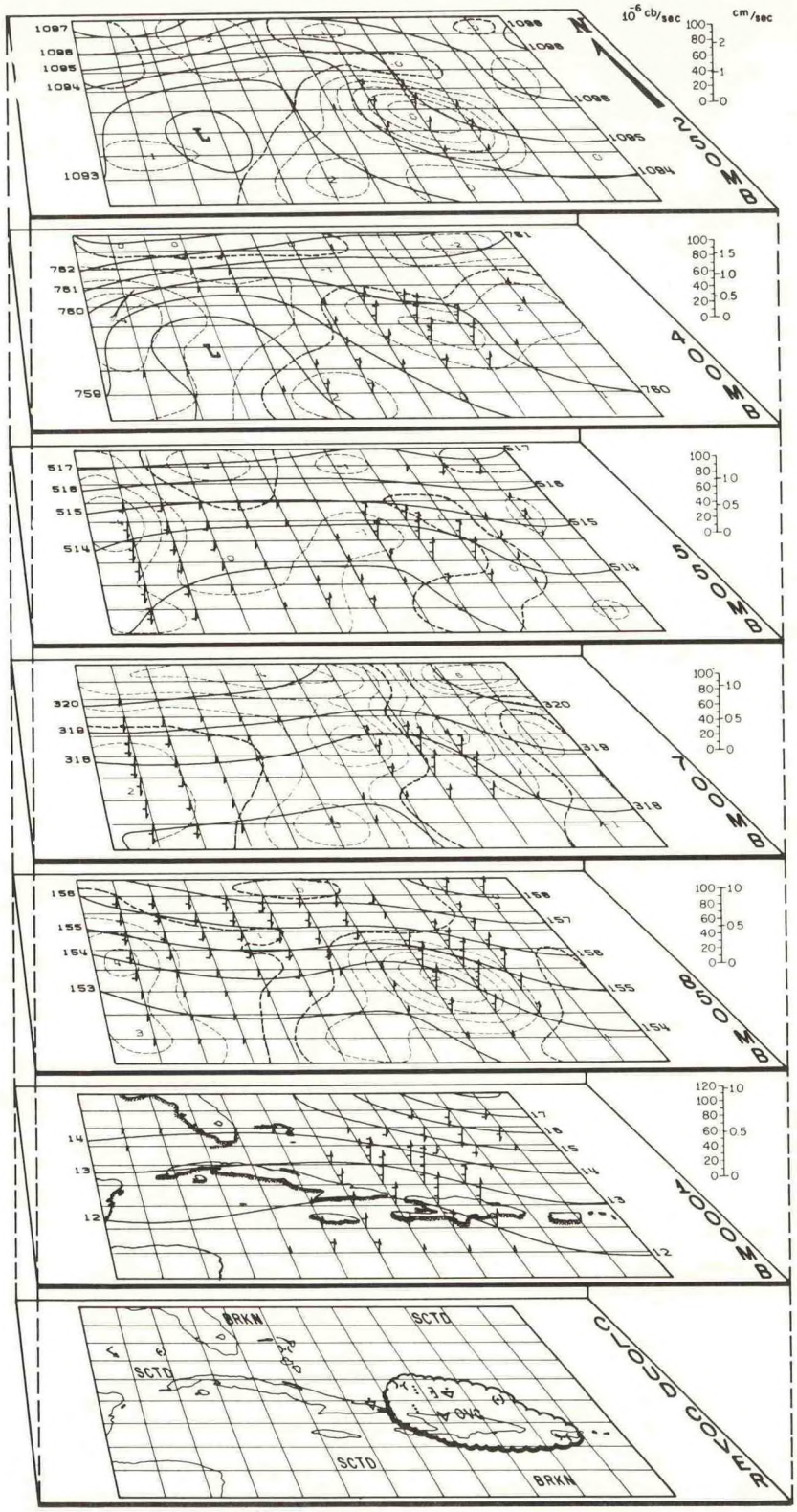
10^{-6} cb/sec
cm/sec
250 MB
400 MB
550 MB
700 MB
850 MB
1000 MB
CLOUD COVER
BRKN
SCTD
SCTD
SCTD
BRKN

Figure 14b. August 3, 1963, 12Z. Streamfunction, vorticity, and total wind fields (see legend figure 7b). The low-level vorticity center is well marked up through 550 mb reaching a maximum between 850 and 700 mb. Above 550 mb it disappears rapidly into the upper tropospheric trough-ridge system (a weak cyclonic vorticity center can still be seen at 400 mb). Retrogression of the upper-tropospheric system is also evident.

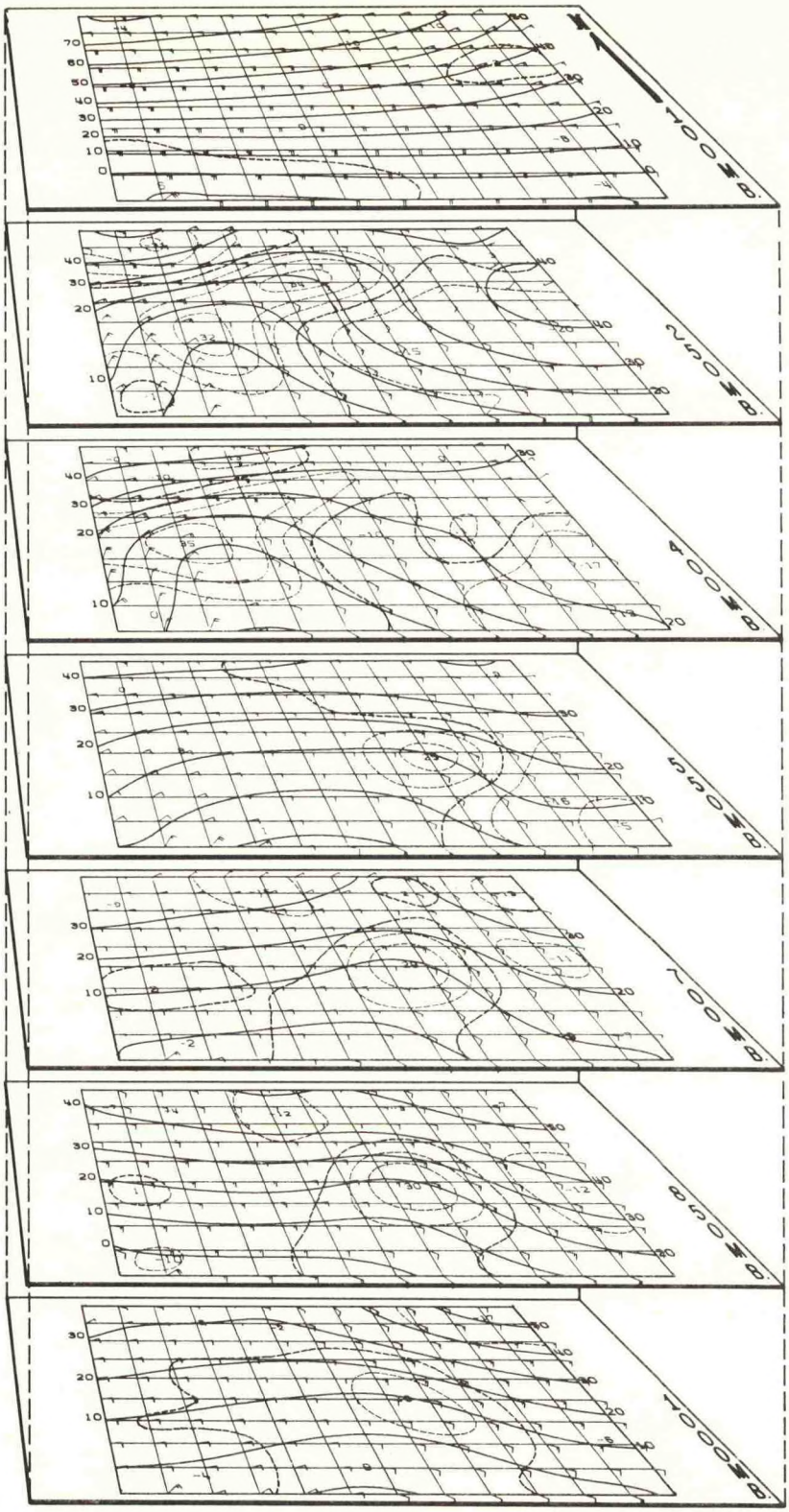

Figure 15a. August 4, 1963, 00Z. Weather, vertical motion, contour and divergence fields (see legend figure 7a). The easterly wave continues to move westward but at a slower rate than that at which the upper troposphere system is retrograding. The wave appears best marked at the 850-mb level and is accompanied by a fair area of convergence. Aloft the divergence seems to be weakening.

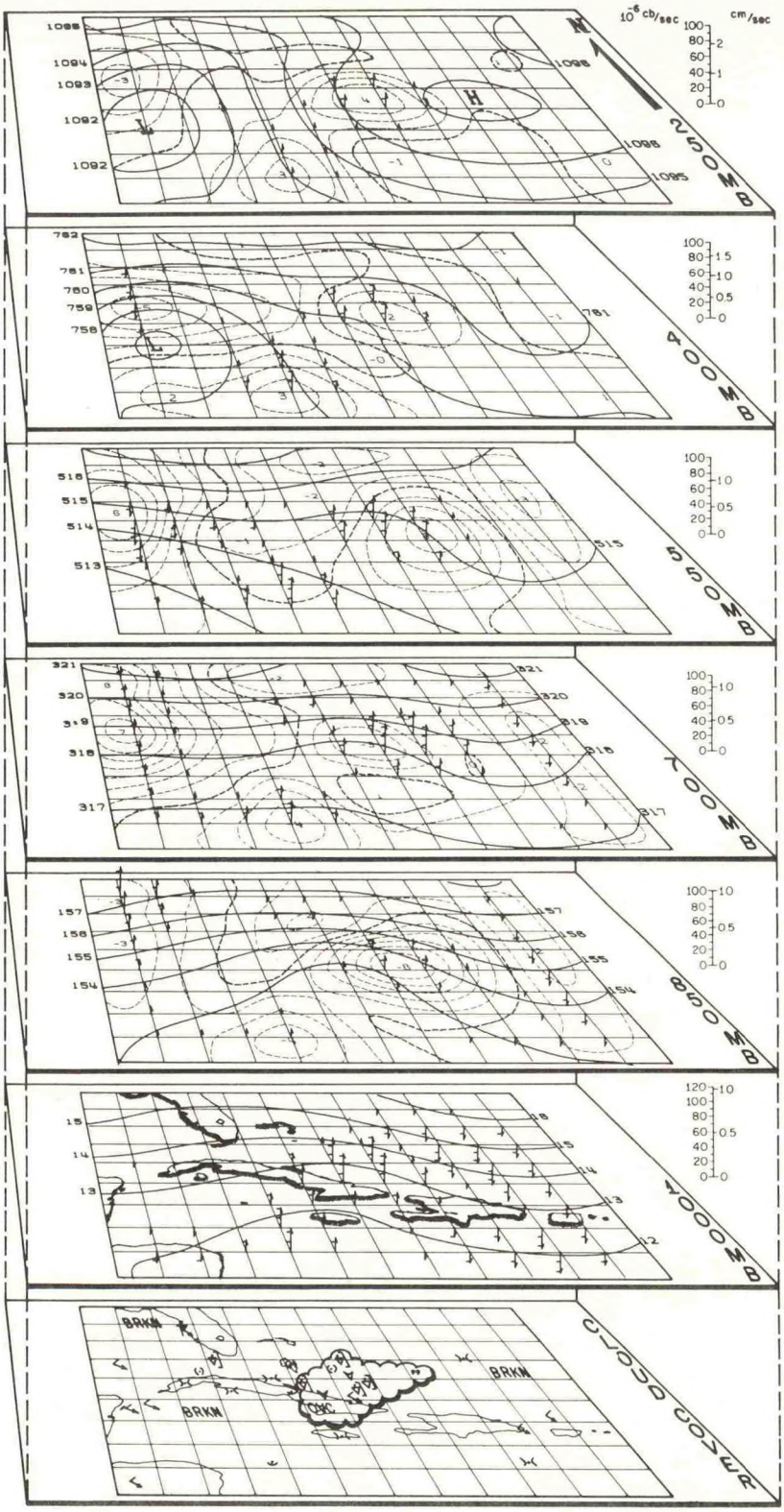
10^{-6} cb/sec
cm/sec
250 MB
400 MB
500 MB
700 MB
850 MB
1000 MB
CLOUD COVER
BRKN
OVC

Figure 15b. August 4, 1963, 00Z. Streamfunction, vorticity and total wind fields (see legend figure 7b). Traces of the easterly wave can be detected up through the 400-mb level. Immediately above, at 250 mb, a strong anticyclonic circulation dominates the scene.

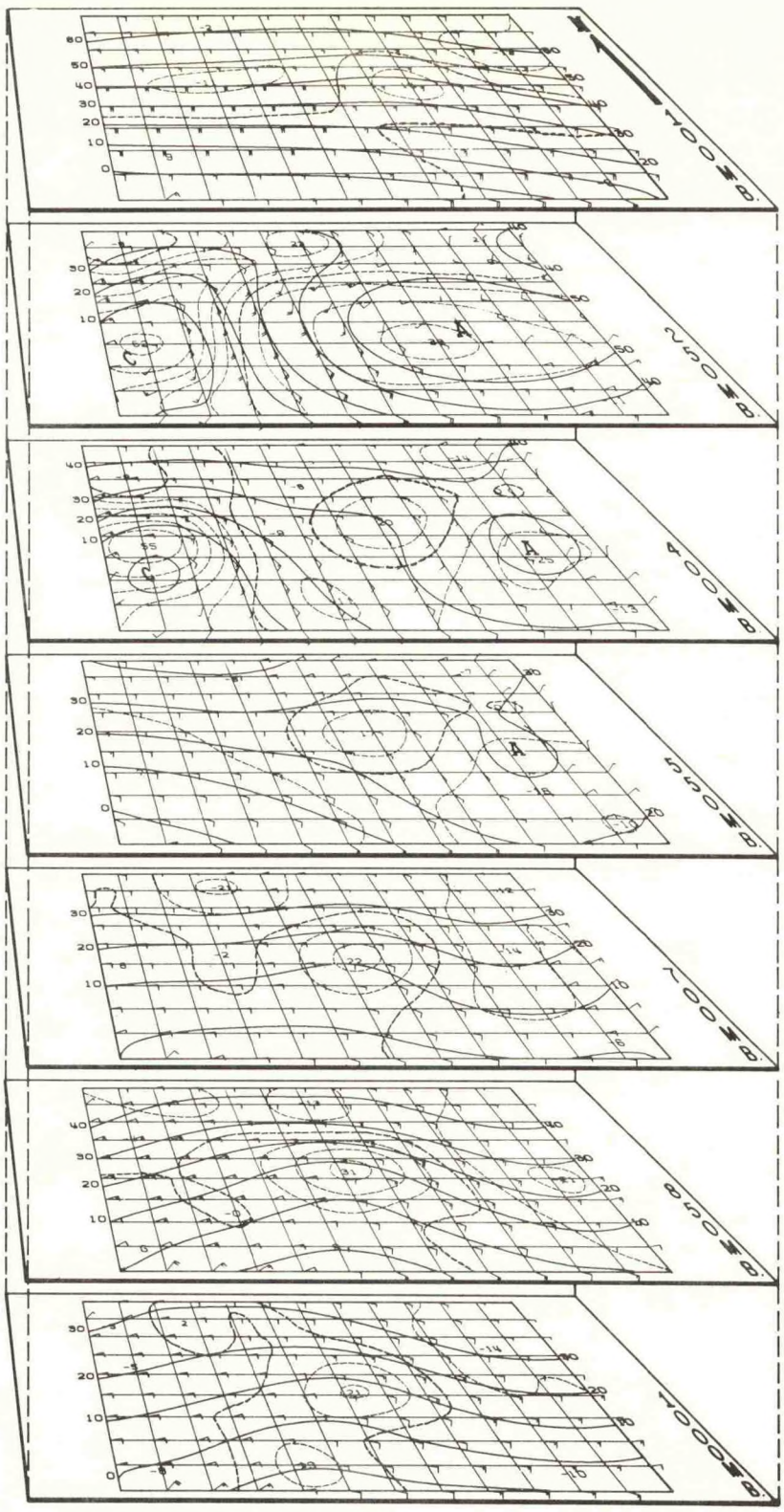

Figure 16a. August 4, 1963, 12Z. Weather, vertical motion, contour and divergence fields (see legend figure 7a). Contour curvature identified with the wave becomes weaker as the sequence progresses. Similarly, the low-level vertical updrafts are weaker and cover a smaller area.

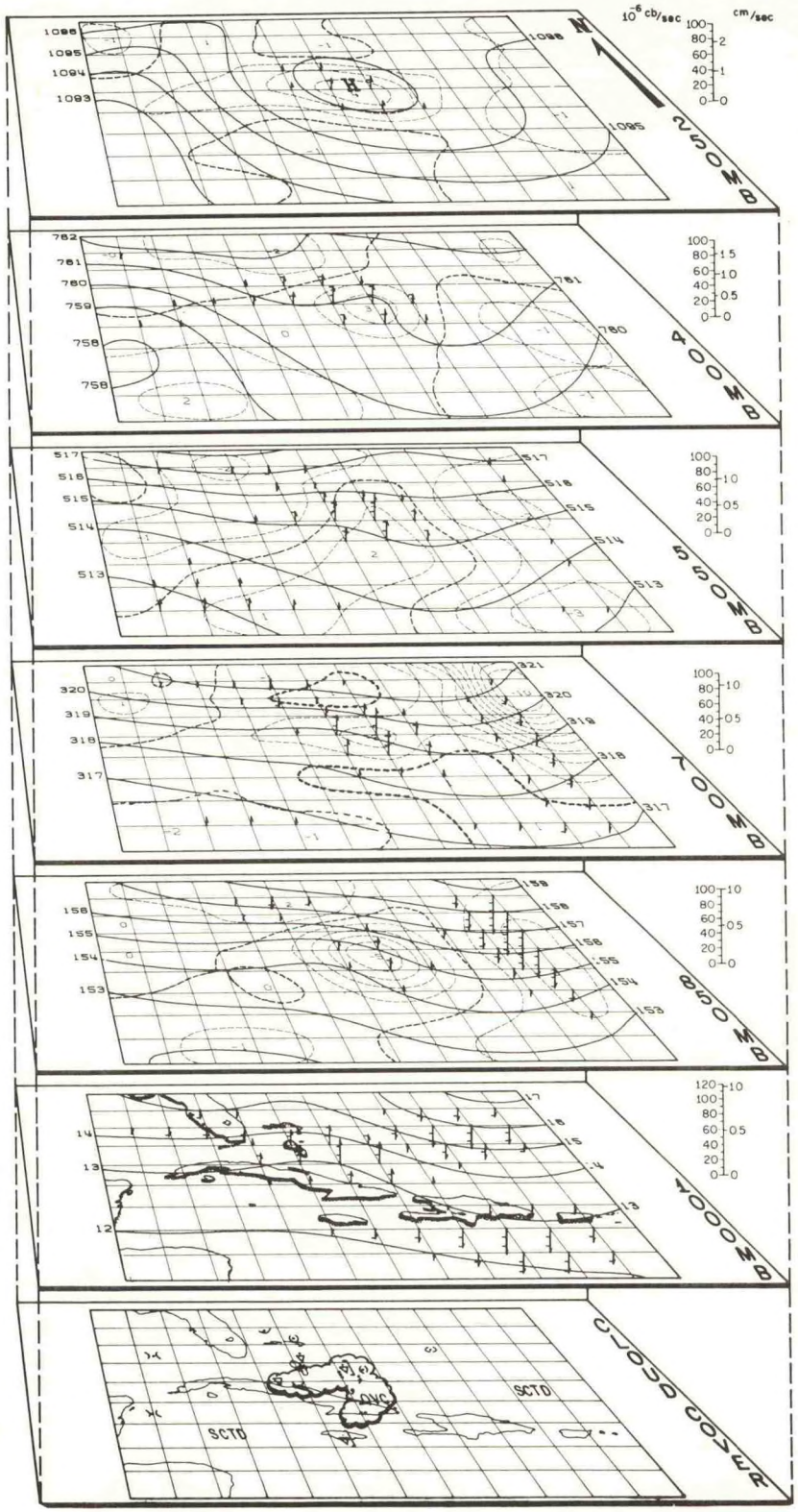
10^{-6} cb/sec
cm/sec
1086
1095
1094
1093
1088
1085
H
L
250 MB
782
781
780
759
758
758
781
780
400 MB
517
518
515
514
513
517
518
515
514
513
500 MB
320
319
318
317
321
320
319
318
317
700 MB
158
155
154
153
159
158
157
158
155
154
158
850 MB
14
13
12
17
16
15
14
13
1000 MB
SCTD
SCTD
CLOUD COVER

Figure 16b. August 4, 1963, 12Z. Streamfunction, vorticity and total wind fields (see legend figure 7b). In the lower levels there is only a slight decrease in the cyclonic vorticity accompanying the wave despite the decrease in curvature. The anticyclone at 250 mb is larger, stronger and further west than ever.

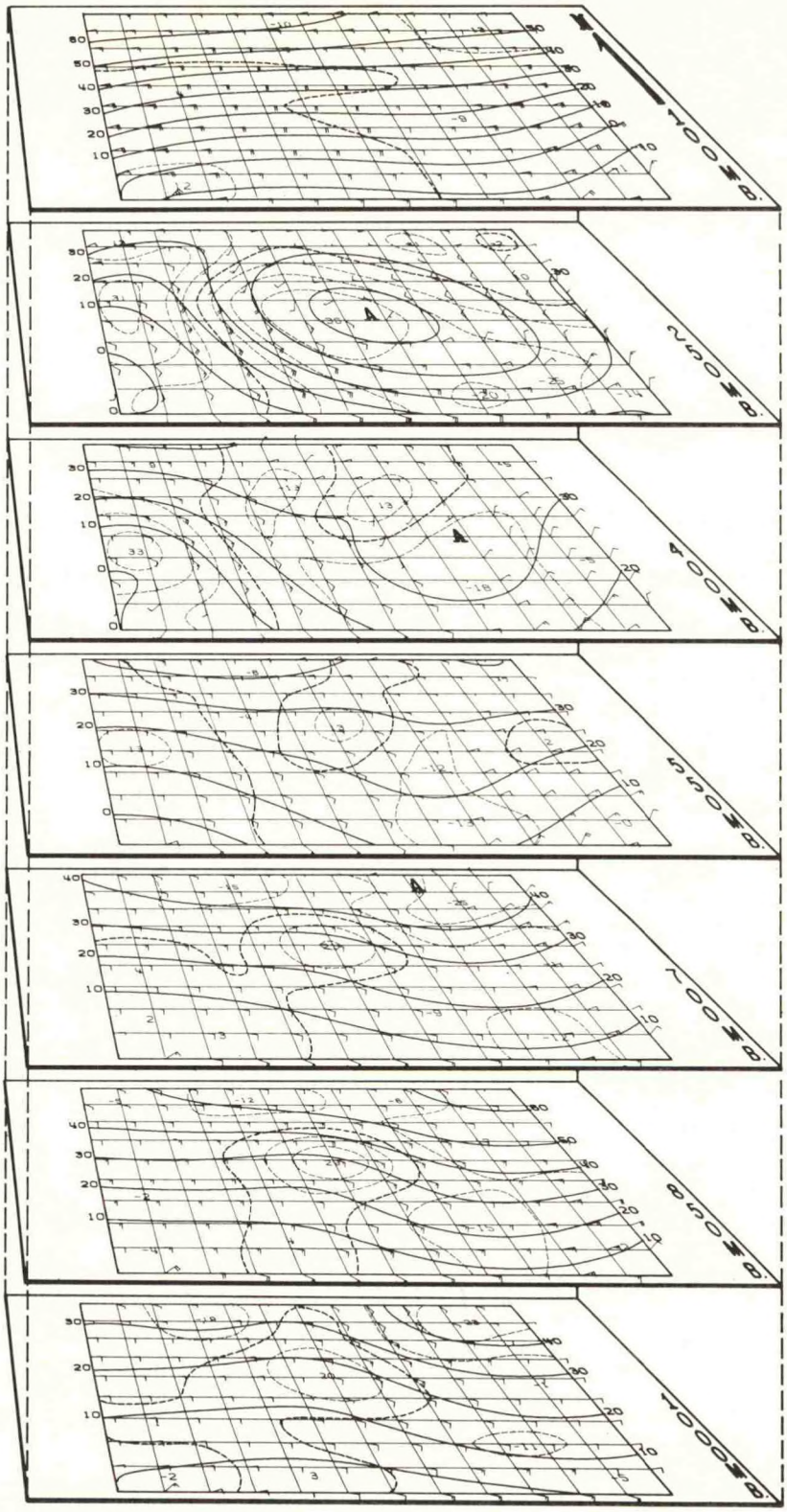

Figure 17a. August 5, 1963, 00Z. Weather, vertical motion, contour and divergence fields (see legend figure 7a). A further decrease in wave amplitude and in the low-level convergence fields associated with the wave is now evident. The upper level anticyclone dominates our grid area aloft and ridge conditions extend further down to lower levels.

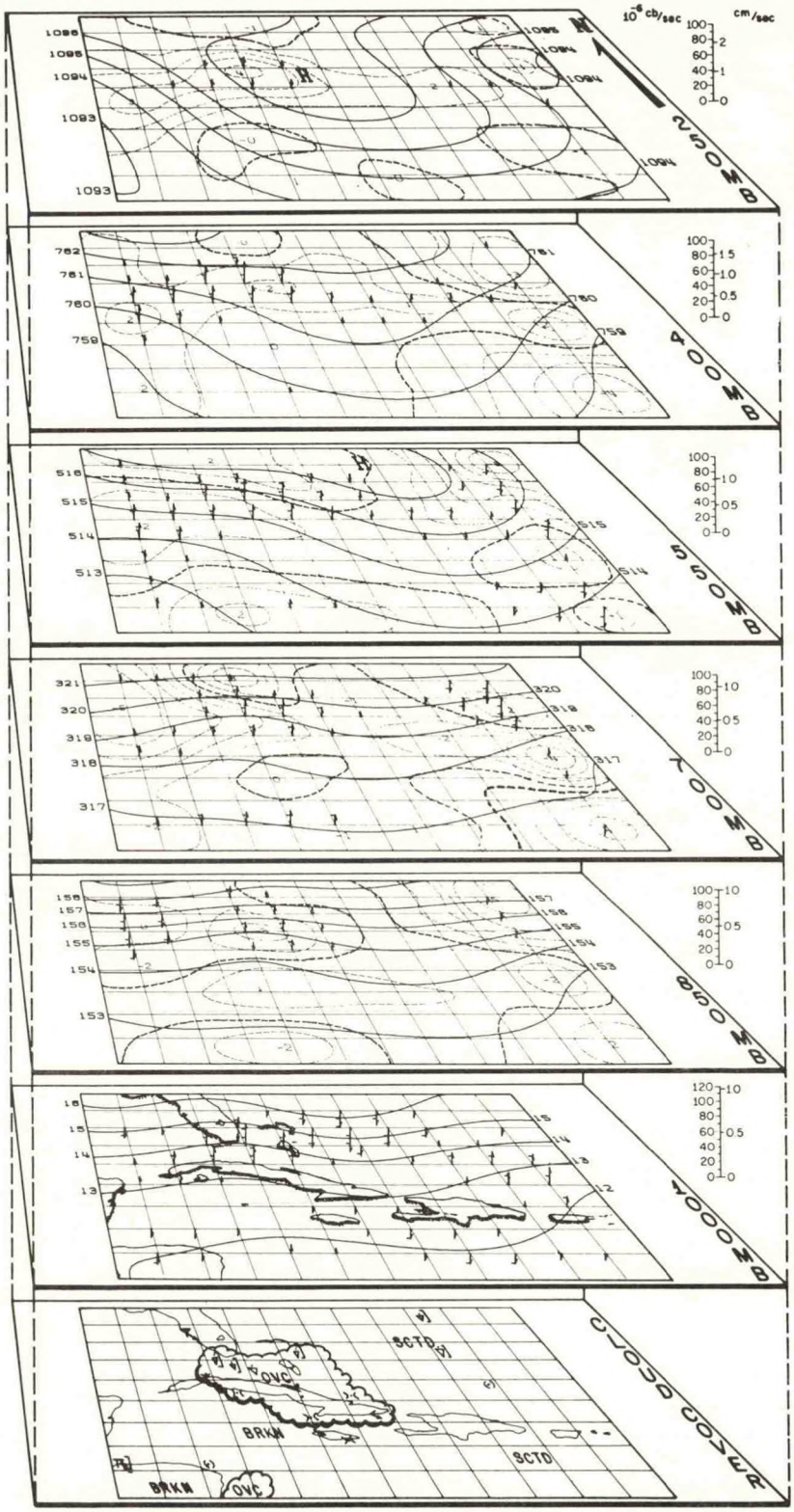
10^{-6} cb/sec
cm/sec
1000 MB
850 MB
700 MB
500 MB
400 MB
CLOUD COVER
OVC
BRKN
SCTD

Figure 17b. August 5, 1963, 00Z. Streamfunction, vorticity, and total wind fields (see legend figure 7b). The anticyclone at 250 mb now reaches its maximum intensity (vorticity $\approx$ - 42 x 10^{-6} sec^{-1}) and the trough to its east has now become apparent on the eastern extremities of the grid. Cyclonic vorticity accompanying the wave has weakened slightly at all levels.

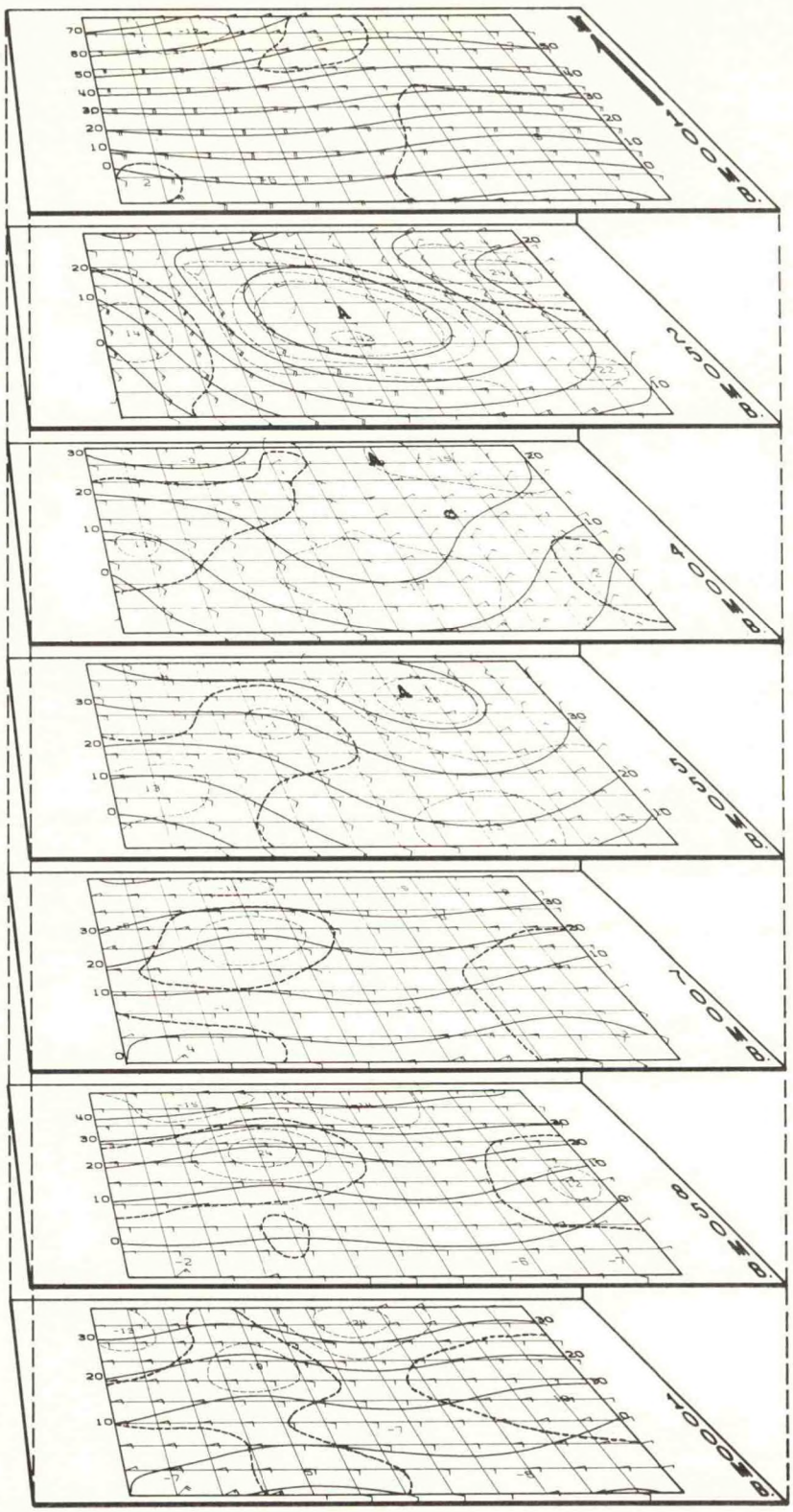

Figure 18a. August 5, 1963, 12Z. Weather, vertical motion, contour and divergence fields (see legend figure 7a). The wave has almost disappeared but can still be traced. Convergence at 850 mb has strengthened slightly, and upper-level divergence southeast of the upper-level high continues. The extreme downward velocities at the eastern edge of the grid were associated with questionable values of the static stability and do not appear to be a required feature of the dynamics of the situation. The velocities above and below do not support such extreme velocities.

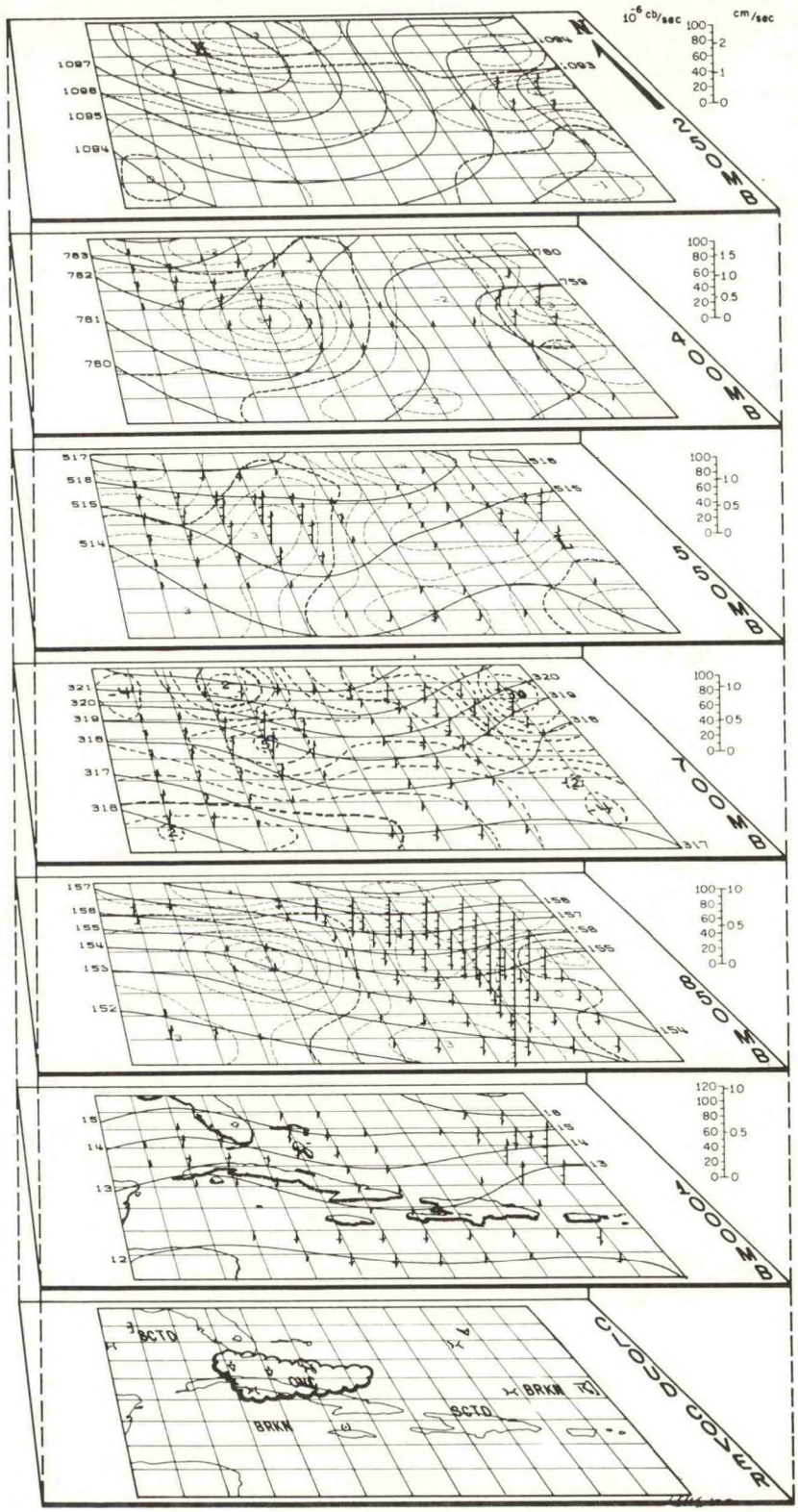
10^{-6} cb/sec
cm/sec
250 MB
400 MB
500 MB
700 MB
850 MB
1000 MB
CLOUD COVER
BCTD
OVC
BRKN
SCTD
BRKN

Figure 18b. August 5, 1963, 12Z. Streamfunction, vorticity and total wind fields (see legend figure 7b). The lower-level portion of the wave continues to weaken as cyclonic vorticity values continue to decline. The area of bad weather is quite restricted and the wave itself becomes difficult to trace.

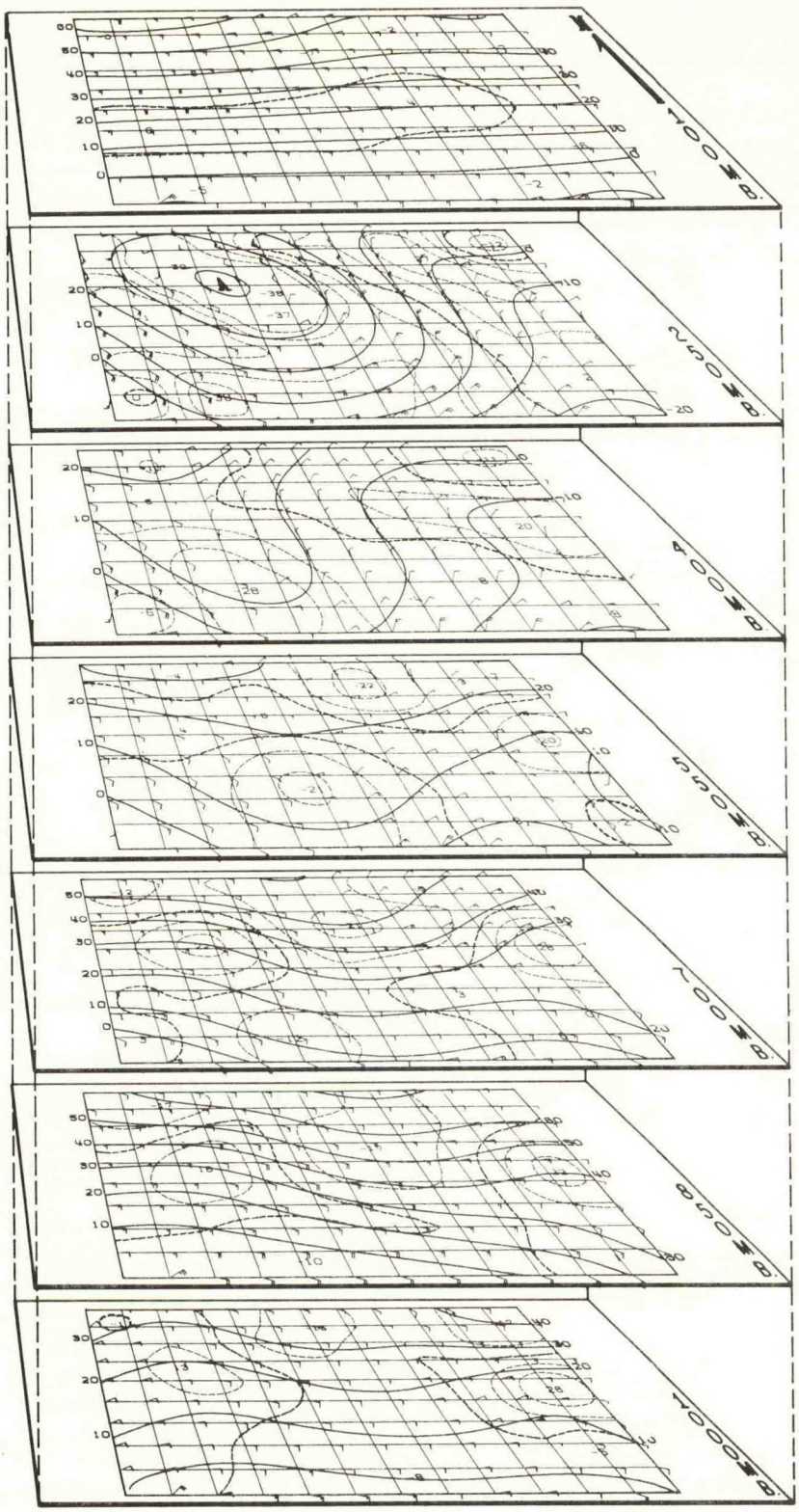

IV. DEVELOPMENT OF THE DIAGNOSTIC MODEL

A. Introduction

The coding and checking out of the diagnostic program were carried out as the results from the Sequence #1 analysis became available. In the course of these early runs many decisions had to be made with regard to tolerances for relaxations, relaxation coefficients, best first guesses, heating coefficients, as well as the task of debugging the program itself. The following is a brief description of the more significant of these items.

B. Finite Difference Approximations, Relaxation Procedures and Tolerances

All finite difference approximations were of the simple centered difference form unless one-sided differences were necessary. Where i is the row index and j is the column index $\psi_x = \frac{\psi_{i,j+1} - \psi_{i,j-1}}{2d_i}$ where d_i is the grid spacing and includes the map factor. Similarly

$$\psi_y = \frac{\psi_{i+1,j} - \psi_{i-1,j}}{2d_i} \quad \text{and}$$

$$\nabla^2\psi = \frac{\psi_{i+1,j} + \psi_{i,j-1} + \psi_{i-1,j} + \psi_{i,j+1} - 4\psi_{i,j}}{(d_i)^2}$$

Originally some of the more elaborate and accurate finite difference expressions were employed. When results were compared with results obtained using the simpler expressions, differences were negligible. This statement is not meant to infer that such refinements are not useful and often necessary in lengthy iterations where certain integral

properties must be conserved. But for diagnostic purposes, the simplest expressions were found to be adequate.

The relaxation scheme employed is that known as the Extrapolated Liebmann Method. If FF is the forcing function, and k is the vertical level index, expressions are reduced to the form

$$\text{Res} = f(\psi_{i\pm1,j\pm1,k\pm0,1}) - A\,\psi_{i,j,k} - B(FF)$$

where A is a constant coefficient which equals 4.0 if the Laplacian is being relaxed and B is a coefficient which may vary with latitude, i.e., it is equal to $(d_i)^2$ when the Laplacian is being considered. We set

$$\psi^{N+1}_{i,j,k} = \psi^{N}_{i,j,k} + \alpha\,\text{Res}^{N}_{i,j,k}$$

where α is the relaxation factor and N, the scan index, refers to the number of scans. Thus the new value of ψ is placed immediately in the active ψ array and may be used in the calculation of other ψ values on the same scan. The object of the iteration is to reduce Res to zero, or failing that, to make it equal to or smaller than, some preassigned tolerance.

The speed with which the iterations converge is a function of α, and Stuart (1961) has shown that the optimum coefficient depends on a number of factors: the nature of the equation in regard to the derivatives of ψ, the value of the coefficients, the order in which the grid points are treated and probably even the number of the scan, N. More practically, he has shown that too large values of $\alpha(\alpha > .5)$ would seldom lead to convergence in the 2- and 3-dimensional arrays with which he was concerned. We have used $\alpha = .35$ for the two dimensional arrays; $\alpha = .25$ for the three-dimensional geostrophic omega arrays and $\alpha = .70$ for the one-dimensional streamfunction boundary arrays. (O'Brien (1968) has analytically studied one and two-dimensional square arrays and arrived

at similar conclusions.) Scan counts were made during all of the relaxations, and the computation was terminated if the counts became excessive; usually more than 50 or 60 scans were considered unacceptable and the program was terminated. Experience showed that such excesses could be traced to coding errors. In every instance in which a first guess superior to zero was available, then the better first guess was used.

For relaxations involving ψ, the streamfunction, the tolerance used was 60 m^2/sec. This is far finer than the accuracy of the wind measurements demand and is a luxury which can be afforded in a diagnostic model where the whole series of relaxations is done only once and not repeated for many time-steps. If ψ at two points, 2 grid distances apart, were to differ from the relaxation values by the maximum, 60 m^2/sec, then the resulting error in the wind would be

$$u \sim \psi_y = \frac{\psi_{i+1,j} - \psi_{i-1,j}}{2d_i} \doteq \frac{120}{2x205x10^3} \doteq .3 \times 10^{-3} \text{ m/s}$$

Similarly for the height values, the tolerance of .3 m^2/sec^2 was used for relaxation. By similar reasoning the effect on the geostrophic wind at 15°N could be as much as

$$\frac{1}{f}\Phi_y \doteq \frac{.6}{4x10^{-5}x2x2x10^5} \doteq .04 \text{ m/s}$$

In both instances these tolerances result in no significant degradation of the fields since they have been deliberately chosen to be quite stringent.

For the three-dimensional relaxation of the geostrophic omega field, a tolerance of 10^{-7} cbs/sec was used, i.e., the geostrophic vertical velocities cannot be considered accurate to better than 10^{-7} cbs/sec.

The test for the convergence of the final loop in the program, which involves the successive values of the divergence at all of the interior points, was set at 3×10^{-7} sec^{-1}. This value was arrived at after some

experience with the model and trials with various tolerance estimates. Some difficulty was encountered in meeting a finer tolerance and an examination of the successive omegas revealed that they seemed to be oscillating about a final value but were not always converging towards the center of oscillation. By trial we found that averaging the array of omegas for every third cycle with their corresponding number in the second cycle array brought the mean close enough to the center of oscillation so that convergence ensued in all cases.

C. Empirical Adjustments of Δt

A point of passing interest was the value of Δt to be used in estimating the vorticity at time t_2. This may almost be looked on as an initialization procedure. The time interval, Δt, is to be used just once on the vorticity equation to provide ${}_{t_2}\zeta$, from which we determine ${}_{t_2}\psi$ and ${}_{t_2}\Phi$. The latter is used to evaluate the thickness tendency in which process the time interval is divided into the finite difference expression for the change in thickness. The simplest mathematical treatment is to allow Δt to equal one second so that no actual multiplication and division must be programmed or executed. This was tried and found to be unsatisfactory. Presumably round-off and truncation tended to obscure and degrade the very small effects which were actually present. Trials were made with Δt = 10, 100, 1000 and 10,000 seconds. The latter two showed small differences of little consequence, the 100 and 1000 intervals were quite alike but not as similar as the former pair. At 10 seconds some sense was emerging, but it was not deemed acceptable. The choice was made to use a Δt of 1000 seconds (~17 minutes). This seemed to allow plenty of time for the various terms to have a realistic effect yet not

so long that the original boundary values (where relaxations were involved) would unduly constrain the new field of values. (As pointed out previously, new boundary values were obtained for this later time by extrapolating the internal change field out to the boundary.)

D. Effect of Latent Heating

The earliest runs with the model were made without the low-level frictional convergence and without any latent heating effects. The omega fields were quite small at this stage. When the frictional convergence alone was added there was a notable increase in the magnitude of the larger vertically upward motions, but they were still quite small by middle latitude standards. The addition of latent heat effects to the model had a slightly more pronounced effect on the omega magnitudes but left them still rather small. In view of our previous rationalization of the possible defect in the Kuo parameterization, it was decided to arbitrarily increase the heating effect by multiplying dQ/dt by a coefficient ELL. Values of ELL were tried which ranged from 2 to 10. When the heating effect was increased by an order of magnitude the model failed to converge and patterns of the various fields of parameters became highly erratic and unreal.

In order to help resolve this problem, one may consider the climatological values of N.

$$N = \frac{1}{g}\left\{ \int_{P_T}^{P_B} \frac{C_P}{L}(T_S - T)\,dp + \int_{P_T}^{P_B} (q_S - q)\,dp \right\}$$

is computed in Appendix C. We note that 3/4 of the moisture is used to bring ambient air (at q) up to cloud humidity (q_S), and only 1/4 is used to raise the temperature from T to T_S. We postulate that cumulus activity

does indeed moisten the ambient atmosphere to some extent, but it is probably unrealistic to insist that the moisture used to heat versus the moisture used to moisten be fixed in the ratio 1:3. This is especially true in areas of persistent cumulus updrafts (which should be the ones indicated by our grid scale upward velocities) where, we have pointed out, $q > q_s$ and $T > T_s$, so that N becomes much smaller than the climatological N. On the basis of the trial runs and the previous consideration, it was decided to arbitrarily increase the Kuo parameterization by a factor of 3. This value proved to give fairly reasonable magnitudes to the vertical motions in the October situations yet did not result in disorganizing the various fields. Consequently, in the remainder of this paper, when runs with latent heating are referred to, they will mean runs for which the Kuo parameterization has been increased three-fold unless it is otherwise specifically indicated.

E. Merging the Streamfunction and Geopotential Fields

One of the objectives of this research was to try and gauge the contribution which the contour fields might make to the diagnosis over and above that made by the streamfunction. We have already pointed out that the contours can hardly be considered independent information because of the way in which they were derived. Runs were made in which the whole result was based essentially on the streamfunctions (from which the geopotentials were derived) to runs in which they were weighted half and half, to the final extreme where everything was weighted on the geopotentials. The results of these runs may be summarized as follows:

1. Differences in the runs were very small regardless of the weightings. This was, in part at least, due to the method by which the

contours were drawn, i.e., by paying close attention to the wind direction and speed.

2. Fitting "geostrophic" boundaries (as described in chapter II, B, 3e) to the contour fields was of no great benefit. As previously pointed out, it was these derived boundary relationships that, almost exclusively, led to troubles with the static stability. Furthermore, the computed boundaries gave rise on occasion to discontinuities in the vorticity fields since the computed boundaries surrounded the analyzed data and both were used in the computation of the Laplacian which is used to determine ψ as defined in the balance equation. Consequently, it became apparent that if the contour values were to be used it was simpler to use them as analyzed, i.e., without computed "geostrophic" boundaries.

3. One of the more optimistic notes of this phase of the investigation was the complete elimination of the analyzed contour values. The contour heights were derived by computing the boundaries as described, setting the mean of these values equal to the normal height for that level and then relaxing the Laplacian of phi in the balance equation to find the interior values. This approach was deemed so successful that it has been used in all cases except where otherwise specified.

V. RESULTS OF APPLYING THE DIAGNOSTIC MODEL

In the evaluation of results obtained with the diagnostic model many pages of printout tabulations have been produced. It is manifestly impossible to present all of these data for consideration, and it would probably be unwise to do so in any event because of the confusion which would accompany such a mass of statistics. Consequently, we have tried to select representative statistics with which to support general statements about the results of the runs.

A. Vertical Motion Studies

1. Magnitudes of Vertical Velocities

Traditionally it has been difficult for low latitude researchers to produce vertical velocities on a synoptic scale which are comparable to those that their colleagues have found at higher latitudes. This has led to a certain amount of uncertainty on the part of the professional meteorologist as to whether such results (at low latitudes) should be treated with respect. We hope that the present study will in part alleviate the suspicions with which some of the former works have been regarded

In the first place it does not seem very realistic to expect the synoptic-scale vertical motions to be strictly comparable in all situations. We are well aware that the bulk of ascending vertical motion at lower latitudes takes place in cumulus towers. The bulk of the descent, it is true, takes place on a slightly larger scale but not necessarily on a synoptic scale. Consequently, we have gradually come to accept the idea that while synoptic-scale upward motion undoubtedly exists and is

detectable in the tropics, it is primarily a triggering mechanism which touches off deep cumulus activity. The cumulus activity is accompanied by strong local updrafts and more widespread 'local' downdrafts so that a certain amount of local compensation takes place at less than synoptic scale.

Our experience with results from the diagnostic model fit well into this framework of thinking. For instance, the vigorous October low has maximum vertical velocities on the order of centimeters per second (where frictional convergence drives three times the Kuo Heating). This seems reasonable in view of the structure of the low, lateness of the season, etc., i.e., the omegas should be expected to approach middle latitude omegas in magnitude. Maximum velocities of the order of 3×10^{-4} cb/sec (about 8.5 cm/sec) were attained at 400 mb on 03Z October 14, 1956. Most of the vertical velocities were considerably smaller than this, but on each day of the October sequence there were vertical velocities of the order of centimeters per second.

Perhaps a note on the October vertical velocity scale is in order. The omegas have been scaled by 10^6, and the horizontal tick marks are for every 50 of these scaled units. Thus every two tick marks represent 100 of the scaled units. If one uses Jordan's (1958) normal tropical sounding for average temperatures and the approximation

$$w = - \frac{RT}{gP} \omega$$

we can establish the conversion factors to convert from <u>hundreds</u> of the scaled (by 10^6) vertical velocities to cm/sec.

Pressure Level	10^{-4} cb/sec
1000	.86 cm/sec
850	.98 cm/sec
700	1.15 cm/sec
550	1.41 cm/sec
400	1.83 cm/sec
250	2.65 cm/sec

Thus any time the vertical velocities reach 100 x 10^{-6}cb/sec, i.e., two tick marks on the October series, the velocities are of the order of one cm/sec. The average absolute value of the interior vertical velocities for Sequence #1 was of the order of 10 to 70 (times 10^{-6}) cb/sec. These statements apply to both the refined and geostrophic omegas.

The values of vertical velocity in the two easterly wave sequences were much weaker than that in the October closed low. A comparison of the average absolute values of the refined omegas is presented in figure 19. It is readily apparent that the October 1956 omegas are significantly larger than either of the easterly wave cases. It is also apparent on the last day of Sequence #2 that as the closed low intensifies, the maximum vertical velocities are increasing, and some of them have reached the cm/sec order of magnitude (see figure 12a). It should be noted that for both Sequences #2 and #3, Figures 7 - 18a, the scaling factor has been increased to 5 x 10^{6}.

One significant aspect of the three sequences is the range of vertical motions they present. A well-defined closed vortex, Sequence #1, contains vertical motions quite comparable to those which accompany analogous systems at higher latitudes. The weaker wave, Sequence #3,

Figure 19. Average absolute values of the diagnostic vertical velocities. For each of the three synoptic sequences and in chronological order from left to right are the average absolute omegas in units of 10^{-6} cb/sec. There were two overlapping synoptic times in the 1962 sequence when the grid was shifted two rows to the north to follow the disturbance; they have both been retained since 1/4th of the data are new. To eliminate any duplication, ignore the two middle bars in the 1962 presentation. The 1956 sequence was by far the most active with the 1962 sequence next and showing some small tendency toward increased activity with time. The 1963 sequence reflects the relatively inactive state with some tendency for values to decline as time progresses; on the last day, values are distorted by the unrepresentative downdrafts previously noted at the 850-mb level.

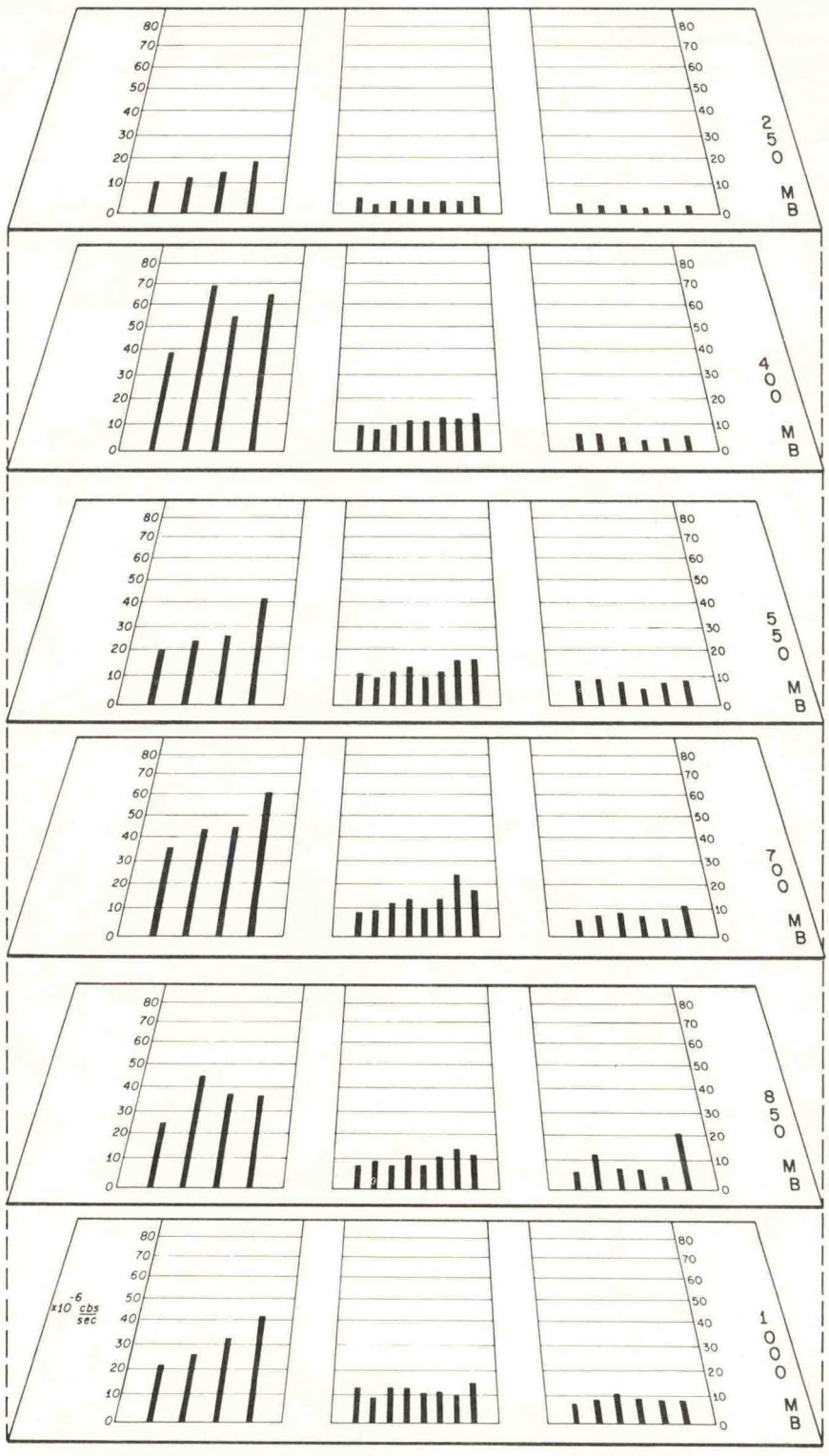
80
70
60
50
40
30
20
10
0
250 MB
400 MB
550 MB
700 MB
850 MB
1000 MB
x10 -6 cbs/sec
OCTOBER 1956
AUGUST 1962
AUGUST 1963

never really approaches this level of activity. In Sequence #2 we tend to bridge the gap with a transitional sequence which seems to fit logically between the extremes. It should be noted that the unusually strong downdrafts in the northeast corner of the grid in figure 18a appear to be due mainly to questionable values of the static stability where σ approached the minimum allowed. The geostrophic omegas (not shown) did not contain a similar extreme maximum so the gross dynamics of the situation did not require so marked a maximum.

2. Relation of the "Geostrophic" to the Refined Vertical Velocities

The geostrophic omegas were originally introduced as a first estimate when successive divergences failed to meet the tolerance requirement in one of the October sequence runs. The motivating thought was that by providing a reliable first guess, convergence should be fairly swift and sure. It turned out, however, that the "geostrophic" vertical velocities were quite an accurate first guess and were correlated quite highly with the more sophisticated vertical velocities. There are reasons for the positive correlations but their magnitude was something of a surprise.

Figure 20 shows the correlations of ω_g with ω_r for the interior levels where the heights have been derived from the wind field, the latent heating is frictionally driven and is three times the "Kuo rate". The bulk of the correlations are +.9 and over with only a few less than +.8. It must be recalled that the contours used in these "geostrophic" computations are not independent of the wind field but are related through the balance equation and that the latent heating is the same in either case, being driven by the low-level frictional effects. One might have expected the October sequence to differ a bit from the other two since

it is concerned almost exclusively with a large closed cyclonic circulation which we would expect the geostrophic approach to systematically overestimate. This does not appear to be the case.

Correlations tended to be a minimum at the 850-mb level and reasons can be adduced to support the reality of this trend. The prime cause for it appears to be associated with the fact that the static stability at that level is small and because the value of σ may range by a factor of possibly 5 or so over the horizontal grid. For instance, the average static stability at 850 mb is about 1.4 m/cb^2 with a range of individual values from .3 to 2.2 m/cb^2. At 700 mb the average is about 2.0 m/cb^2 with a range from 1.5 to 2.8 m/cb^2. At higher levels the stabilities are bigger and the value of σ over the field ranges by a factor of less than 2. Since the "geostrophic" omegas employ a static stability which is a function of pressure only, we used the average value for the pressure level (at that map time) in computing ω_g. However, the full range of field values is used in computing the refined omegas, and this variability at a given level has no counterpart in the geostrophic procedure. In addition to this effect and, in all probability, a much smaller effect is the likelihood that at low levels the ageostrophic effects are a maximum and may contribute to lowering the correlations with the geostrophic omegas.

3. Effect of Latent Heat on Vertical Motion

The effects of including the release of latent heat in the model were slightly more subtle than originally expected. It was, of course, immediately apparent that there was a pronounced tendency to increase the magnitude of the centers of upward motion. This tendency increased with altitude up to 250 or 400 mb. The increases were not of an order

of magnitude but were by a factor of 2 to 5 usually, i.e., the magnitude of the center of updraft would be increased through the addition of latent heating by a factor of some 2 to 5 at the upper levels.

In the strong well-defined patterns such as Sequence #1, this had only a rather small effect on the remainder of the field. In fact, the average absolute value was changed hardly at all, and the correlations between the refined omegas with and without the heating (see figure 21) were all above +.8 except at 250 mb.

This was not quite the case for the weaker patterns of August 1962 and 1963 as is shown in the same figure. Again the effects are small at low levels, and once again the changes become more pronounced with height. But, in addition to increasing the magnitude of the updraft centers, there seems to be an increasing trend for the addition of latent heating to change the patterns of up and down motion at the higher levels of the weaker patterns. In view of the fact that some of these patterns are so very weak, it cannot be held as of great moment that they are readily changed. The correlations (figure 21) show that removing the latent heating does result in lowering correlations (at 250 and 400 mb) more for the weak patterns than it does for the strong.

The effects of latent heating on the "geostrophic" omegas were nearly identical to their effects on the refined omegas.

4. Effect of Surface Friction on Vertical Motion

In addition to allowing one to eliminate the effects of latent heating, the program options also allowed for the deletion of the surface friction, i.e., for setting the frictional velocity, ω_H, at the top of the boundary layer equal to zero. Since this is the vertical velocity used to drive the latent heating, there is no latent heating possible when running in this mode.

The frictional effect is closely related to the vorticity, so, when the cyclonic vorticity is strong as it is in Sequence #1, the frictional vertical velocities are strong. Since these affect the computation of the 850-mb vertical velocities, the difference between having a meaningful low-level velocity and setting it equal to zero is most strongly felt at the 850-mb level. The central updraft velocities may be increased by up to 50% with vorticity centers as strong as those shown in Sequence #1. The effect on the downdrafts was less well marked and usually less than 20% in significant centers. At higher altitudes the effects on magnitude were quite small but, nevertheless, perceptible. The patterns of vertical velocity, however, were changed very, very little and, in general, correlations with the patterns obtained setting the latent heat equal to zero were greater than +.9.

5. Diagnostic Versus Kinematic Divergences

Much has been said about the pitfalls of using kinematic divergences. These dangers have not been exaggerated if the results of applying the diagnostic model to these three sequences are representative. Figure 22a shows the correlations between our 'standard' divergences and those computed from the input winds (read from the analyses) after they had been smoothed horizontally to take the 'noise' out of the signal.

In general, the best correlations are obtained at the 1000-mb level where the data coverage is best and, one might hope, the analysis most meaningful. One must recall, however, that the diagnostic divergence at 1000 mb is taken as a one-sided difference in the vertical velocities at 850 mb. This must be a partial recommendation of the quantity and quality of the low-level data and the analysis they permit. Even at these best levels the correlations are disconcertingly low and none

Figure 20. Correlation of "geostrophic" omegas with those obtained from the balanced diagnostic model. Correlations are almost uniformly high partly because the heights used to derive the geostrophic values were obtained from the wind field analysis using the balance equation, not from independent height analysis. They are also attributable to the fact that on the average the terms retained in deriving the "geostrophic" omega equation were the most important in these synoptic sequences.

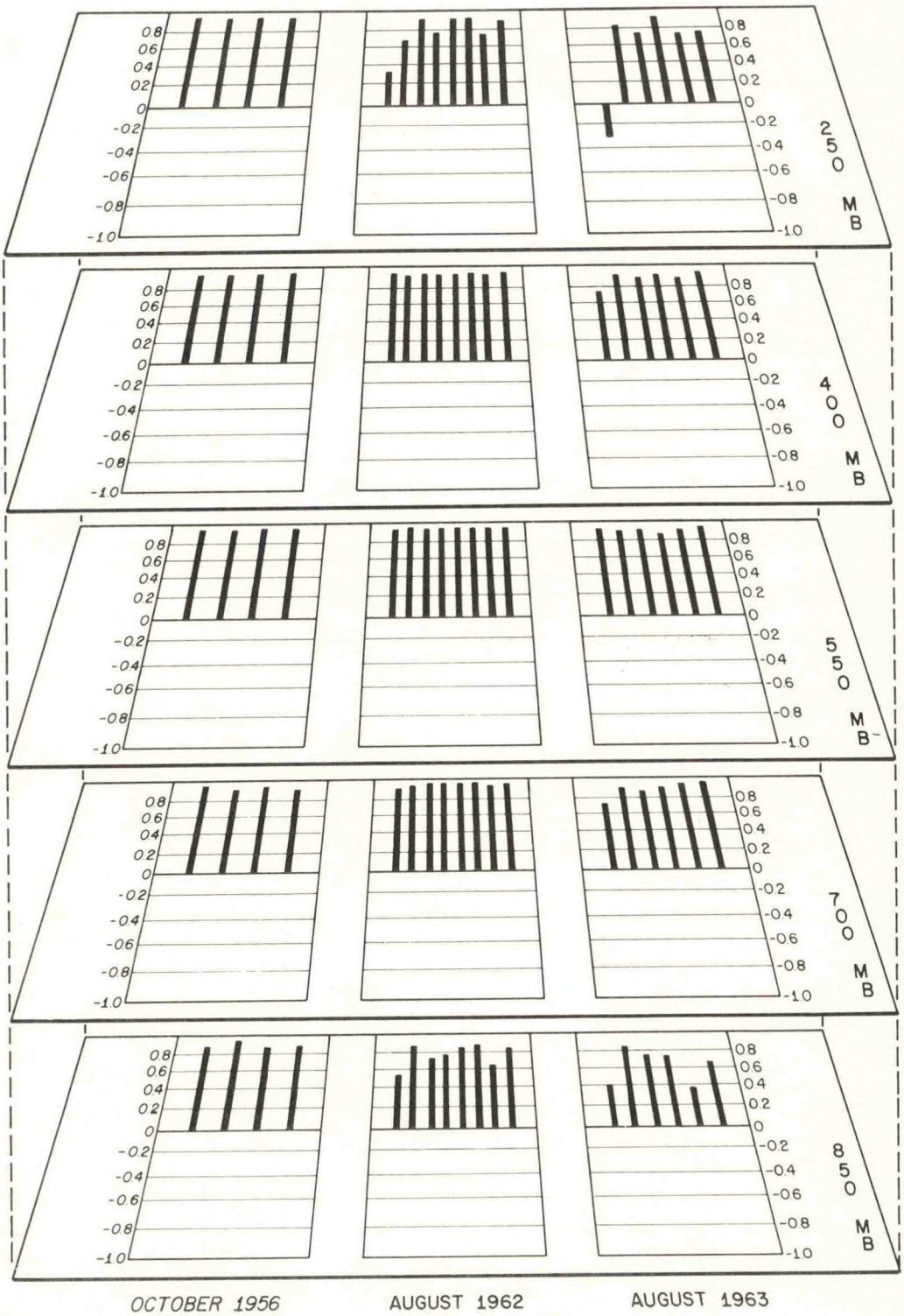
08
06
04
02
0
-02
-04
-06
-08
-10
250 MB
400 MB
550 MB
700 MB
850 MB
OCTOBER 1956
AUGUST 1962
AUGUST 1963

Figure 21. Correlations between balanced diagnostic vertical velocities with and without latent heat release. The pattern of the omega field is relatively stable, i.e., the addition of latent heating does not grossly alter fields, particularly if they are strong. Weak vertical velocity fields are most apt to be altered and the effect most noticed at higher elevations where heating effects are strongest.

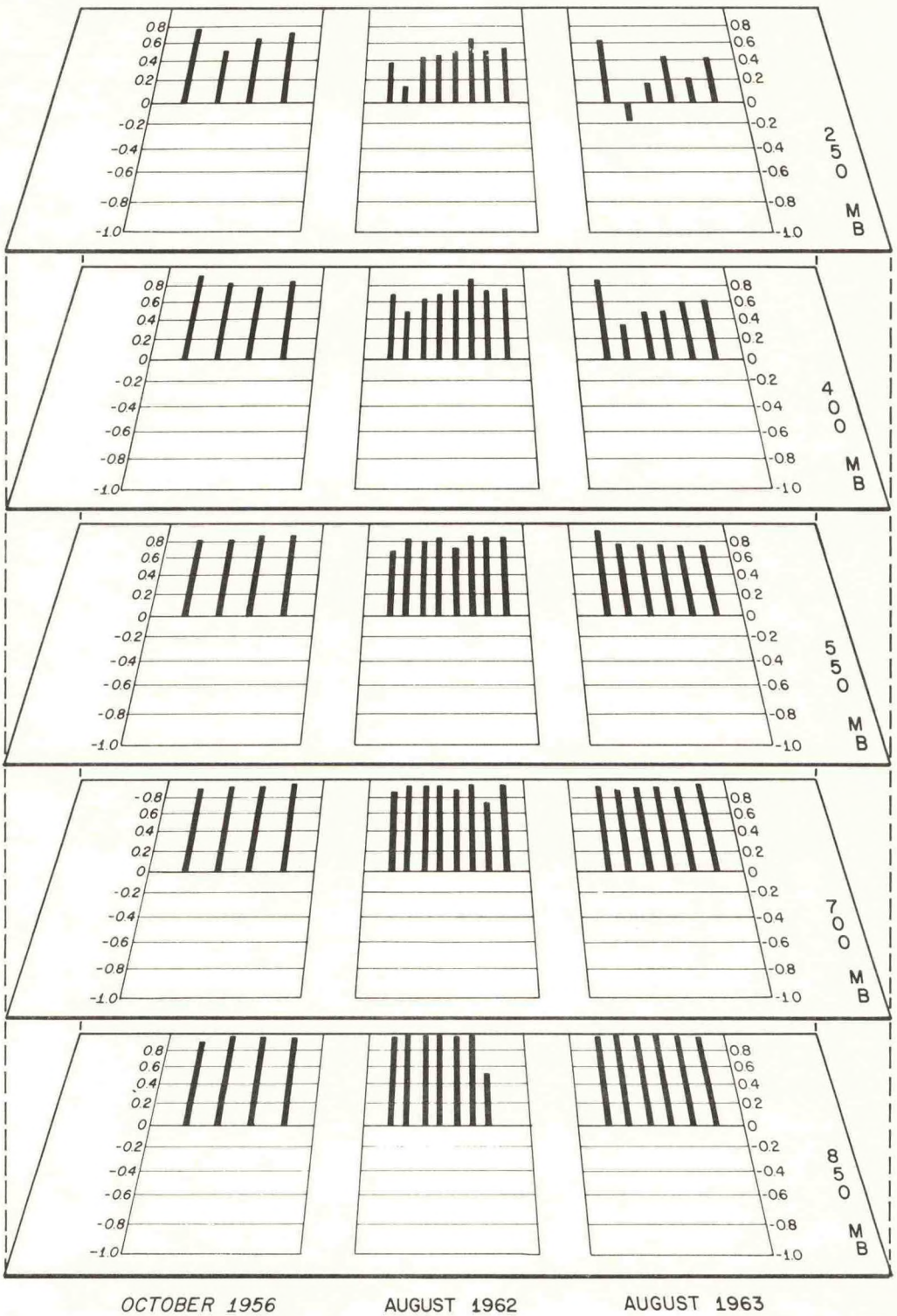
0.8
0.6
0.4
0.2
0
-0.2
-0.4
-0.6
-0.8
-1.0
250 MB
400 MB
550 MB
700 MB
850 MB
OCTOBER 1956
AUGUST 1962
AUGUST 1963

Figure 22a. Correlations of the diagnostic and the kinematic divergences. The diagnostic divergences are calculated point by point from the diagnostic omegas and the kinematic divergences are computed from the smoothed input winds (from the analysis) after they have been broken into u and v components. These correlations are rather small; they are largest at the lower levels where the data are most plentiful. Also, there is a tendency for the correlations to be highest where the divergences are large.

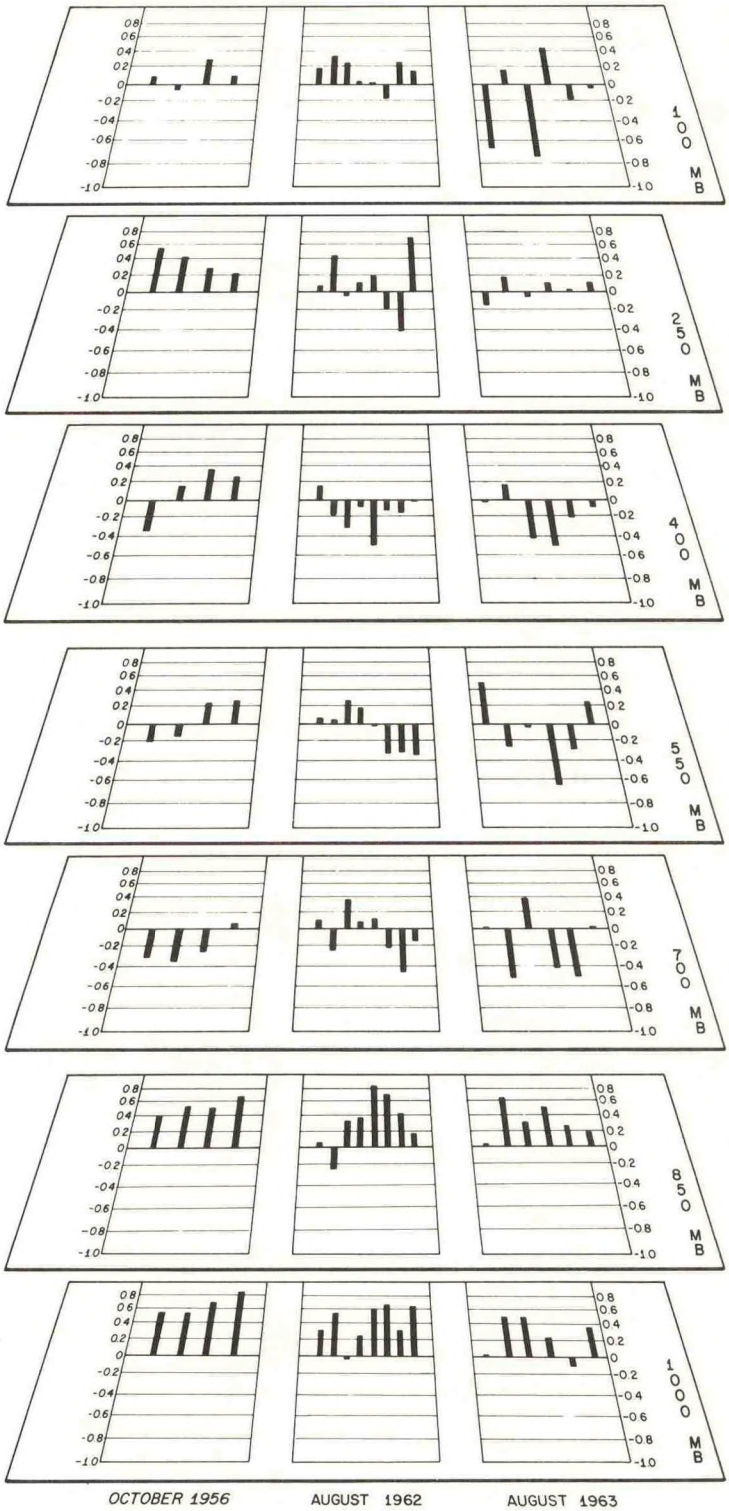
100 MB
250 MB
400 MB
550 MB
700 MB
850 MB
1000 MB
OCTOBER 1956
AUGUST 1962
AUGUST 1963

average over +.7. The October situation affords the better correlations, possibly because the divergences accompanying this "stronger" situation were of greater magnitude.

In addition to presenting a rather poor picture of the pattern of divergence, the kinematic divergences suffered from another defect. They were almost uniformly too large. If one compares the mean absolute value of the kinematic divergence with the refined divergence, it becomes apparent that most of the kinematic values exceed the other by factors varying from 2 to 10 (figure 22b). The latter is most applicable to the weakest divergence patterns.

Consequently, while it may have been expected that kinematic estimates would have difficulty in replicating weak fields of divergence, we find they do not do too well even on strong fields. Furthermore, there is a uniform tendency to overestimate the divergence when it is kinematically evaluated. It would appear to be a dubious method to employ and should be used only as a last resort even if one were to take advantage of O'Brien's (1970) suggestions. Lateef (1967) has recently employed the data from the weakest case (August, 1963) to compute divergences and vertical velocities as discussed previously. His magnitudes of both divergence and vertical velocity tend to be larger than those determined diagnostically.

6. Contour Height Analysis and Vertical Motions

For the first two sequences, October 1956 and August 1962, contour analyses were available for all synoptic times and levels of data. We have already pointed out that the height analyses were made while paying close attention to the wind analyses as well as the reported heights at observing stations. The most difficult part of this type of analysis is

in judging the effects of curvature on the pressure gradient so as to better estimate the wind called for by the analysis. In this instance both analyses (October and August) appear to be less than ideal in much the same respect.

The common weakness appears to be in an overestimate of the pressure gradients. When we run the model allowing the contours to dominate the merging of winds and heights (so that the wind analysis is weighted zero), we find the following interesting relationships come to view after we compare the results obtained with those obtained when the wind analyses are allowed to dominate the merging:

a. The vorticity centers "calculated from the height fields" overestimate the cyclonic centers computed from the wind field, i.e., the gradients are too strong and the effects of cyclonic curvature in reducing the geostrophic to gradient wind have been overestimated.

b. The strength of the wind field itself is overestimated as a general rule due to the reason cited in a.

c. The vertical motions are, as a result, mostly larger than those obtained from the wind analyses. This is not uniformly true, for the mean absolute values may be smaller on occasion. However, in extreme cases the mean absolute vertical velocity may be almost doubled by using contours alone.

d. Perhaps the most curious aspect of this situation is the fact that the overall patterns of vertical motion remain so similar. Figure 23 presents the correlations between the standard "winds-weighted-only," and the "contour-weighted-only" vertical velocities. Both runs were with surface friction and full latent heating. The October case which was dominated by cyclonic circulation shows little variation with pressure

Figure 22b. Average absolute value of the diagnostic (solid bar) and kinematic (open bar) divergences in units of 10^{-6} sec^{-1}. Diagnostic divergences in the 1956 sequence were generally larger than in the other two. The 1963 sequence has the smallest diagnostic divergences (with the exception of the last map-time at lower levels which has already been discussed). All of the kinematic divergences are overestimates in magnitude and tend to average around 3 or 4 x 10^{-6} sec^{-1} regardless of the diagnostic divergences or the analyst involved. A notable exception was the 250-mb level of the 1956 sequence where wind speeds were stronger than in the other sequences and ranged around 40 to 50 knots.

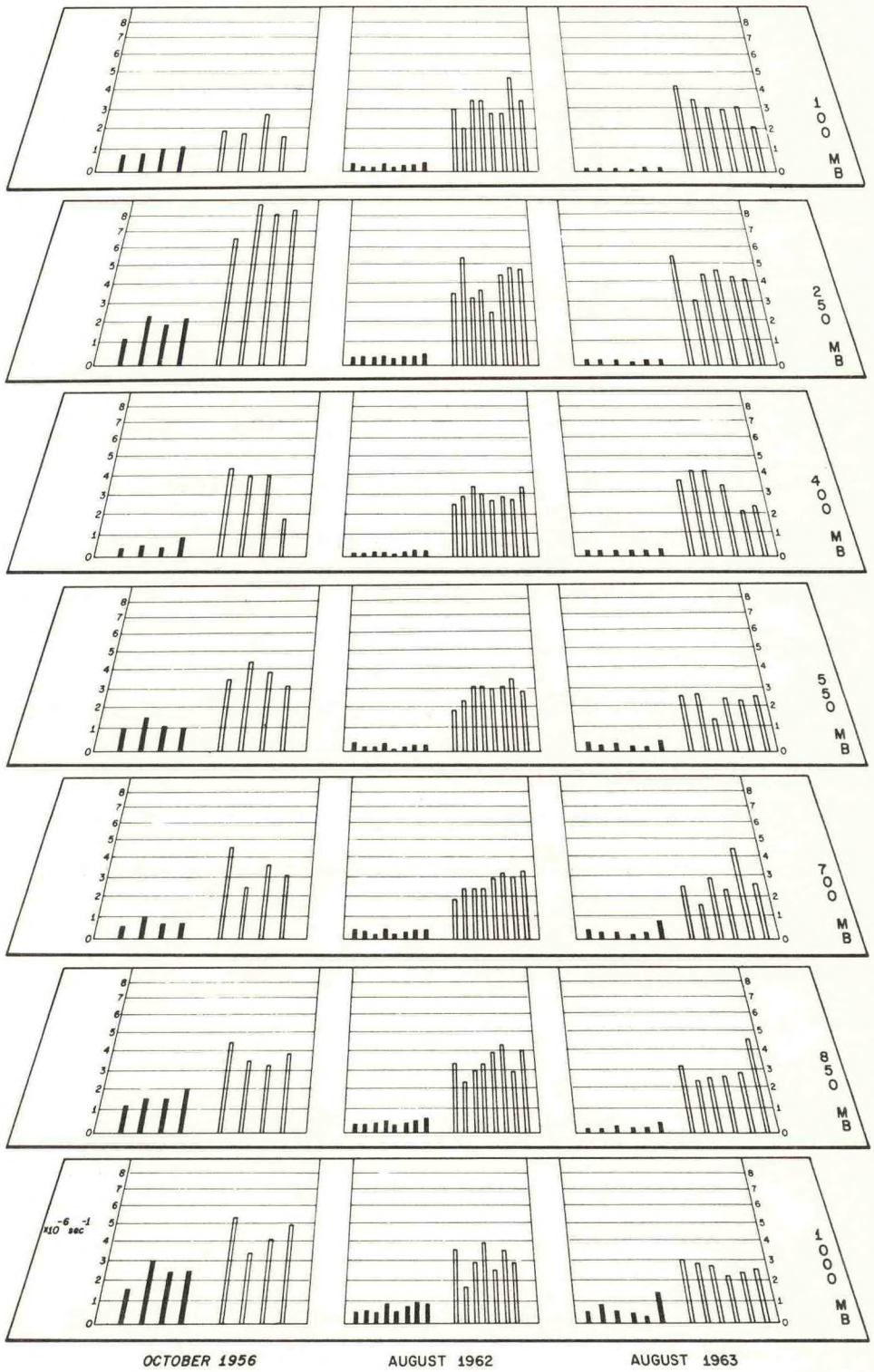
100 MB
250 MB
400 MB
550 MB
700 MB
850 MB
1000 MB
x10⁻⁶ sec⁻¹
OCTOBER 1956
AUGUST 1962
AUGUST 1963

Figure 23. Correlations of balanced diagnostic omegas: one derived using the wind analysis only as independent input data and the other derived using only analyzed contour data. It is pointed out elsewhere that the contour analyses are by no means independent of the wind data and wind analyses. The current state of the raob network at low latitudes and raob accuracy make independent height analyses impossible. Consequently, it is not surprising that the correlations are seldom less than +0.6. No contour analyses were available for the 1963 sequence.

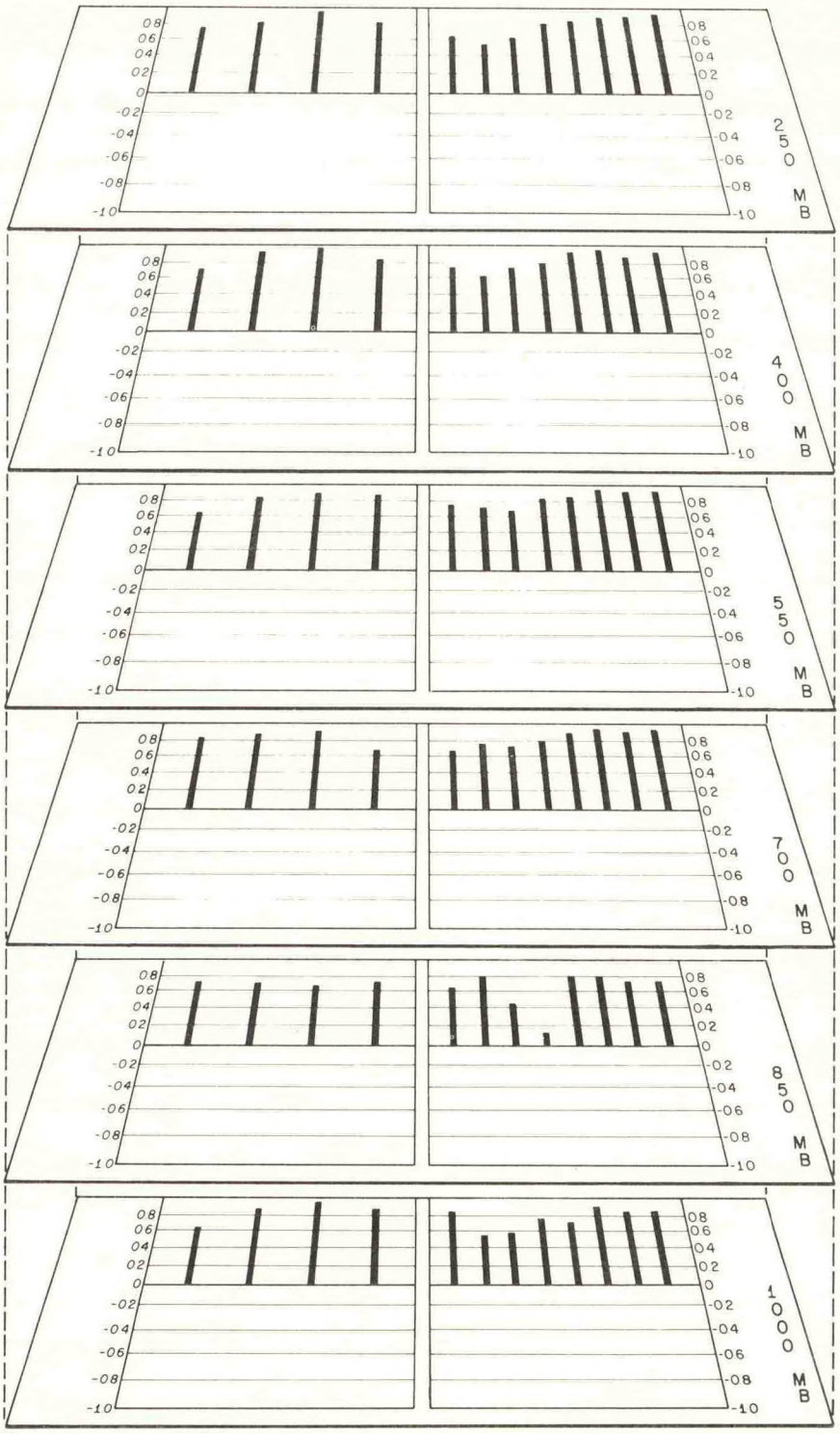
08
06
04
02
0
-02
-04
-06
-08
-10
250 MB
400 MB
550 MB
700 MB
850 MB
1000 MB
OCTOBER 1956
AUGUST 1962

and all correlations averaging above +.8 except for 850 mb where +.7 is more representative. The pattern is much the same for August 1962 except that the spread is somewhat larger and the average correlation a little lower. In view of the fact that the data net is none too good and, occasionally, data are missing, we have deliberately chosen to lean on the wind analyses because the station heights are so often misleading. Nevertheless, we have not managed to render the wind field very effectively despite the freedom taken with reported raob heights. The net result of this contretemps is that the author sees little advantage in careful contour analysis. If the reported values cannot be trusted and drawn to, then one must rely on the wind analysis for guidance. The time may better be spent on refining the wind analysis. Height reports are useful in some instances. From isolated stations like Bermuda, heights may give information as to whether a high or low is near the station, a fact which may be difficult to determine without such data.

The other contribution from the height analyses is the static stability. It seems patently unnecessary to perform the whole height analysis, merely to acquire σ, the static stability. Heights derived through the balance equation (using normal height values for the mean boundary height), will retain more consistent thickness patterns. Certainly they will be so in a relative sense and, probably in an absolute sense as well. The general stability of the vertical motion patterns does much to recommend this philosophy.

7. Vertical Velocities and the Weather

The frictionally induced vertical velocities which should be characteristic of the top of the boundary layer, are portrayed on the 1000-mb level presentation of the contour heights in figures 3a-18a.

These velocities are a function of the vorticity, upward where relative vorticity is positive (cyclonic) and downward where relative vorticity is negative. It would be unrealistic to propose that the sea-level vorticity alone determines the local weather, although it is undoubtedly a meaningful index of the weather when the vorticity is large. Rather, it is felt that extensive cloudiness and significant weather should occur with upward vertical velocities of sensible magnitudes at both 1000-mb and 850-mb levels (and, probably, at the 700-mb level as well). Consequently, when the "weather" (depicted on the lowest slab) is compared to the vertical velocities, it is suggested that consideration of the vertical velocities include the lowermost 2 or 3 levels. On all levels above the 1000-mb level both the contour height (solid lines) and the divergence fields (dashed) are presented. Figures 3b through 18b present the wind field, streamfunction and (dashed) the relative vorticity field. Perhaps it should be mentioned that the "present-weather" analyses were executed by someone not involved in any of the analyses and without recourse to the diagnostic fields.

a. Sequence #1, October 13-15, 1956

(1) October 13, 15Z (figures 3a, b)

An extensive area of overcast and rain covers Cuba and the area north and northeast of Cuba. For the most part this area is one of upward vertical motion at the 1000, 850 and 750-mb levels with maximum omegas between 100 and 200 ($\times 10^{-6}$) cb/sec or 0.5 to 1.0 cm/sec. South of Cuba there is little significant bad weather with broken skies to the south of the low; over part of this area the vertical velocities are weakly upward at 1000 mb but too small to be plotted at 850 and 700 mbs. The southeastern and northwestern corners of the grid enjoy the best

weather with the latter most favored under descending motion at 850 and 700 mbs.

(2) October 14, 03Z (figures 4a, b)

The weather over Cuba, to the North, and over southeastern Florida has changed but little. The upward velocities have become a bit stronger at the center of rising motion and now exceed 150 ($\times 10^{-6}$) cb/sec or 1.5 cm/sec at the lower levels. The northwestern grid area enjoys scattered cloudiness under descending motion at 850 and 700 mb while the southwestern quadrant has broken coverage under little significant vertical motion - some of this is cumulus activity in the cool air being advected southward. The extension of overcast conditions south-southwestward from Hispaniola does not contain much weather of note, but it is not readily explainable in terms of the very weak vertical motion and convergence fields which accompanied it.

(3) October 14, 15Z (figures 5a, b)

The western third of the grid still has scattered to broken cloud coverage with the northwest again enjoying the finest weather associated with the descent and divergence at the 850-mb level. The main bulk of the bad weather has shifted slightly to the north of Cuba along with the disturbance and its attendant centers of vorticity and convergence. The area south of the Windward Passage remains overcast but now there is a sizeable cyclonic circulation in the region due to the trough elongation in this direction. Weak upward motion, convergence and cyclonic vorticity characterize the area. The extreme southeast has broken sky cover under weakly anticyclonic circulation (figure 5b). The magnitude of the vertical velocities at the center of upward motion has increased slightly since the previous map.

(4) October 15, 03Z (figures 6a, b)

The last maps in this sequence show the intensifying disturbance. The center is located just north of central Cuba with the strongest low-level vorticity center (55×10^{-6} sec^{-1}) encountered yet. The upward vertical velocities have again increased somewhat in magnitude and are quite widespread. Fine weather with only scattered cloudiness persists over the northwestern third of the grid under weak descent and anti-cyclonic vorticity in the low levels. The southwestern quadrant has broken to scattered cloudiness right into the northwesterly cyclonically-curved flow (with weak divergence and subsidence) southwest of the surface low. An extensive area of overcast skies, rain, showers and squalls characterize the strong cyclonic area where high values of vorticity and strong upward vertical velocities dominate the scene.

Summary of Sequence #1

The series is dominated by a large, strong cyclonic circulation which is characterized by strong upward vertical motions mainly to the north and northeast of the center. An extensive area of overcast skies, showers, thundershowers and rain coincides quite well with these features perhaps extending a bit further to the south than one might prefer. Fair weather far to the northwest in weakly anticyclonic flow and intermediate weather to the southwest seem reasonably appropriate to the attendant circulations. Consequently, it is judged that the observed weather and the diagnostic parameters are in reasonable agreement.

b. Sequence #2, August 25-27, 1962

The vertical motions in this situation were decidedly smaller for the most part than those of the October sequence. Because of this, the vertical motion arrows have been expanded for both this and the next

sequence. In order to show more variability, one tick mark on the vertical motion arrows now corresponds to 10 ($x10^{-6}$) cb/sec. Conversion scales (to cm/sec) for each pressure level are printed at the right hand side of the slab for that level.

(1) August 25, 00Z (figure 7a, b)

The sequence opens with a moderately strong easterly wave (vorticity of 24 x 10^{-6} sec^{-1}) well delineated by both curvature and shear. East of the wave axis the vertically upward, friction-driven velocities (shown at the 1000-mb level) are at their strongest, nearly 50 x 10^{-6} cb/sec (almost 0.5 cm/sec). Above, at the 850 and 700-mb levels vertical velocities are upward but weaker. This region is associated with an area of overcast, rain and showers which reaches to the southeast of Hispaniola. The curious aspect of this situation is the area of broken cloudiness followed by a second area of overcast well to the west of the wave axis. There is a detached area of weak updrafts at the 850 and 700-mb levels which coincides fairly well with this secondary weather area, and the frictionally driven upward velocities are prolonged in this direction along the axis of positive vorticity, (figure 7b) but they do not go to zero over central Cuba and the southern Bahamas. The southwestern quarter of the grid is mainly characterized by fair weather and scattered cloudiness under weak northeasterly air flow.

(2) August 25, 12Z (figures 8a, b)

The wave is less well marked by curvature of pattern and the 1000-mb vorticity has decreased to about a half of the value it had 12 hours previously. However, at the 850 and 700-mb levels there has been little change in vorticity, and the wave is delineated by both cyclonic shear and curvature. The bulk of the weather, i.e., overcast skies and showers,

occurs to the east of the wave axis where the 850-mb convergence is a maximum. The 1000-mb upward velocities (which are weak in any event) do not extend as far east and north as the cloud shield. However, both the 850 and 700-mb levels show upward velocities even to the east of the overcast. The extension of the northern edge of this overcast westward to the east central Florida coast is more difficult to account for although there is a weak field of 850-mb convergence in this region. The southwestern half of the grid is an area of scattered to broken cloudiness under very weak vertical velocities and weak low level divergences.

(3) August 26, 00Z (figures 9a, b)

The third synoptic time of this series is highlighted by the appearance of a closed low over northern Cuba with an increase of the 1000-mb vorticity field, while the vorticity at 850 and 700 mbs changes but little. However, the 850-mb convergence has increased to almost .5 x 10^{-5} sec^{-1}, and the magnitude of the vertical velocities has perceptibly increased. Maximum low level velocities are noted of from 40 to 50 (x 10^{-6}) cb/sec or about 0.5 cm/sec. The area of bad weather has expanded slightly and is located mainly east of what may be considered the old wave axis with considerable north-south extent. The 1000-mb vertical motions and the stronger vertical motions at 850 and 700 mbs would appear to delineate the bad weather quite well. Fair weather on the western third and eastern quarter of the grid accompanied weak to negligible vertical velocity and divergence fields.

(4) August 26, 12Z (figures 10a, b)

The vortex at 1000 mb is now located over the southern tip of Florida. Upward vertical velocities of 40 to 50 (x 10^{-6}) cb/sec, nearly 0.5 cm/sec, are to be found (at 1000 mb) northeast of the center.

The most severe weather occurred in this area as depicted in the lowest slab of figure 10a. Overcast conditions extend southeastward to north of Hispaniola in connection with extension of a rather strong field of 850-mb convergence northeast of the low. The northwestern portion of the grid has scattered to broken skies with some weather of a showery character in the northern Gulf of Mexico under weak fields of vertical motion, convergence and vorticity. The southwest portion has only scattered cloudiness marked by anticyclonic vorticity.

(5) August 27, 00Z (figures 11a, b)

The low has moved up the Florida east coast and is situated near Cape Kennedy. Vorticity associated with the center (figure 11b) has increased at 1000 mb and upward motion is slightly more pronounced. Once again upward velocities at the 850 and 700-mb levels extend further east of the low in the convergence field at 850 mb than do the 1000-mb upward velocities. The former agree quite well with the extensive area of bad weather east and northeast of the low. A southern extension of the bad weather through eastern Cuba is accompanied by very weak upward velocities and southern extensions of the convergence and cyclonic vorticity fields. A relatively unusual feature of the series was the relatively strong downward motions and divergence at 850 and 700 mb on the southeast portion of the grid. Generally fair weather characterized this area. On the western side, cloud cover was mostly broken under weak fields of vertical motion and divergence.

(6) August 27, 12Z (figures 12a, b)

The low is off Jacksonville and is at the strongest stage of this series. Frictional omegas reach more than 80 ($\times 10^{-6}$) cb/sec or almost 1 cm/sec. Both the 850 and 700-mb upward velocities have also increased

in magnitude. Weather in and particularly east of the center is overcast with showers and squalls. The southeastern grid area has mainly broken cloud cover with preponderantly downward vertical motion at lower levels. The western quarter of the grid enjoys scattered cloudiness under weak diagnostic fields.

Summary of Sequence #2

This strong easterly wave-tropical low series shows the gradual increase in magnitude of the vertical motions as the wave becomes a closed center. Despite weaker velocities initially, the weather coincides reasonably well with regions of upward motion in the lower levels. Broken cloudiness may be associated with weak or indifferent fields and scattered clouds usually require some definite signs of subsidence.

c. Sequence #3, August 3-5, 1963

The easterly wave in this series is rather poorly marked at 1000 mb at the start. However, at the 850 and 700-mb levels, it appears about as strong (vorticity about 3×10^{-5} sec^{-1}) as the wave considered in the previous sequence. In the early period it follows much the same path as the other wave and at the lower levels appears to be of comparable strength. The wave fails to deepen significantly as upward vertical velocities fail to grow larger and the area of bad weather remains relatively restricted.

(1) August 3, 00Z (figures 13a, b)

The weak 1000-mb wave over eastern Hispaniola gives rise to exceedingly weak frictional omegas. Nevertheless, the weather over eastern Hispaniola and Puerto Rico appears to be in response to the 1000-mb upward omegas plus the weak support they find at 850 and 700 mbs. This is also the area (at 850 mb) of strongest cyclonic vorticity and

convergence. Thundershowers are also occurring over the Florida peninsula presumably as a result of diurnal heating. Elsewhere the weather is generally fair with weak descending currents and with some widely scattered shower activity over the western Caribbean.

(2) August 3, 12Z (figures 14a, b)

The low-level frictionally driven velocities have more than doubled as the low-level definition of the wave sharpens and the cyclonic vorticity increases. Supporting upward motion is found at the 850 and 700-mb levels in the compact mass of showers and overcast around Hispaniola. This is just about the only significant bad weather area on the grid. Over western grid sectors there is descending air at 850 mbs with generally similar motion at the levels above and below. This district is characterized by fair weather with mostly scattered but some broken cloudiness and one report of lightning with rain in sight over the Gulf of Mexico. It is the most extensive fair weather area seen on the grid yet.

(3) August 4, 00Z (figures 15a, b)

The wave has progressed to eastern Cuba and Jamaica and is reasonably well delineated with upward "frictional velocities" reaching 30 ($\times 10^{-6}$) cb/sec or about .25 cm/sec. Similar upward velocities occur at 700 mb with somewhat smaller values in between. The major bad weather is well situated with respect to this area of rising air. Over the western third of the grid broken cloudiness maintains with scattered showers and thundershowers. For the most part these are occurring with very weak updrafts at 1000 mb and/or similar flows at 850 and 700 mb but with fairly strong divergence at 700 mb. Weather conditions seem slightly better over the eastern quarter of the grid where the indications are that weak downdrafts prevailed.

(4) August 4, 12Z (figures 16a, b)

The wave has progressed to east central Cuba. There is less bad weather and more good weather over the grid at this time than at any other map time considered. A small area of weak updrafts over and just north of eastern Cuba accompanies the limited region of overcast and showers stretching eastward from near the wave axis. This area extends a bit further to the east than the weak low-level upward motions accompanying the wave might suggest. In part the eastern portion may have been due to diurnal shower activity over the Cuban land mass which could be associated with the weak circulation characteristics. The eastern grid area showed mostly fair weather with weak descending motion at 700 and 850 mb over portions of the area but mostly weak upward frictional omegas at 1000 mb.

(6) August 5, 12Z (figures 18a, b)

The final maps in the series show the weakened wave over western Cuba. A small area of overcast and showers accompanies the very limited area of weak upward motion at the two lowest levels. Again the bad weather area is prolonged a bit farther east than might be anticipated. The excessive downward motions over the extreme eastern grid at 850 mb are due to the previously cited difficulty occasionally encountered in computing the static stability on the edges of the grid. The weather over the eastern half of the grid is scattered to broken with a very few showers which occurred mainly along with some updrafts suggested at 1000 mb. Weather over the southern third of the grid was mainly fair under low-level downdrafts.

Summary of Sequence #3

The last sequence, that of a weakening easterly wave, shows significant weather occurring over very limited regions. This region is usually in and to the east of the wave axis and in an area of weak upward motion. The bad weather area tends to become more restricted as the wave weakens. The area of fair weather increases but not necessarily because of stronger more persistent (through a deep layer) downdrafts. All in all the weather seems satisfactorily located with respect to the focal point of our interest, the easterly wave, and, despite the size of the velocities involved, the lower level vertical motions taken together appear to indicate where significant bad weather is occurring. These results may be compared with those obtained by Lateef (1967) using a kinematic approach. It is our opinion that our low level vertical velocities are somewhat better located with respect to the weather than those obtained kinematically.

B. Heating Effects

Since the latent heating has such an important influence on the vertical motions, it is of some interest to examine the thermal changes which are called for by the model. The changes were studied by manipulating the thermodynamic equation so that thickness changes (or temperature changes) are expressed in terms of the mean virtual temperature change expected over a 12-hour period if thickness changes occurred as called for by the model. The layers are taken to be 300 mb deep so there is an overlap between adjacent levels. We consider

$$\Delta\overline{T}_{*} = \frac{\Delta P \Delta t}{R \ell n P_2/P_1} \left[\overline{\vec{V}\cdot\nabla\Phi_p} + \overline{\omega\sigma} + \overline{\frac{R}{C_p P}\frac{dQ}{dt}}\right]$$

where ΔT_{*} is the mean virtual temperature change over the 300-mb layer,

and the quantities under the bar are assumed to be constant (or representative) over the 300-mb layer as well as the 12-hour time period. (This latter assumption is made only to gain a feeling for the magnitudes involved.) We evaluate each of the 3 terms on the right-hand side (the horizontal advection of thickness, the changes due to vertical motion, and the latent heating itself). The sum is also computed to indicate the overall effect.

1. Sequence #1, October 1956

We have seen that Sequence #1 has the strongest vertical motions of the situations studied thus far. It also has the strongest latent heating. In general, the maps of the heating for this sequence are fairly similar. Consequently, only one presentation of the heating effect is made - that for October 14, 1956, 03Z (figure 24). Only interior grid points have been portrayed and from left to right about the gridpoint are graphed the changes due to: horizontal advection of thickness, latent heating, the net total (plotted just to the right of the gridpoint), and vertical motion. Tick marks indicate intervals of one degree Celsius heating (up) or cooling (down) in 12 hours.

Both the latent heating and the adiabatic compensation terms frequently give rise to changes of the order of 4° to 5°C in 12 hours in the centers of vertical motion. However, under normal conditions, they must be of opposite sign. The equivalent temperature change accompanying horizontal thickness advection is usually small but on occasion amounts to a degree or two. (For simplicity, changes of 0.6°C or less per 12 hours are not plotted at all.) The overall picture is one in which the dominant terms tend to cancel one another, and the net is a rather small residual. Since the latent heating term is so large, it is somewhat

Figure 24. Terms in the thermodynamic equation for October 14, 1956, 03Z. Across each grid intersection are arrayed in order the following terms: latent heating, horizontal thickness advection, (then to the right of the intersection) the net change or sum of all contributions, and, on the extreme right, the vertical advection or adiabatic compensation. Ticks to the left of each hollow bar indicate mean virtual temperature change rates of 1°C per 12 hours over a 300-mb thick layer centered on the level in question. Temperature rises are plotted above the line and falls below. The most interesting thing about these terms is the fact that although the horizontal advection may be appreciable, it very seldom equals 2°C/12 hours; the latent heating and vertical advection may equal 4 to 5°C/12 hours, yet the combinations are so balanced that the net computed change (just to the right of the grid point) is seldom as large as 1°C/12 hours.

2500 m.
4000 m.
5500 m.
7000 m.
8500 m.

reassuring to find adiabatic compensation, but it is a little disconcerting to find the compensation so complete. These results, at first glance, would seem to imply that it would be difficult to account for the upper level warming known to accompany hurricane formation (Hawkins and Rubsam, 1968) using the Kuo (or modified Kuo) parameterization of the release of latent heat. However, it seems more likely that the grid-scale (200 km) used in this study is probably too large to measure the large convergences needed for rapid heating.

These results were common to the entire October sequence. The maximum net temperature changes called for by the model in the area of strong vertical motions were less than .5°C per 12 hours. Heating rates greater than this have certainly been observed during hurricane genesis. On the other hand, the changes in temperature which occurred during the October sequence (not shown) were generally small, and the reliable ones were not out of keeping with the calculated.

2. Sequence #2, August 1962

Sequence #2 offers few surprises. The horizontal thickness advection is similar in magnitude to the October series. However, both the vertical motion and the latent heating terms are small. No term exceeds 1.6°C in 12 hours until the last synoptic time. On this latter occasion, as the storm intensifies, both the vertical motion and the heating term have maximum absolute values between 2° and 3°C per 12 hours. Thus, in this sense also the August 1962 sequence provides a bridge between the strongly disturbed and the more moderately disturbed states.

Figures 25 and 26 for August 25, 12Z and August 27, 12Z 1962 provide a comparison of the transitional with the moderately disturbed state. The vertical temperature scale has been expanded for the earlier time

when magnitudes were so small. The adiabatic compensation for the release of latent heat continues to be the rule with the net effect of all terms at any gridpoint quite small, almost always less than 1.0°C/12 hours.

3. Sequence #3, August 1962

As may be anticipated, the final sequence had only two occasions where changes of 1.0°C/12 hours or greater were indicated. Since these occurred near the border, there may be some doubt of their validity. The advective changes were much the same as before, perhaps a little smaller with the weaker winds. Since the vertical velocities were small, so was the adiabatic compensation. The frictional velocities were weak, so the latent heating was also weak. On an expanded scale, figure 27 presents the temperature-change data for August 3, 1963 at 12Z.

C. Vorticity

Study of the vorticity budget was undertaken after some preliminary consideration of the following. Usually vorticity verifications are not made rigorously point by point nor are point values felt to be necessarily representative. We made a number of trials using one-sided differences, averages of 2 tendencies 12 hours apart, and centered differences. These were tested on a point by point basis and also after use of the 9-point Shuman smoothing routine. We felt the most representative values and possibly the most conservative values were obtained by using smoothed, centered differences. For this reason, the correlation figures we use here and the mean absolute values will be derived from smoothed tendencies.

Figure 25. Terms in the thermodynamic equation for August 25, 1962, 12Z (see legend figure 24). The tick marks in this figure represent 0.25°C/12 hours so the heating rates are much smaller than in figure 24. Net cumulative heating is still small so that even the weaker individual terms nearly compensate one another on this not very active day (see figure 8a).

2500 ft.
4000 ft.
5500 ft.
7000 ft.
8500 ft.

Figure 26. Terms in the thermodynamic equation for August 27, 1962, 12Z (see legend figure 24, but note the tick marks represent temperature change rates of 0.5°C/12 hours). The slowly intensifying system has given rise to increasing vertical velocity maxima and larger latent heating rates than in figure 25. Net calculated changes remain small.

2500 ft.
4000 ft.
5500 ft.
7000 ft.
8500 ft.

Figure 27. Terms in the thermodynamic equation for August 3, 1963, 12Z (see legend figure 24, but note the tick marks represent temperature change rates of 0.5°C/12 hours as in the preceding illustration). The very small size of the bars is indicative of the lack of significant developments and vertical motions on this relatively quiescent day (reference figure 14a).

2500 ft.
4000 ft.
5500 ft.
7000 ft.
8500 ft.

1. The Average Magnitude of Terms in the Vorticity Equation

As indicated earlier, the model was coded in such a way that the individual terms in the vorticity equation were computed and could be presented separately. Figures 28, 29 and 30 show the mean absolute values for each term (after smoothing) plus the mean absolute value of their sum and the observed. The "instantaneous" tendencies have been evaluated for the change in vorticity which would occur if the rate of change which we computed persisted for 12 hours, and it is these values to which reference is made. The observed tendency (for 12 hours) is obtained by subtracting vorticity values (after smoothing) over two maps 24 hours apart and dividing by two. These 'tendencies' are compared with the tendencies (evaluated for a 12-hour period) obtained at the map time midway between the original maps used to derive the 24-hour changes.

a. October, 1956

There are two centered verification periods possible in the October sequence and they occupy adjacent synoptic times separated by 12 hours. The average absolute value of the terms for each of these times is shown in figure 28. The graphs show quite clearly that the term representing the horizontal advection by the total wind greatly exceeds all other terms except at the 1000 and 100 mbs. The next most important term is usually the divergence term which slightly exceeds the advective at 100 mb (and once at 1000 mb) but, at the interior levels, is generally significantly smaller than the advective. This result is in agreement with our scaling of the vorticity equation in Appendix A where deliberate underestimates of the coriolis parameter led to divergence term estimates similar to those for the vertical advection and twisting terms, but notice was made that we should expect the divergence term to be on the average

larger than the vertical advection and twisting terms. The vertical advection and twisting terms are, on the average, quite small, i.e., almost an order of magnitude less than the advective terms. However, even on the average, these terms equalled or exceeded the divergence term at 400 mb and were not an order of magnitude less than the advection term.

The sums of the individual terms for the computed tendencies tend to exceed the observed at just about all levels. There is no ready explanation for this difference which, we will see, is also common (but to a lesser extent) to particularly the lower levels of the other sequences. There was some indication that the large October vortex (which was moving very slowly) was somewhat erratic in motion and that the 24 hours tendency evaluation was over too long a period. Thus, it may be dangerous to conclude that the advective term will be a gross overestimate in other strong circulation situations.

b. August, 1962

Sequence #2 shows many of the same general characteristics (figure 29) as the October series. The advective term exceeds the divergent at all levels on all occasions and exceeds the observed (with one exception) at level 700 mbs and lower. At 550 mbs, the advective term, the net sum of terms and the observed are closely grouped. At 400 and 250 mbs the observed exceeds the advective and the computed. The net sum tends to be dominated by the advective term except at 400 mb where advection appears to be at a minimum and, to a lesser extent, at 1000 mb where the divergence term is at a maximum. The vertical advection and the twisting terms remain quite small on the average and seldom exceed a change of 2×10^{-6} sec^{-1} in vorticity for the 12-hour period.

Figure 28. Average absolute value of terms in the vorticity equation for October 14, 1956, 03 and 15Z. The various terms are designated: A, horizontal advection; D, divergence term; V, vertical advection; T, twisting term; C, the computed sums of terms; O, the observed. Evaluation is made after space smoothing the grid-point values in all cases. All values are tendencies expressed in units of vorticity change in 12 hours, i.e., 10^{-6} sec^{-1}/12 hours. The observed values are computed by taking the 24 hour vorticity changes centered on the synoptic times and dividing by 2 (after space smoothing). No vertical advection and twisting term evaluations are made at 1000 and 100 mbs.

At levels other than 100 and 1000 mbs, the horizontal advective term tends to dominate and is usually twice the divergence term. The computed tendencies were larger than the observed in absolute magnitude at all levels with the excess diminishing with elevation.

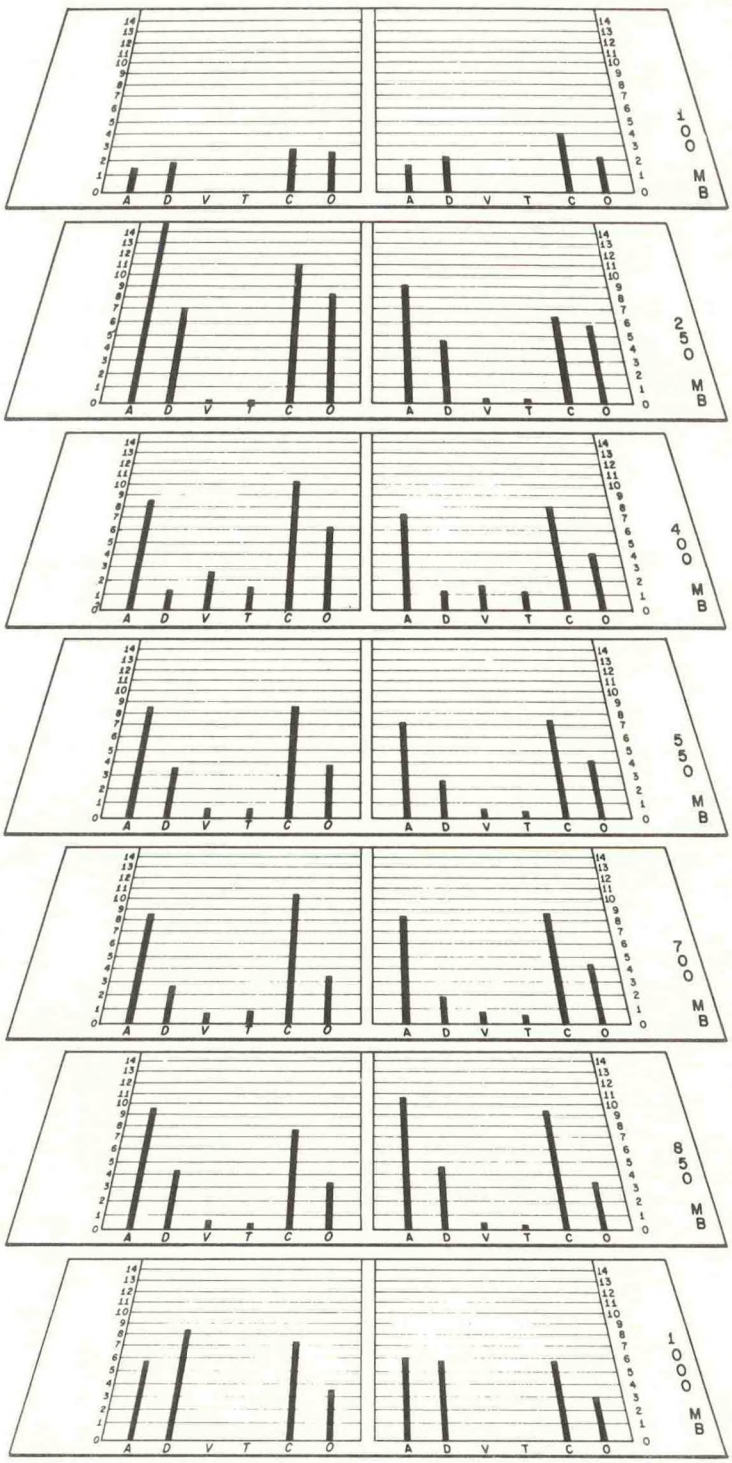
100 MB
250 MB
400 MB
550 MB
700 MB
850 MB
1000 MB
A D V T C O
OCTOBER 14, 1956
0300 GMT
OCTOBER 14, 1956
1500 GMT

Figure 29. Average absolute value of terms in the vorticity equation for August 25, 12Z, to August 27, 00Z, 1962 (see legend figure 28). The magnitude of the vorticity changes observed is quite similar to that noted in the 1956 sequence (cf. figure 28). In the present sequence the horizontal advective term is even more dominating than before (at all levels). However, the computed tendency does not consistently overestimate the observed tendency except at the lower levels and even at these levels the overestimates are not particularly large.

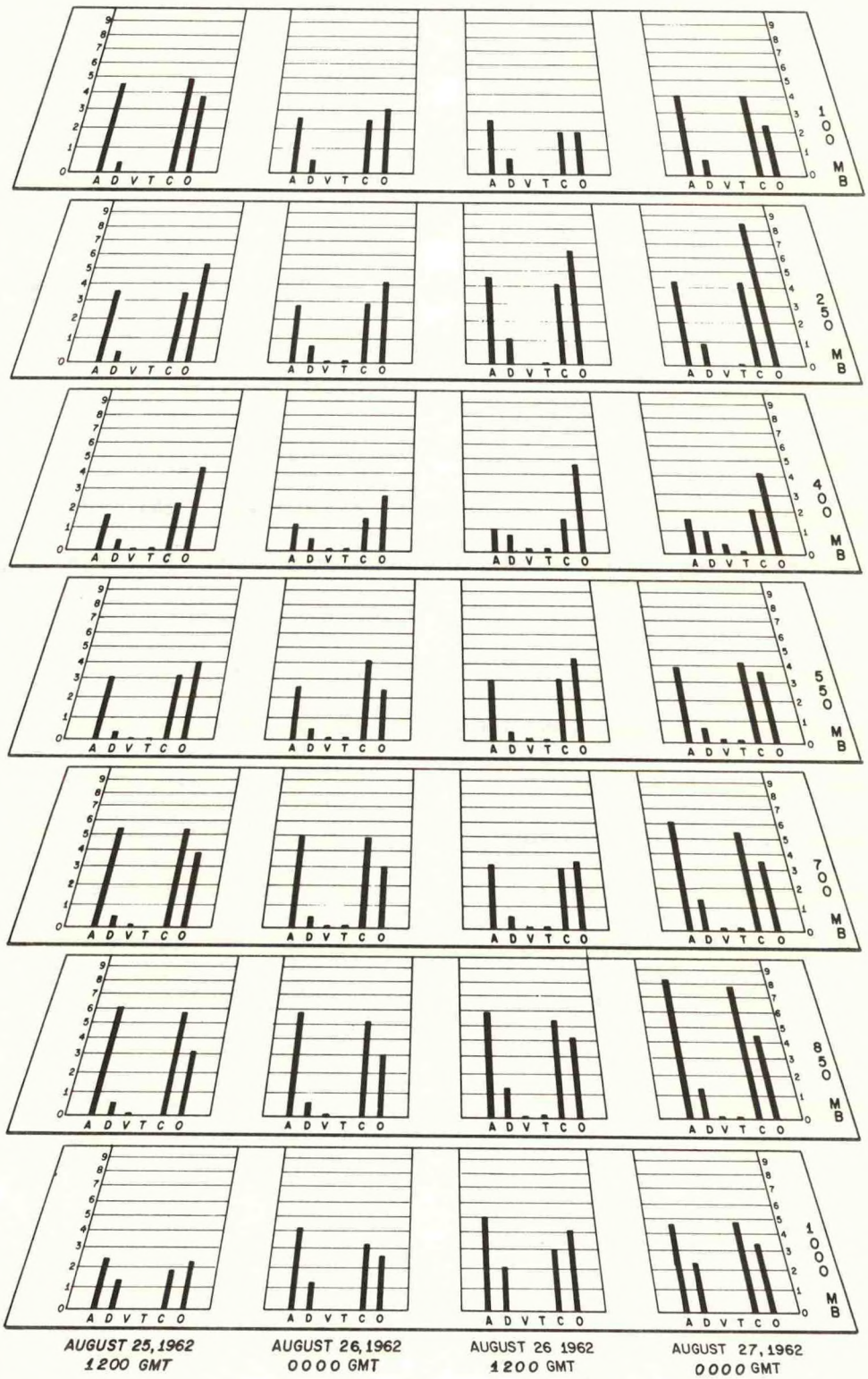
A D V T C O
100 MB
250 MB
400 MB
550 MB
700 MB
850 MB
1000 MB
AUGUST 25, 1962
1200 GMT
AUGUST 26, 1962
0000 GMT
AUGUST 26 1962
1200 GMT
AUGUST 27, 1962
0000 GMT

c. August, 1963

Sequence #3 has been described in a number of contexts as the weakest of the three series. The low level statistics of figure 30 bear this out; the vorticity changes are indeed small at the four lower levels. However, at 250 and 400 mbs the changes are quite sizeable, averaging almost 10^{-5} sec^{-1} for the 12 hours. The advective term dominates again and is more consistently separated from the divergence term. The latter term is almost everywhere small (as was the divergence itself) and closely approaches the magnitude of the vertical advection and twisting terms. Lateef (1967) found very similar relationships in his evaluation of the vorticity equation for this series. On the whole, the magnitudes of the advective and net sum terms are reasonably related to that of the observed. They tend to exceed the observed at 1000 and 850 mbs but not markedly. At higher levels the magnitudes are quite comparable.

The most interesting part of this phase of the work was the realization that the advective term was, on the average, of such overwhelming importance. One might have presupposed that the divergence term would be of lesser importance, since the low-latitude divergence on a synoptic scale has usually been found to be small. But the general dominance indicated in these samples is most impressive. The maximum observed (and forecast) vorticity changes that occurred at 250 mb (where the winds and vorticity tend to be at a maximum) was caught by the advective term although the divergence term was quite significant here in the October case. In the August 1962 series the advection failed to rise to the requisite heights and the observed tendencies at 250 mb were underestimated.

2. Individual Values of Terms in the Vorticity Equation

In the preceding section we have dealt exclusively with the mean magnitude of the terms in the vorticity equation and these have been space smoothed for the presentation. While this is relevant when considering certain aspects of the matter, it is not necessarily informative as to whether individual or groups of individual values become sizeable enough that they should be retained for inclusion in a model despite the fact that their average magnitude is small. This information can only be gathered by examination of the individual maps.

Such an examination shows that there are times and areas where the vertical advection and the twisting term do contribute significantly to the calculated tendency at a given level. One such example is presented in figure 31 which presents the unsmoothed grid point values for each term on the right-hand side of the vorticity equation for October 15, 1956, 03Z. (The terms are plotted about the grid point in the following order: vertical advection, horizontal advection, twisting and divergence.) We can see that at 400 mb, for instance, the twisting term has a (12-hour) value of 2×10^{-5} sec^{-1} over a considerable area at the 400-mb level. At 700 mbs the vertical advection term reaches a peak of 1.6×10^{-5} sec^{-1} per 12 hours. The lengths of the other bars at these grid points indicate that these would both be contributions of some significance. Other days of this same sequence had maximum "minor term" values approaching the one illustrated here but none equalled it. The August sequences were generally of lesser magnitude, and even in the strongest of the transitional series (August 27, 12Z) both the vertical advection and twisting terms fell far short of effecting a 12-hour vorticity change of 10^{-5} sec^{-1}. Thus, we tentatively conclude that for

Figure 30. Average absolute value of terms in the vorticity equation for August 3, 12Z to August 5, 00Z, 1963 (see legend figure 28). This is the least disturbed of the sequences considered. Observed vorticity tendencies are quite small at lower levels (around 2 or 3 x 10^{-6} sec^{-1}/12 hours) increasing to more than twice that magnitude at 250 mb. Except at the very lowest level, the advective term is by far the dominant term. Its magnitude compares well with that of the observed tendency as does that of the computed tendency.

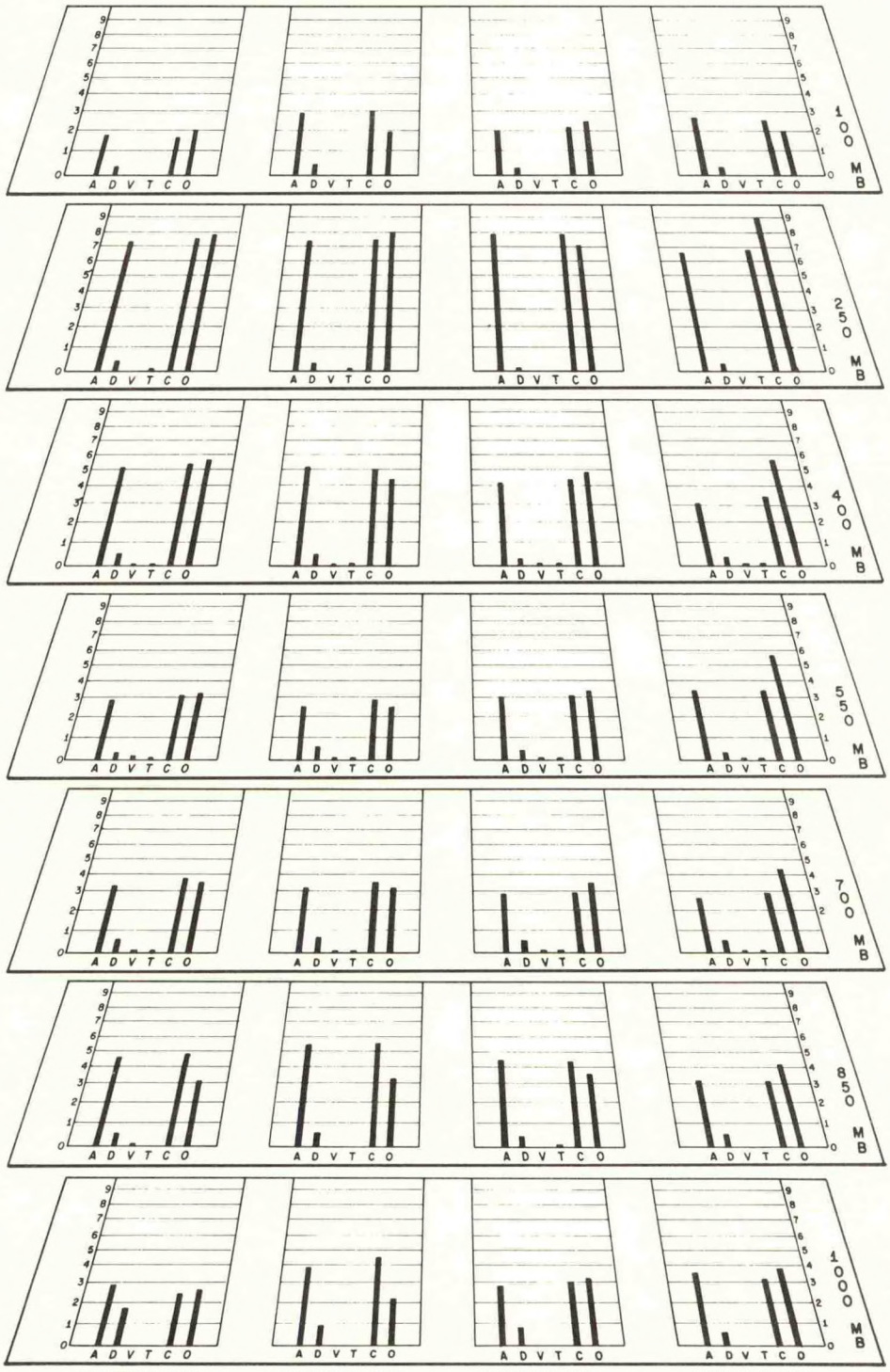
A D V T C O
100 MB
250 MB
400 MB
550 MB
700 MB
850 MB
1000 MB
AUGUST 3, 1963
1200 GMT
AUGUST 4, 1963
0000 GMT
AUGUST 4 1963
1200 GMT
AUGUST 5, 1963
0000 GMT

Figure 31. Individual unsmoothed terms in the vorticity equation for October 15, 1956, 03Z. The terms are arranged across the grid intersections from left to right: vertical advection, horizontal advection (both to the left of the intersection), and then, the twisting term and divergence term. One tick mark corresponds to a vorticity tendency of 25×10^{-6} sec^{-1}/12 hours; above the line indicates increasing cyclonic vorticity.

The example was chosen to illustrate that on occasion the twisting and vertical advection terms can significantly influence the computed tendency. This is shown here at the 400-mb level. It should be noted that the horizontal advection and divergence terms were exceptionally small and the total tendency was small, hence the significance of these occasions may be doubtful.

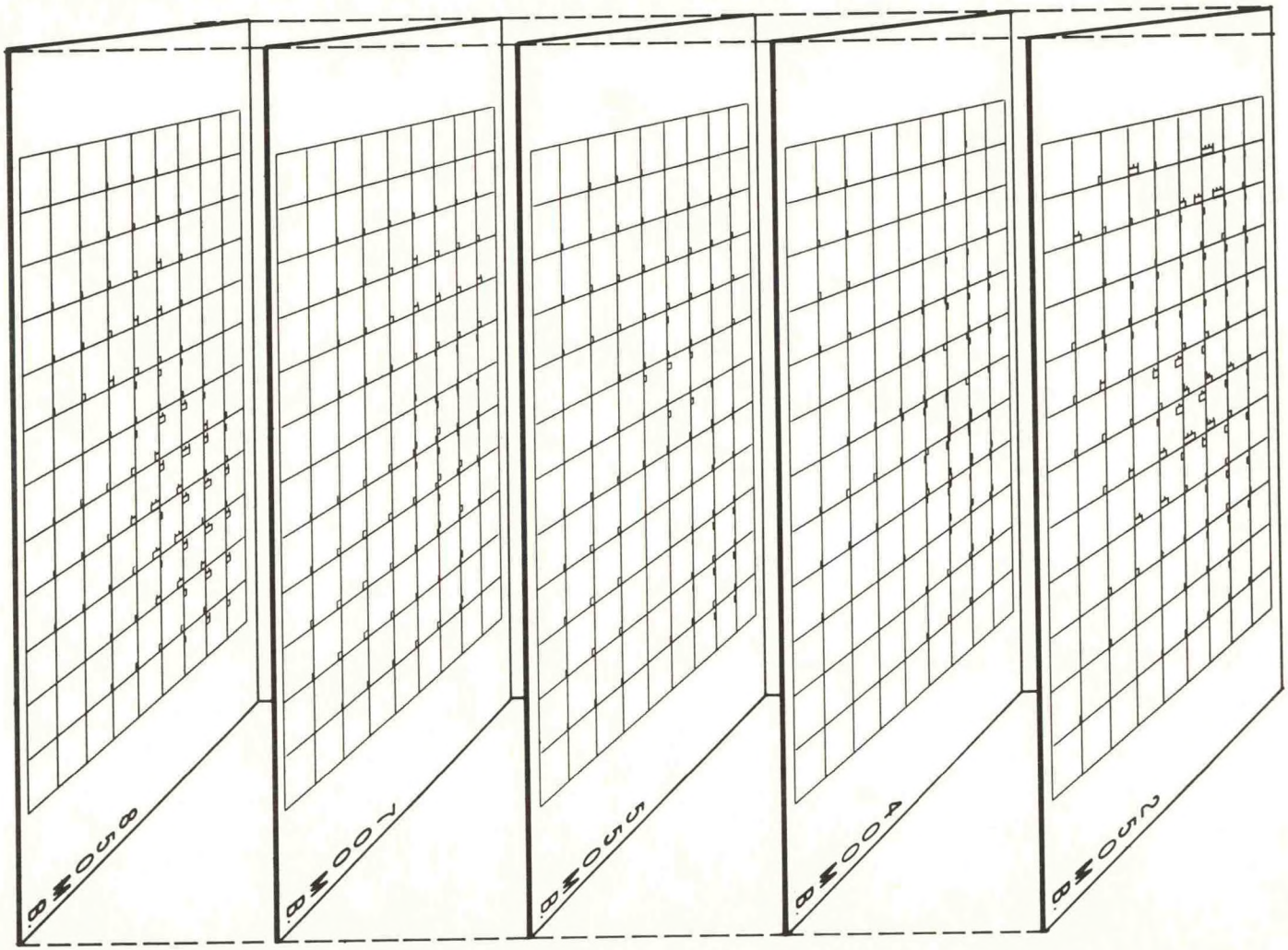

Figure 32. Correlations of the computed and the observed vorticity tendencies. The observed tendencies were time centered differences and both the computed and observed were space smoothed before correlation. Correlations appear to be poorest for the 1956 sequence, the most active situation; they were best for the most quiescent situation, 1963, and were intermediate for the transitional sequence of 1962.

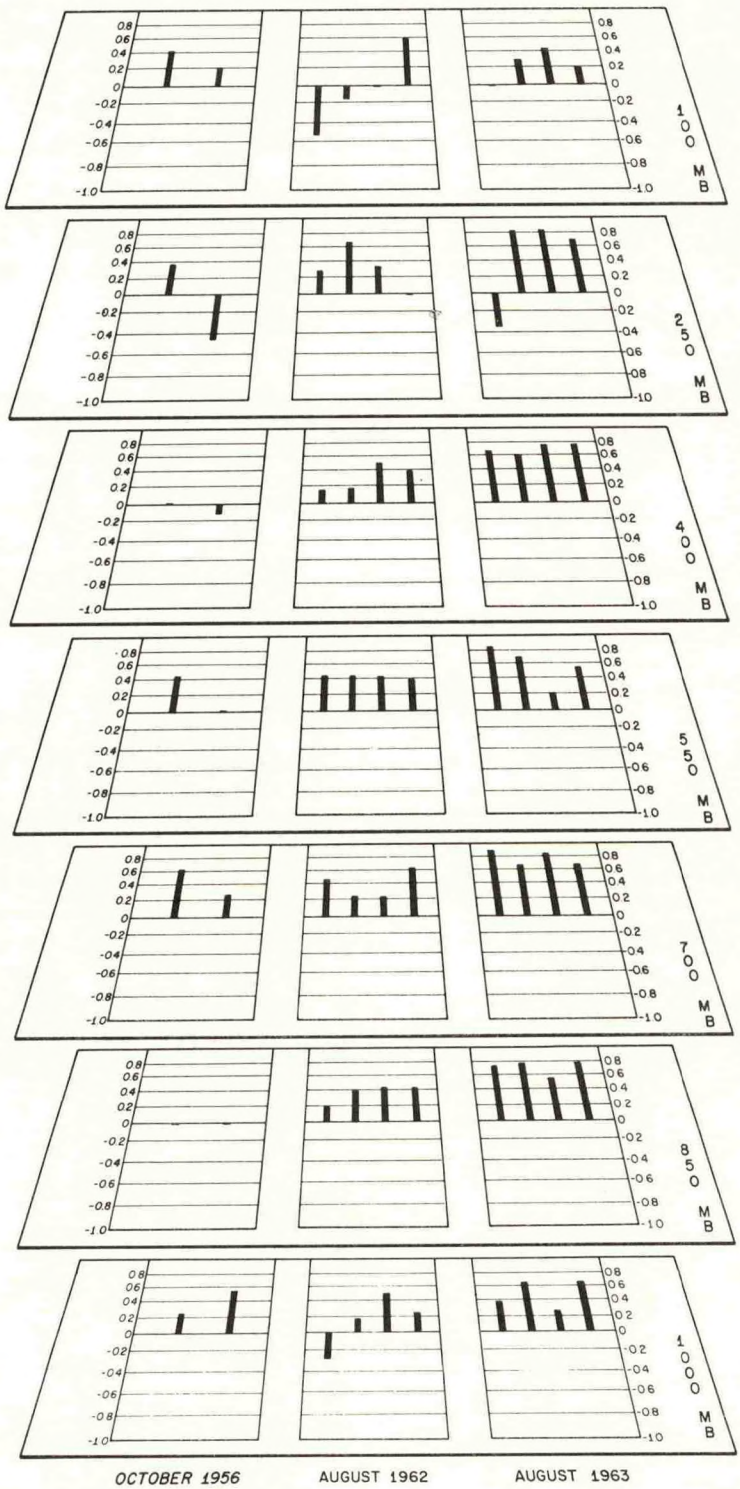
0.8
0.6
0.4
0.2
0
-0.2
-0.4
-0.6
-0.8
-1.0
1000 MB
250 MB
400 MB
550 MB
700 MB
850 MB
1000 MB
OCTOBER 1956
AUGUST 1962
AUGUST 1963

the average easterly wave or incipient vortex the vertical advection of vorticity and the twisting term are seldom, if ever, important. However, for closed vortices with marked synoptic scale vertical motions, they may, on occasion, make significant contributions.

3. Correlations of Calculated and Observed Vorticity Tendencies

We have already commented on characteristics of the terms in the vorticity equation with regard to their average magnitude and to their variability. We next take up the question of their accuracy, i.e., how well do they or their sums correlate with the observed. Figure 32 presents the correlation statistics for the 10 cases for which centered difference calculations were possible.

The most striking fact about the correlations is that the weakest situation, August 1963, has the best over all correlations. The second best correlations are less easily decided but may go to the transitional case, August 1962. Results for the 1963 sequence are quite comparable to those obtained by Lateef (1967, table 4) despite differences in models and evaluations. While differences due the analysts cannot be ruled out a priori, we have found that the analyses have had many common characteristics, i.e., dominance of the advective term, poor correlations of diagnostic to kinematic divergence, too large estimates (kinematically) of the divergence, etc. Consequently, it is deemed unlikely that these differences are due principally to the analytical skills of their authors.

It may be that the relatively steady uniform motion of features at their various levels in August 1963 was mainly produced by horizontal advection and was fairly well explained by this term alone. We have already pointed out that the 24-hour evaluation period for October 1956 may have been too long. Investigation showed the 12-hour changes were

of the same magnitude or, on occasion, bigger than the 24-hour; in some instances the tendencies reversed from one 12-hour period to the next. Nevertheless, it seems worthwhile to investigate the 'errors' in light of another process which must be present.

4. Study of Tendency Errors

We have seen in the preceeding section that the computed vorticity tendency, when related to the observed vorticity tendency, correlated most poorly in the sequence which had the most marked convection. Now there are any number of reasons why the correlations might be low including the time span used to evaluate the 'instantaneous' tendencies, irregular motion of the vortex, faulty parameterization of the latent heat release etc., etc. (The possibility that systematic errors in the divergence fields might be associated with the 'errors' was examined at some length but no apparent relation could be gleaned from comparison of maps of these parameters, and correlation studies revealed no meaningful relationships.) Nevertheless, the fact that the correlations are lowest when convection is the strongest suggests there may be a possible connection between the two.

The suggestion is made, therefore, that possibly the local vorticity changes are being modified by the cumulus activity. It seems obvious that strong convection must transport low-level values of vorticity upwards. The descent takes place on a larger scale and a downward mixing of vorticity is less obvious and more questionable, i.e., it is presumably slower and on a larger scale. Gray (1967) has emphasized the significance of cumulus transport of momentum in hurricanes and elsewhere in the tropics. So, the question is: can a relation be found between the vorticity tendency errors and the convective transport of vorticity upwards?

Figure 33. Correlations of the error (computed minus observed) in vorticity tendency with a measure of the effect of cumulus transport of vorticity in the vertical. At each point where the upward vertical velocity exceeded 10^{-7} cb/sec the vorticity difference between 1000 mb and the level in question ($\zeta_{1000} - \zeta_K$) is weighted by the frictionally forced ($-\omega_H$) and scaled by a factor S; these points are filed in an array and correlated with the "error" at those points. The number of points selected by this criterion is tabulated below the bar for that level. Negative correlations show that cumulus transport parameterized in such a fashion would help to account for the error in vorticity tendency.

The only indications of a significant relationship are in the lower levels of the most active sequence, 1956. The other more quiescent sequences do not show a meaningful relationship.

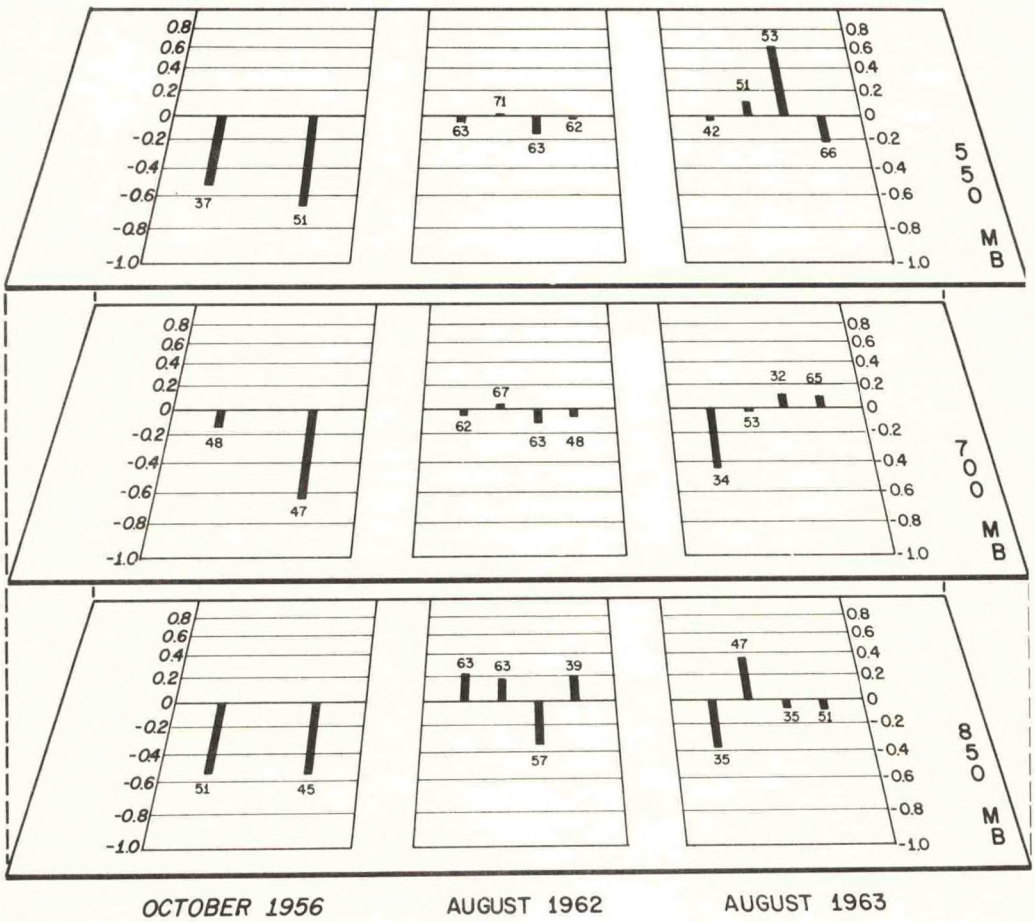
0.8
0.6
0.4
0.2
0
-0.2
-0.4
-0.6
-0.8
-1.0
37
51
71
63
63
62
53
51
42
66
550 MB
48
47
67
62
63
48
32
65
53
34
700 MB
51
45
63
63
39
57
47
35
35
51
850 MB
OCTOBER 1956
AUGUST 1962
AUGUST 1963

A number of different schemes were evaluated in testing this hypothesis. Results varied but not a great deal when the schemes were reasonably similar. One of the better ones is also the simplest and most direct and is presented here. There are a number of basic assumptions involved in this approach:

a. That significant convection occurs only when the synoptic scale vertical motion is directed upward and exceeds a certain amount in this case taken to be 10^{-7} cb/sec.

b. That the convective transports draw most heavily on the lowest level, i.e., the 1000-mb level, and that vorticity being carried up will be closely related to the 1000-mb vorticity values.

c. The net effect at any level is proportional to the vertical gradient of vorticity between that level and the 1000-mb level and

d. That this effect may be weighted by the frictionally induced vertical velocity assuming that the result will be proportional to the intensity of the cumulus activity which is closely related to the synoptic scale vertical motion in the boundary layer.

Following this line of reasoning, correlations were run between the vorticity tendency errors, $\zeta_t\Big|_{error} = \zeta_t\Big|_{calc} - \zeta_t\Big|_{obs}$, and $(\zeta_{1000} - \zeta_K)(-\omega_H)S$ where S is a scaling factor. Points were selected only where the upward vertical velocity exceeded 10^{-7} cb/sec. When the formulation is posed in this fashion, negative correlations indicate that the hypothesized effect of cumulus transport <u>does</u> help to account for the errors in the vorticity tendency. Figure 33 presents these

correlations for all of the sequences and also shows the number of grid points which contributed to each correlation.

It is immediately apparent that the largest, most consistently negative correlations are those for the 850, 700 and 550-mb levels of October 1956. Values here ranged from -.65 to -.52 with one -.12. In contrast, the same levels for August 1963 range from -.44 to +.62 and 5 out of 12 of the correlations are positive. The August 1962 correlations may be classified as intermediate. They are mostly small and do show a tendency to turn negative as the period progresses. But their magnitude precludes any definitive statement. It is unfortunate that no centered verifications are possible for August 27, at 12Z when the convection was beginning to approach that of October.

It is, of course, impossible to conclude from this small sample of data whether this effect is real. Similarly, it is impossible to claim that it is significant. Nevertheless, the effect is in the desired direction and is supported by a reasonable hypothesis. It would appear to be a matter worthy of further consideration.

VI. CONCLUSIONS AND RECOMMENDATIONS

A. General Summary

Our diagnostic model has been applied to three different sequences which offered a reasonable sample of Caribbean weather. We find the stronger vertical motions to be of the order of centimeters per second in the most intense of these disturbances and a tenth of this value in the weakest system considered. In view of the cumuliform nature or origin of most of the cloudiness at these latitudes, we have reasoned that grid-scale vertical velocities of this magnitude are quite acceptable. The cumulus scale motions will be of course sensibly larger.

These velocities were achieved by utilizing an idealized release of latent heat which depended on the normal tropical humidities and was driven by a parameterized expression of surface friction. A heuristic rationale has been offered for this approach. The inclusion of frictional effects increases the central updraft velocities up to 50% in strong systems while the inclusion of latent heating increases central updrafts by an additional factor of 2 to 5. The latter effect was particularly noticeable at 250 and 400 mb.

In obtaining the final vertical velocity, the "geostrophic omegas" were used as a first guess. These were not obtained from an independent height analysis but from contour heights obtained through the balance equation using a streamfunction computed from the wind analysis. These velocities were fairly simple to obtain compared to the more sophisticated omegas and were highly correlated with the "refined" omegas in a consistent

fashion. If one seeks only the vertical velocities and their derivative fields, it seems likely that the geostrophic omegas will satisfy most requirements. (This may not be true at even lower latitudes or if the situations have greater curvature or we consider a smaller scale.)

When the diagnostic vertical velocities are used to compute the associated divergence patterns, these are found to relate very poorly to the kinematic divergences. This characteristic was true of each of the three series and presumably does not reflect analytical skills. We found that the kinematic estimates came closest at the lowest levels where the data were most plentiful. However, the correlations decreased with altitude, and the kinematic estimates grossly overestimated the magnitude of the divergence on all occasions.

In the matter of testing the separate contributions of wind versus height analysis, no clear cut answer was possible. The data network is so sparse and the data of such quality that height analysis without recourse to the wind field is impossible; this renders the question almost academic. We have managed to demonstrate that one can ignore the height information and still derive vertical velocities, divergences, etc. that relate in a reasonable and meaningful fashion to the concomitant weather.

In developing the model, adequate reason was found to depart from the Kuo parameterization of latent heating. This, apparently, more realistic partitioning of the latent heat increased the heat release in the various atmospheric layers. In turn the additional heat release stimulated stronger upward vertical velocities in the center of updrafts. Despite the heat released (particularly at higher levels) which approached warming equivalent to 4 to 5°C/12 hrs., no such warming

occurred nor was demanded in the net computed effect. The vertical motion accompanying the heat release was just about enough to counteract the heating through "adiabatic" expansion. Thus the net heating calculated was a very small residual.

The vorticity budget was quite informative. In the weaker disturbances where divergence is small, almost all of the change can be attributed to advection. In stronger systems where the significant vertical velocities and divergences occur, then the divergence term can become quite important, even dominant. The vertical advection and twisting terms seldom become very large of themselves, but on occasion where the advective and divergence terms are weak they may contribute in a significant way to the vorticity change at that level. (These findings are not at variance with the scale analysis of Appendix A.) When one considers the relation between the observed vorticity change and the rate of change calculated diagnostically, it becomes apparent that the better correlations occur with the more quiescent atmospheric states, i.e., the smaller and weaker the disturbance, the smaller the divergence fields, and the more the horizontal advective term dominates the changes and accounts for the observed change. On the other hand, it is possible that these characteristics are simply a reflection of the fact that our estimates of vertical velocity and divergence may not be very good. In the strongly disturbed state we have seen that, at least up through the 550-mb level, there is evidence that the cumulus scale activity seems to be effecting vorticity changes which are proportional to the vertical gradient of vorticity (from 1000 mb to the level under consideration) multiplied by the frictionally driven omega at the top of the boundary layer. This is an interesting observation which, to our knowledge, has not been

documented in this fashion before, although Gray (1967) has studied analogous effects in hurricanes. It implies that in intensely convective situations the synoptic scale vertical velocity used to transport vorticity is too small and that the transport may indeed occur at something approaching cumulus scale velocities.

B. Suggestions for Future Research

There are a number of obvious avenues along which this work should be continued. The most obvious continuation is to expand the work to include the energetics of the perturbations in order to see if we can determine why and how one wave deepened and the other filled, etc. The next most pressing need is for an expansion of the grid to cover a greater area so that the boundary effects will be well removed from the area of major interest. After that, there are several desirable options which include: application to a wider variety of synoptic situations; specific inclusion and analysis of humidity, possibly as a check of the parameterization currently used; further examination of the vertical transport of vorticity due to intense and widespread cumulus action; experiments with less vertical resolution, i.e., one could drop the 850, 550 and 250-mb levels, retain the 1000, 700, 400 and 100-mb levels and compare the results obtained with those available from the current model; run the model using analyses provided by one or more of the objective analysis techniques now either available or becoming available.

At the present time tentative plans are being considered for a tropical weather "experiment" to be run in connection with the Global Atmospheric Research Program. If a truly dense data network does become operative and is not located too close to the equator, the application

of diagnostic models to the results will be most helpful in expanding our current knowledge of tropical weather systems.

ACKNOWLEDGMENTS

The author is grateful to Dr. Stanley L. Rosenthal who in the early stages of this work did much to encourage and shape the endeavor. Since the work was performed *in absentia* he very frequently served as a substitute figure for Dr. Noel E. LaSeur, my leading professor. Their guidance and suggestions have been most generous, always helpful and much appreciated.

The work was undertaken without previous experience in programming. Advice and assistance were graciously provided in various amounts by Messrs. Billy M. Lewis, James W. Trout, Peter P. Chase and W. James Koss when a programming problem exceeded accrued experience.

Acknowledgment must be made for the synoptic analysis presentations. The idea of superposing various atmospheric levels on one page is not original. But the superposition and pseudo-perspective is a unique development. Mr. Robert L. Carrodus was mainly responsible for the concept; its application to the Calcomp plotter was the work of Messrs. Billy M. Lewis and Eugene M. Page, carried out under the guidance of the author. A tremendous amount of material is presented on a given page and the interrelationship of various items is made visible at a glance. Also special thanks must be expressed to Mrs. Mary Jane Clarke who typed the final copy so beautifully.

In addition, two of the weather sequences examined in this investigation had been analyzed for other purposes by colleagues Mr. C. L. Smith and Dr. M. A. Lateef. They very kindly made the results of their analyses available to the author and in this manner contributed significantly to the scope of the present application.

Finally, I would like to acknowledge the continuing impetus provided by Dr. R. Cecil Gentry. He has conscientiously tried to make time available for me to carry out this work and has encouraged this effort unfailingly.

APPENDIX A

SCALE ANALYSIS

Definitions.

For the purposes of scale analysis we assume the following:

Horizontal scale $\equiv S \sim 10^6 m$

Vertical scale $\equiv H \sim 10^4 m$

Characteristic horizontal velocity $\equiv V \sim 10$ m/sec

Characteristic horizontal phase velocity $\equiv C \sim 10$ m/sec

Gravity $\equiv g \sim 10$ m/sec^2

Pressure $\equiv \pi \sim 10^2$ cb

Angular velocity of the earth $\equiv \Omega \sim 10^{-4}$ sec^{-1}
(but in tropics, $f \sim 10^{-5}$)

Mean radius of earth $\equiv a \sim 10^7 m$

Basic Relationships.

1. In considering u_x we treat the average value over a half wave length, i.e. $u_x \sim \frac{\Delta u}{S} \sim \frac{V}{S} \sim \frac{10}{10^6} \sim 10^{-5}$

and $uu_x \sim \frac{V^2}{S} \sim 10^{-4}$

2. $u_t \sim Cu_x \sim C\frac{V}{S} \sim 10^{-4}$

3. $\Phi_x \sim fv \sim fV \sim 10^{-5} \times 10 \sim 10^{-4}$

Magnitude Estimate for Omega.

We employ equation 3 from Chapter II:

$$\omega = -\frac{(\Phi_{pt} + \vec{V}\cdot\nabla\Phi_p + \frac{R}{C_P P}\frac{dQ}{dt})}{\sigma}$$

$$\Phi_{pt} \sim C\Phi_{px} \sim C(fv)_p \sim C\frac{fv}{\pi} \sim \frac{10\times10^{-5}\times10}{10^2} \sim 10^{-5}$$

$$V\cdot\nabla\Phi_p \sim V\Phi_{px} \sim V(fv)_p \sim \frac{V^2 f}{\pi} \sim \frac{10^2\times10^{-5}}{10^2} \sim 10^{-5}$$

$$\frac{R}{C_P P}\frac{dQ}{dt} \sim \frac{R}{C_P P} C_P (T_S - T) \frac{\omega_H q_H}{gN} \sim \frac{10^2}{10^2} \times 1 \times \frac{\omega_H q_H}{10N} \sim \frac{\omega_H q_H}{10N}$$

Now q_H and N must be observed to determine their scale, since they depend on the lapse rate of temperature and the distribution of moisture.

So, $q_H \sim 10^{-2}$ and $N \sim 10^{-2}$ by observation (see Appendix C).

$$\omega_H = \frac{\rho_H g C_d}{f}\left[(u\sqrt{u^2+v^2})_y - (v\sqrt{u^2+v^2})_x\right]$$

$$\sim \frac{\rho_H g C_d}{f}(uV_y + Vu_y - .....)$$

$$\sim \frac{\rho_H g C_d}{f}\left(\frac{V^2}{S} + \frac{V^2}{S} - ....\right)$$

$$\sim \frac{10^{-3}\times 10\times 10^{-3}}{10^{-5}}\left(\frac{10^2}{10^6} + \frac{10^2}{10^6} - ..\right) \sim 10^{-4}$$

where $C_d \sim 10^{-3}$ empirically.

Consequently, $\frac{R}{C_P P}\frac{dQ}{dt} \sim \frac{\omega_H q_H}{10N} \sim \frac{10^{-4}\times 10^{-2}}{10\times 10^{-2}} \sim 10^{-5}$

Therefore, $\omega \sim 10^{-5}/\sigma$

The static stability, σ, cannot be estimated by scaling alone since it is a function of the lapse rate of temperature and moisture in the atmosphere. We have computed σ for each of the internal levels of the model at each synoptic time. The values range from about unity at 850 mb to almost 20 at 250 mb. Since we have used a low estimate for f (10^{-5}, rather than 5×10^{-5} which is applicable at 20°N) we will use a small static stability, i.e., unity, to partially compensate for this effect.

$$\omega \sim \frac{10^{-5}}{\sigma} \sim 10^{-5}(\text{cb/sec})$$

It is apparent that all three of the terms in the omega equation may contribute significantly to the vertical motion. As we will see in Appendix C, the quantity $(T_S - T)$ becomes a maximum in the region 250 to 400 mb. This does not necessarily mean that its effect on the vertical velocities is a maximum here because the contribution to ω through latent heating is weighted by $\frac{1}{P\sigma}$. Although P decreases with altitude, σ increases and, in some pressure intervals, at a faster rate so that

the increased "warming" with elevation need not produce increasing vertical velocities.

Scaling the Vorticity Equation.

$$\zeta = v_x - u_y + \frac{u\tan\phi}{a} \sim \frac{V}{S} - \frac{V}{S} + \frac{V}{a} \sim 10^{-5} - 10^{-5} + 10^{-6} \sim 10^{-5}$$

$$\zeta_t + \vec{V}\cdot\nabla\zeta + \vec{V}\cdot\nabla f + \omega\zeta_p + \zeta\nabla\cdot\vec{V} + f\nabla\cdot\vec{V} + \hat{k}\cdot\nabla\omega\times\vec{V}_p = 0$$

$$C\zeta_x \qquad V\zeta_x \qquad Vf_y \qquad \omega\zeta_p \qquad \zeta\omega_p \qquad f\omega_p \qquad \omega_x v_p$$

$$\frac{C\zeta}{S} \qquad \frac{V\zeta}{S} \qquad \frac{Vf}{S} \qquad \frac{\omega\zeta}{\pi} \qquad \frac{\zeta\omega}{\pi} \qquad \frac{f\omega}{\pi} \qquad \frac{\omega}{S}\frac{V}{\pi}$$

$$10^{-10} \qquad 10^{-10} \qquad 10^{-10} \qquad 10^{-12} \qquad 10^{-12} \qquad 10^{-12} \qquad 10^{-12}$$

This scaling for the tropics suggests that in ordinary circumstances the local vorticity tendency will be dominated by the horizontal advective term. We have underestimated f although not by an order of magnitude. The only term involving undifferentiated f in the numerator is the divergence term. Consequently, we should expect the divergence term, on the average, to be larger than the vertical advective and twisting terms but to be closer in magnitude to them than to the horizontal advective term. Of course, where the divergence becomes quite large (especially if it coincides with large values of vorticity) the divergence term may dominate the whole expression. Similarly with strong vertical motions the vertical advection term may become significant (given reasonable values of ζ_p); or, if strong horizontal gradients of ω are combined with strong shears of the horizontal wind with height, the twisting term will assume importance. These latter two possibilities are much less likely than the former due to the underestimate of f.

Scaling the Divergence Equation.

Divergence, $D \equiv u_x + v_y = -\omega_p \sim \frac{\omega}{\pi} \sim \frac{10^{-5}}{10^2} \sim 10^{-7}$

If we use the complete divergence equation in the form in which it appears preceding equation (2), Chapter II, we get

$$D_t + \vec{V}\cdot\nabla D + \omega D_p + \nabla\omega\cdot\vec{V}_p - f\zeta + \nabla^2\Phi$$

$$CD_x \quad uD_x \quad \omega D_p \quad \omega_x u_p \quad f\zeta$$

$$C\frac{D}{S} \quad V\frac{D}{S} \quad \omega\frac{D}{\pi} \quad \frac{\omega}{S}\times\frac{V}{\pi} \quad f\zeta$$

$$10^{-12} \quad 10^{-12} \quad 10^{-14} \quad 10^{-12} \quad 10^{-10}$$

continued

$$+ \vec{V}\cdot(\nabla\times f\hat{k}) + D^2 + 2J(v,u) - \frac{\vec{V}\cdot\vec{V}}{a^2} - \frac{\mathrm{Tan}\,\phi}{a} 2(\vec{V}\cdot\vec{V})_y = 0$$

$$vf_y \quad D^2 \quad v_x u_y \quad \frac{V^2}{a^2} \quad \frac{1}{a}(V^2)_y$$

$$V\frac{f}{S} \quad D^2 \quad \frac{V^2}{S^2} \quad \frac{V^2}{a^2} \quad \frac{V^2}{a\times S}$$

$$10^{-10} \quad 10^{-14} \quad 10^{-10} \quad 10^{-12} \quad 10^{-11}$$

This tropical scaling produces slightly different results from those obtained in middle latitudes. If we recall that f has been underestimated, we can reclaim the geostrophic relationship by pointing out that $\nabla^2\Phi$ must, in the first estimate, be balanced by $-f\zeta$, i.e. $\nabla^2\Phi = f\zeta$. However, it is obvious that as latitude decreases, the relation becomes less valid. If we retain terms of $10^{-10}\,\mathrm{sec}^{-2}$, we find the balance equation:

$$\nabla^2\Phi - f\zeta + \beta u + 2J(v, u) = 0$$

This expression includes the variation of f with latitude and the Jacobian which involves the streamline curvature.

If we scale the irrotational, $\vec{V}_\chi = \nabla\chi$, and non-divergent, $\vec{V}_\psi = \hat{k}x\nabla\psi$, parts of the wind field, we find

$$\nabla^2\chi = \chi_{xx} + \chi_{yy} = D$$

$$\frac{\chi}{S^2} + \frac{\chi}{S^2} \sim D \qquad \chi \sim S^2 D \sim 10^5$$

$$\nabla^2\psi = \psi_{xx} + \psi_{yy} = \zeta$$

$$\frac{\psi}{S^2} + \frac{\psi}{S^2} \sim \zeta \qquad \psi \sim S^2\zeta \sim 10^7$$

Consequently,

$$\vec{V}_\psi \sim \psi_y \sim \frac{\psi}{S} \sim \frac{10^7}{10^6} \sim 10$$

$$\vec{V}_\chi \sim \chi_x \sim \frac{\chi}{S} \sim \frac{10^5}{10^6} \sim 10^{-1}$$

and the irrotational part of the wind is more than one order of magnitude smaller than the non-divergent part. This fact may be employed in the previous expression of the balance equation. If the wind components, u and v, are split into their non-divergent and irrotational components, it is obvious that the terms involving the irrotational part of the wind will be more than an order of magnitude smaller than those corresponding terms involving the non-divergent part of the wind. Since this is so, we can write

$$f\nabla^2\psi + \beta\psi_y - 2J(\psi_x, \psi_y) = \nabla^2\Phi$$

where the left-hand side is a function of ψ and involves the non-divergent part of the wind only.

APPENDIX B

ENERGETIC CONSISTENCY

The perils of ignoring energetic consistency are not so immediately obvious in diagnostic modelling. With forecast models which are run long enough, effects of energetic inconsistencies usually become obvious in forecast deterioration. This is not a hazard in diagnostic work, but it is nevertheless true, that the results will be unrepresentative to the extent that energetically inconsistent formulations are used. The following is an examination of the energetic consistency of the principal working equations.

Let $\hat{P}_E$ be the potential energy/unit area.

$$\hat{P}_E = -\int_{P_0}^{0} Z\delta p = Z_0 P_0 + R \int_0^{\infty} \rho T \delta Z$$

Let $\hat{I}$ be the internal energy/unit area.

$$\hat{I} = C_v \int_0^{\infty} \rho T \delta Z$$

$$\hat{P}_E + \hat{I} = Z_0 P_0 + \frac{C_p}{g} \int_0^{P_0} T \delta p$$

If we sum these quantities over the whole atmosphere to find the Total Potential Energy, P^*

$$P^* = \int_S Z_0 P_0 \delta A + C_p \int_M \theta \left(\frac{P}{P_0}\right)^{\kappa} \delta M$$

Where δA is an element of area and δM is an element of mass.

Following Lorenz (1960) we now introduce identically numbered subscripts to designate those variables related to each other by an identity.

$$P({}_1\alpha) = R({}_1T), \qquad {}_1\Phi_p = -{}_1\alpha, \qquad {}_2\vec{V} = \hat{k}\times\nabla\, {}_2\psi$$

$${}_3\vec{V} = \nabla\, {}_3\chi \quad , \qquad {}_2\zeta = \nabla^2\, {}_2\psi, \qquad {}_3D = \nabla^2\, {}_3\chi$$

The kinetic energy per unit mass, $\hat{K}$ is

$$\hat{K} = \frac{\vec{V}\cdot\vec{V}}{2} = \frac{\vec{V}_2\cdot\vec{V}_2}{2} + \frac{\vec{V}_3\cdot\vec{V}_3}{2} + \vec{V}_2\cdot\vec{V}_3$$

$$= \frac{\nabla\,{}_2\psi\cdot\nabla\,{}_2\psi}{2} + \frac{\nabla\,{}_3\chi\cdot\nabla\,{}_3\chi}{2} + \hat{k}\times\nabla\,{}_2\psi\cdot\nabla\,{}_3\chi$$

where the latter term is also $J\,({}_2\psi, {}_3\chi)$ which vanishes when summed over the atmosphere. The total kinetic energy, K is equal,

$$K = \int_M \hat{K}\delta M = \int_M \frac{\nabla\,{}_2\psi\cdot\nabla\,{}_2\psi}{2}\,\delta M + \int_M \frac{\nabla\,{}_3\chi\cdot\nabla\,{}_3\chi}{2}\,\delta M = {}_2K + {}_3K$$

We can show that the rate of change of the total potential and internal energy, P^* of the atmosphere is

$$P^*_t = \int {}_1\alpha\,{}_3\omega\delta M$$

where ω is taken to be zero at the upper and lower limits of the atmosphere. Similarly, it can be shown that the rate of change of the total kinetic energy is $K_t = -\int_1 \alpha\,{}_3\omega\delta M$. So that $K_t + P^*_t = 0$ or $(P^* + {}_2K + {}_3K)_t = 0$. This does not mean that ${}_2K$ and ${}_3K$ cannot change between themselves.

Further manipulation shows that we can also write

$${}_2K_t = -\int {}_2\psi\,{}_2\zeta_t\delta M \text{ and } {}_3K_t = -\int {}_3\chi\,{}_3D_t\delta M$$

which relate the kinetic energies to the vorticity and divergence equations.

If we assume for the moment that we consider non-viscous, adiabatic processes only, we will write our basic equations in subscripted form.

1. First law of thermodynamics

(1) (1,2) (1,3) (1,3)

$${}_1\theta_t = -J({}_2\psi, {}_1\theta) - {}_3\vec{V}\cdot\nabla\,{}_1\theta - {}_3\omega\,{}_1\theta_p$$

2. Vorticity Equation

$$
\begin{aligned}
{}^{(2)}_{2}\zeta_t = &- J({}_2\psi, {}_2\zeta) - J({}_2\psi, f) - \nabla\cdot f\, {}_3\vec{V} - {}_3\vec{V}\cdot\nabla\, {}_2\zeta - {}_2\zeta\, {}_3D - {}_3\omega\, {}_2\zeta_p \\
&- \nabla\, {}_3\omega\cdot\nabla\, {}_2\psi_p - J({}_3\omega, {}_3\chi_p)
\end{aligned}
$$

3. Divergence Equation

$$
\begin{aligned}
{}^{(3)}_{3}D_t = &- \nabla^2\, {}_1\Phi + \nabla\cdot(f\nabla\, {}_2\psi) + J(f, {}_3\chi) - \nabla\cdot({}_2\vec{V}\cdot\nabla\, {}_2\vec{V}) \\
&- \nabla\cdot({}_2\vec{V}\cdot\nabla\, {}_3\vec{V}) - \nabla\cdot({}_3\vec{V}\cdot\nabla\, {}_2\vec{V}) - \nabla\, {}_3\omega\cdot {}_2\vec{V}_p \\
&- \nabla\cdot({}_3\vec{V}\cdot\nabla\, {}_3\vec{V}) - \nabla\, {}_3\omega\cdot {}_3\vec{V}_p - {}_3\omega\, {}_3D_p
\end{aligned}
$$

We also write 3 additional equations.

4. Total potential energy of the atmosphere.

$$
{}^{(1)}_{}P_t^* = \frac{C_p K}{P_0} \int_M \left(\frac{P}{P_0}\right)^{\kappa-1} {}_3\omega\, {}_1\theta\, \delta M
$$

5. Kinetic energy of the non-divergent wind component.

$$
\begin{aligned}
{}^{(2)}_{2}K_t = &\int {}_2\psi\nabla\cdot f\, {}_3\vec{V}\delta M + \int {}_2\psi\, {}_3\vec{V}\cdot\nabla\, {}_2\zeta\delta M + \int {}_2\psi\, {}_2\zeta\, {}_3D\delta M \\
&+ \int {}_2\psi(\nabla\, {}_3\omega\cdot\nabla\, {}_2\psi_p)\delta M + \int {}_2\psi J({}_3\omega, {}_3\chi_p)\delta M
\end{aligned}
$$

6. Kinetic energy of the irrotational component of the wind.

$$
\begin{aligned}
{}^{(3)}_{3}K_t = &\int {}_3\chi\nabla^2\, {}_1\Phi\delta M - \int {}_3\chi\nabla\cdot(f\nabla\, {}_2\psi)\delta M + \int {}_3\chi\nabla\cdot({}_2\vec{V}\cdot\nabla\, {}_2\vec{V})\delta M \\
&+ \int {}_3\chi\nabla\cdot({}_2\vec{V}\cdot\nabla\, {}_3\vec{V})\delta M + \int {}_3\chi\nabla\cdot({}_3\vec{V}\cdot\nabla\, {}_2\vec{V})\delta M \\
&+ \int {}_3\chi\nabla\, {}_3\omega\cdot\, {}_2\vec{V}_p\delta M
\end{aligned}
$$

In any model (particularly one which requires iteration) we require that it be energetically consistent, i.e., that $(P^* + {}_2K + {}_3K)_t = 0$. In order for this to be so, certain safeguards must be observed. First of all it must be realized that in the latter expression, the terms cancel class by class. Consequently, if, in order to achieve simplification, one drops certain terms in the divergence equation, then one must make sure that the corresponding cancelling terms in the other equations are similarly dropped. For instance, our scaling of the divergence equation in Appendix A suggests that we retain only the 10^{-10} sec^{-2} terms and only those components involving the non-divergent part of the wind. Thus we would drop all of the terms containing a (3) in the divergence equation. If the effect of this omission is traced through to the development of equation #6, we find that the last three terms, (2,3,3) terms, would not be present to cancel the (2,3,3) term in ${}_2K_t$. This deficiency can be overcome by eliminating the (2,3,3) term in ${}_2K_t$ which derives from the $J({}_3\omega, {}_3\chi_p)$ part of the twisting term (due to the divergent part of the wind) in the vorticity equation.

Hence, one energetically consistent set of equations (where $\vec{V} = {}_2\vec{V} + {}_3\vec{V}$) is:

$$ {}_2\zeta_t = -\vec{V}\cdot\nabla({}_2\zeta+f) - ({}_2\zeta+f)\nabla\cdot {}_3\vec{V} - {}_3\omega\ {}_2\zeta_p - \hat{k}\cdot\nabla\ {}_3\omega\times({}_2\vec{V}_p) $$

$$ \nabla^2\ {}_1\Phi = \nabla\cdot(f\nabla\ {}_2\psi) - \nabla\cdot({}_2\vec{V}\cdot\nabla\ {}_2\vec{V}) $$

$$ {}_1\theta_t = -J({}_2\psi, {}_1\theta) - {}_3\vec{V}\cdot\nabla\ {}_1\theta - {}_3\omega\ {}_1\theta_p $$

which can be expressed

$$ {}_1\Phi_{tp} = -{}_2\vec{V}\cdot\nabla\ {}_1\Phi_p - {}_3\vec{V}\cdot\nabla\ {}_1\Phi_p - {}_3\omega\cdot\ {}_1\sigma $$

This set will conserve total energy in an iterative process and should give dependable diagnostic results. To the last equation, of course,

we add the term which parameterizes the release of latent heat and destroys this conservation. However, this is a deliberate and purposeful step and we know that any total energy changes will be due to the heating term and not due to inept modelling.

If we examine further possible simplifications, we can study the result of dropping the (2,2) class term in the divergence equation which then reduces to

$$\nabla^2 {}_1\Phi = \nabla\cdot(f\nabla {}_2\psi) = -\beta\, {}_2u + f\nabla^2 {}_2\psi$$

a geostrophic-like relationship. This means the (2,2,3) term will be missing in ${}_3K_t$, and the four (2,2,3) terms in ${}_2K_t$ must be dropped since they can no longer be cancelled by the same class term in ${}_3K_t$. This, in turn, implies that the (2,3) terms in the vorticity equation which give rise to the four terms should also be dropped. The new cruder but still consistent set is:

$${}_2\zeta_t = -{}_2\vec{V}\cdot\nabla({}_2\zeta+f) - \nabla\cdot f\ {}_3\vec{V}$$

$$\nabla^2 {}_1\Phi = \nabla\cdot(f\nabla {}_2\psi)$$

$${}_1\Phi_{pt} = -{}_2\vec{V}\cdot\nabla\ {}_1\Phi_p - {}_3\vec{V}\cdot\nabla\ {}_1\Phi_p - {}_3\omega\ {}_1\sigma$$

Phillips (1960) has pointed out that a reduced and consistent form of the quasi-static, quasi-geostrophic set of equations is:

$${}_g\zeta_t = -{}_g\vec{V}\cdot\nabla({}_g\zeta+f) - \nabla\cdot f_0\ {}_3\vec{V}$$

$$\nabla^2 {}_1\Phi = f_0\nabla^2 {}_2\psi \text{ or } f\hat{k}\times {}_g\vec{V} = -\nabla\ {}_1\Phi$$

$${}_1\Phi_{tp} = -{}_2\vec{V}\cdot\nabla\ {}_1\Phi_p + P^{\sigma}\ {}_3\omega$$

The advection of thickness by the irrotational component of the wind has been omitted, and the static stability, σ, has been made a function of pressure only ($_P\sigma$) in order that energy be conserved in the following way:

$$\int({}_gV^2 + \frac{\Phi_p^2}{P^{\sigma}})\ \delta M + \rho_0 \int \Phi_0^2\ \delta A = \text{constant where } \Phi_0\ (x,y,t)$$

is the geopotential of the 1000-mb surface and ρ_0 is a suitable constant value of the density for this level.

The geostrophic omega equation is derived by manipulating the foregoing vorticity and thermodynamic equations. The expression for latent heating is added to the latter before the elimination of the time dependent term.

$$\frac{1}{f_0^2}\nabla^2({}_P\sigma\ {}_g\omega) + {}_g\omega_{pp} = \frac{1}{f_0}[{}_g\vec{V}\cdot\nabla({}_g\zeta+f)]_p - \frac{1}{f_0^2}\nabla^2({}_g\vec{V}\cdot\nabla\Phi_p) - \frac{1}{f_0^2}\nabla^2\left(\frac{R}{C_pP}\frac{dQ}{dt}\right)$$

APPENDIX C

CLIMATOLOGICAL VALUES FOR THE LATENT HEATING FUNCTION

The Kuo parameterization of latent heating is of the form

$$\frac{dQ}{dt} = -C_P(T_S - T)\frac{I}{N} \quad \text{where} \quad I = \frac{\omega_H q_H}{g} \quad \text{and}$$

$$N = \frac{1}{g}\int_{P_T}^{P_B} \frac{C_P}{L}(T_S - T)\,dp + \frac{1}{g}\int_{P_T}^{P_B}(q_S - q)\,dp$$

and P_T and P_B refer to pressures at the top and bottom of the cloud. We have chosen to use appropriate climatological values for these quantities with the exception of ω_H, the frictional vertical velocity at the top of the friction layer, which is essentially that given by Cressman (1960). What we propose to do is to use Jordan's (1958) mean monthly West Indian sounding for the relevant months.

Figure 34 presents the mean West Indies sounding for August. Specific humidities have been calculated from the relative humidity data and have been extrapolated above the 450 mb level. Air from the 1000-mb level is raised by parcel ascent to its condensation level which occurs at 960 mb and then moist adiabatically to the point where positive buoyancy is reduced to zero (160 mb). This puts the cloud base at around 1600 ft which is a frequently noted level. Mean values of q, q_S, T and T_S for the necessary pressure intervals are worked out graphically on the tephigram in the usual manner. Below are the values computed for the August soundings, figure 34, and for the October sounding which is not shown. For these computations the following values were used:

$C_P = 1004$ kj/t/deg

$g = 9.8$ m/sec

$L = 2.5 \times 10^6$ kj/t

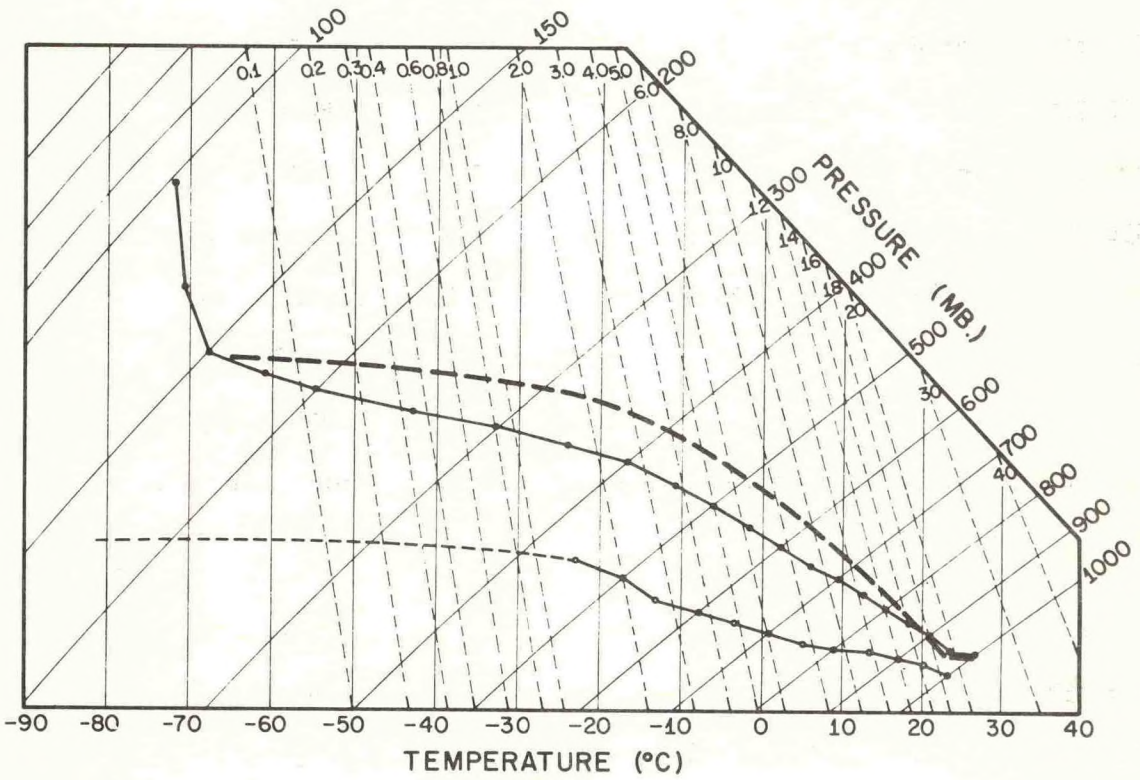

Figure 34. Mean August sounding for the West Indies (Jordan, 1958). Heavy solid lines are the temperature and mixing ratio values (with the mixing ratio extrapolated upward from 450 mb) plotted on a tephigram. Heavy dashes depict parcel ascent dry adiabatically from 1000 mb to the lifting condensation level and moist-adiabatically thereafter. Light solid lines are isotherms and lines of constant pressure; dashed lines are lines of constant mixing ratio, labelled in grams per kilogram of dry air. Dry adiabats are horizontal and are not shown.

COMPUTATION OF N FOR AUGUST

Layer	$\frac{C_P}{g}\frac{\Delta P}{L}$	$\overline{T}_S$ °C	$\overline{T}$ °C	ΔT°C	Product
960-850	$.4508 \times 10^{-3}$	20.5	20.5	0	0
850-700	$.6147 \times 10^{-3}$	14.6	13.2	1.4	$.8606 \times 10^{-3}$
700-550	$.6147 \times 10^{-3}$	6.2	3.0	3.2	1.9670×10^{-3}
550-400	$.6147 \times 10^{-3}$	- 5.5	-10.0	4.5	2.7660×10^{-3}
400-250	$.6147 \times 10^{-3}$	-25.0	-29.8	4.8	2.9506×10^{-3}
250-160	$.3688 \times 10^{-3}$	-51.8	-55.3	3.5	1.2908×10^{-3}
					9.8352×10^{-3}

In the following $\overline{q}_S$ and $\overline{q}$ are in tons of moisture/kiloton but Δq is in tons per ton.

Layer	$\frac{\Delta P}{g}$	$\overline{q}_S$	$\overline{q}$	Δq	Product
960-850	1.1227	17.0	13.7	3.3×10^{-3}	3.7048×10^{-3}
850-700	1.5306	13.8	8.0	5.8×10^{-3}	8.8775×10^{-3}
700-550	1.5306	9.7	3.9	5.8×10^{-3}	8.8775×10^{-3}
550-400	1.5306	5.4	1.7	3.7×10^{-3}	5.6632×10^{-3}
400-250	1.5306	1.7	.25	1.45×10^{-3}	2.2194×10^{-3}
250-160	.9184	.17	.05	$.12 \times 10^{-3}$	$.1102 \times 10^{-3}$
					29.4527×10^{-3}

So the sum, N = .03929 tons of water vapor per square meter which would be required to warm and saturate the environment to cloud conditions. The value of q_H taken from the sounding was .0163 tons of water vapor per ton of moist air which is the value at 960 mb, the cloud base.

The quantity (T_S-T), the difference between cloud and ambient temperatures, is also determined for each level at which heating is to

be calculated. We have determined for August the following:

Level	$(T_S - T)$
850	0.7°C
700	2.2°C
550	3.7°C
400	4.9°C
250	4.7°C

In similar fashion it was determined that N for October was equal to .0436 tons of water vapor per square meter, and the October $(T_S - T)$ values of 2.0, 3.2, 4.5, 6.1, and 6.2°C were tabulated for the levels 850 through 250 mb.

REFERENCES

Aubert, E. J., 1957: On the release of latent heat as a factor in large scale atmospheric motions, J. of Meteor., 14, 527-542.

Baumhefner, D. P., 1968: Application of a diagnostic numerical model to the tropical atmosphere, Mon. Wea. Rev., 96, 218-228.

Bedient, H. A., and J. Vederman, 1964: Computer analysis and forecasting in the tropics, Mon. Wea. Rev., 92, 565-577.

Bellamy, J. C., 1949: Objective calculations of divergence, vertical motion and vorticity, Bulletin Amer. Meteor. Soc., 30, 45-59.

Bushby, F. H., 1952: The evaluation of vertical velocity and thickness from Sutcliffe's theory, Q.J.R.M.S., 78, 354-362.

Charney, J. G., 1962: Integration of the primitive and balance equations, Technical Report of the Japan Meteorological Agency, No. 14, Proceedings of the International Symposium on Numerical Weather Prediction in Tokyo, November 7-13, 1960, 131-152.

Charney, J. G., 1963: A note on large-scale motions in the tropics, J. of Atmospheric Sci., 20, 607-609.

Charney, J. G., and A. Eliassen, 1964: On the growth of the hurricane depression, J. of Atmospheric Sci., 21, 68-75.

Charnock, H., J. R. D. Francis, and P. A. Sheppard, 1956: An investigation of wind structure in the trades Anegada 1953, Philos Trans. of the Roy. Soc. of London, Series A, 249, 179-234.

Colon, J. A., and W. R. Nightingale, 1963: Development of tropical cyclones in relation to circulation patterns at 200 mb level, Mon. Wea. Rev., 91, 329-336.

Craig, R. A., M. A. Lateef, and R. A. Mitchem, 1961: The stratospheric warming over North America in 1957, pt. 2, Height, temperature, vorticity and vertical motion at the 50-mb surface, Contract AF (604)-5471 Scientific Report No. 2, Dept. of Meteorology, Florida State University, Tallahassee.

Cressman, G. P., 1960: Improved terrain effects in barotropic forecasts, Mon. Wea. Rev., 88, 327-342.

Eliassen, A., and W. E. Hubert, 1953: Computation of vertical motion and vorticity budget in a blocking situation, Tellus, 5, No. 2, 192-206.

Epstein, E. S., 1959: Large scale vertical motion in the stratosphere, Final Report Part II, Contract AF 19(604)-2190, Dept. of Meteorology, Pennsylvania State University

Gates, W. L., L. S. Pocinki, and C. F. Jenkins, 1955: Results of numerical forecasting with the barotropic and thermotropic atmospheric models, Geophysical Research Papers, No. 46, Geophysics Research Directorate.

Graham, R. D., 1953: A new method of computing vorticity and divergence, Bulletin Amer. Meteor. Soc., 34, 68-74.

Gray, W. M., 1967: The mutual variation of wind, shear, and baroclinicity in the cumulus convective atmosphere of the hurricane, Mon. Wea. Rev., 95, 55-73.

Hawkins, H. F., and S. L. Rosenthal, 1965: On the computation of stream functions from the wind field, Mon. Wea. Rev., 93, 245-252.

Hawkins, H. F., and D. T. Rubsam, 1968: Hurricane Hilda, 1964, Part I, Genesis as revealed by satellite photographs, conventional and aircraft data, Mon. Wea. Rev., 96, 428-452.

Jordan, C. J., 1958: Mean soundings for the West Indies area, Jour. of Meteorology, 15, 91-97.

Knighting, E., 1960: Some computations on the variations of vertical velocity with pressure on a synoptic scale, Q.J.R.M.S., 86, 318-325.

Krishnamurti, T. N., 1968: A diagnostic balance model for studies of weather systems of low and high latitudes, Rossby number less than 1, Mon. Wea. Rev., 96, 197-207.

Krishnamurti, T. N., 1968: A study of developing wave cyclone, Mon. Wea. Rev., 96, 208-217.

Kuo, H. L., 1965: On formation and intensification of tropical cyclones through latent heat release by cumulus convection, J. Atmospheric Sci., 22, 40-63.

Lateef, M. A., 1967: Vertical motion, divergence, and vorticity in the troposphere over the Caribbean, Aug. 3-5, 1963, Mon. Wea. Rev., 95, 778-790.

Lateef, M. A., 1968: Vertical motion at 100 mb in the tropics, Mon. Wea. Rev., 96, 286-290.

Lateef, M. A., and C. L. Smith, 1967: A synoptic study of two tropical disturbances in the Caribbean, ESSA, Technical Memorandum, IERTM - NHRL No. 78.

Lorenz, E. N., 1960: Energy and numerical weather prediction, Tellus, 12, 364-373.

Miller, A., and H. A. Panofsky, 1957: Vertical motion and weather, Jan. 1-31, 1953, Scientific Report No. 2, Contract No. AF 19(604)-1025, Dept. of Meteorology, Pennsylvania State University.

Miller, B. I., 1966: Energy exchanges between the atmosphere and the oceans, American Society for Oceanography, Public. No. 1, Hurricane Symposium, Oct. 10-11, 1966, Houston, Texas, 134-157.

O'Brien, J. J., 1968: Correspondence - Comments on "Over-relaxation factor in numerical solution of Omega equation", Mon. Wea. Rev., 96, 99-104.

O'Brien, J. J., 1970: Alternative Solutions to the Classical Vertical Velocity Problem, J. of Applied Met., 9, 197-203.

Ogura, Y., 1964: Frictionally controlled, thermally driven circulations in a circular vortex with application to tropical cyclones, J. Atmospheric Sci., 21, 610-621.

Ooyama, K., 1967: Numerical simulation of the life cycle of tropical cyclones, NSF Grant No. GA-623, Dept. of Meteorology and Oceanography, New York Univ., New York, 133 pp.

Palmén, E., 1958: Vertical circulation and release of kinetic energy during development of Hurricane Hazel into an extratropical storm, Tellus, 10, 1-23.

Panofsky, H. A., 1946: Methods of computing vertical motion in the atmosphere. J. of Meteor., 3, 45-49.

Petterssen, S., 1956: Weather analysis and forecasting, Vol. I, New York, McGraw-Hill, 428.

Pfeffer, R. L., 1962: Results of recent research in meteorology at the Lamont Geological Observatory, Technical Report of the Japan Meteorological Society No. 14, Proceedings of the International Symposium on Numerical Weather Prediction in Tokyo, Nov. 7-13, 1960, 249-263.

Phillips, N. A., 1960: Numerical weather prediction, Advances in Computers, Academic Press, 316 pp.

Rex, D. F., 1958: Vertical atmospheric motions in the equatorial central Pacific, Geophysics, 6, 479-501.

Riehl, H., 1954: Tropical Meteorology, McGraw-Hill, New York, 392 pp.

Rosenthal, S. L., 1969: Numerical Experiments with a multi-level primitive equation model designed to simulate the development of tropical cyclones, experiment 1, Technical Memorandum ERLTM - NHRL 82, 0.8.Dept. of Commerce/ESSA.

Rosenthal, S. L., 1970: A circularly symmetric, primitive equation model of tropical cyclone development containing an explicit water vapor cycle, Mon. Wea. Rev., 98, 643-663.

Sanders, F., A. J. Wagner, and T. N. Carlson, 1960: Specification of cloudiness and precipitation by multi-level dynamical models, Scient. Rpt. No. 1, Cont. No. AF 19 (604)-5491, Dept. of Meteor., MIII, III.

Sangster, W. E., 1960: A method of representing the horizontal pressure force without reduction of station pressures to sea level, J. of Meteor., 17, 166-176.

Sawyer, J. S., 1949: Recent research at Central Forecasting Office, Dunstable, Q.J.R.M.S., 75, 185-188.

Shuman, F. G., 1957: Numerical methods in Weather prediction: I. the balance equation, Mon. Wea. Rev., 85, 329-332.

Shuman, F. G., 1957: Numerical methods in Weather prediction: II. smoothing and filtering, Mon. Wea. Rev., 85, 357-361.

Stuart, D. W., 1961: Vertical motion and the baroclinic mechanism of rapid upper-level cyclogenesis, California Rainfall Process Project, Dept. of Meteorology, U.C.L.A.

Stuart, D. W., 1964: A diagnostic case study of the synoptic scale vertical motion and its contribution to mid-tropospheric development, J. of Applied Meteor., 3, 699-684.

Sumner, E. J., 1950: The significance of vertical stability in synoptic development, Q.J.R.M.S., 76, 384-392.

Sutcliffe, R. C., 1947: A contribution to the problem of development, Q.J.R.M.S., 73, 370-383.

Yanai, M., 1961: A detailed analysis of typhoon formation, Jour. of Met. Soc. of Japan, Series II, 39, 187-214.

Yania, M., 1964: An experimental objective analysis in the tropics, Tech. Paper No. 62, Dept. Atmos. Sci., Colorado State Univ., 23 pp.

Yanai, M., and T. Nitta, 1967: Computation of vertical motion and vorticity budget in a Caribbean easterly wave, Jour. of Met. Soc. of Japan, 45, No. 6. 444-446.

GPO 840-211